UNIVERSITA' DEGLI STUDI DI SIENA
DIPARTIMENTO DI BIOTECNOLOGIE, CHIMICA E FARMACIA

DOTTORATO DI RICERCA IN
BIOCHEMISTRY AND MOLECULAR BIOLOGY BIBIM 2.0

CICLO XXXIII

COORDINATORE Lorenza Trabalzini

TITOLO DELLA TESI:

Identification and Characterization of Human Aldose Reductase Differential Inhibitors

SETTORE SCIENTIFICO-DISCIPLINARE: BIO/10

DOTTORANDO
Carlotta Pineschi

TUTOR
Prof.ssa Antonella Del Corso

ANNO ACCADEMICO: 2019/2020

Acknowledgements

I dedicate this thesis to my fiancé, Giovanni, who was my rock. He has always been by my side and supported me even from across the ocean. Your support and love were and are essential for me every day.

I also thank my parents and my brothers for teaching me to never give up and always give the best of me in any situations.

A special thanks to all my mentors in Italy and over ocean. I thank Professor Del-Corso and Professor Mura for teaching me and guide me during these years. Thank you for your patience and your help. Thank you for believing in me and giving me the possibility to do an experience of research in the USA. I also thank all the colleagues in the laboratory in Pisa for the help and the support during these years.

A special thank goes to Professors Anna De-Paoli Roach and Peter J Roach for their hospitality in Indianapolis, for teaching and mentoring me during my period abroad. I will remember for the rest of my life the months spent with you. You helped me to grow up not only from a professional point of view but also as a person. Thank you for hosting me as a real member of your laboratory, I really felt like at home immediately. Regarding that I want to thank also Dyann, you are not only a colleague, with which I am grateful I had the opportunities to work with but you became a very good friend of mine.

TABLE OF CONTENTS

LIST OF TABLES

LIST OF FIGURES

LIST OF ABBREVIATIONS

AGEs	Advanced glycation end-products
AKR	Aldo Keto Reductase
AKR1B1	Aldo-Keto Reductase
ARI	Aldose reductase inhibitor
ARDI	Aldose reductase differential inhibitor
BSA	Bovine serum albumin
C.E.	Crude Extract
DAG	Diaciglycerol
DHN	1,4-dihydroxy-2-nonene
DMSO	Dimethyl sulfoxide
DNA	Deoxyribonucleic acid
DTT	Dithiotreitol
E. coli	Escherichia coli
EDTA	Ethylenediaminetetraacetic acid
FBS	Fetal Bovine Serum
GAL	D,L-glyceraldehyde
GS-DHN	Glutathionyl-1,4-dihydroxynonane
GSH	Glutathione
GSHNE	3-glutathionyl-4-hydroxynonanal
HEK-293	Human Embryonic Kidney 293 cells
HLEC	Human Lens Epithelial Cells
HNE	4-hydroxy-2,3-nonenal
HTS	High throughput screen
IkB	Inhibitor of NF-*k*B
IPTG	Isopropyl ß-D-1-thiagalactopyranoside
LB	Luria-Bertani
LOPAC	Library of Pharmacologically Active Compounds
MEM	Minimum Essential Medium Eagle
NAD^+	Nicotinamide Adenine Dinucleotide

NADH	Nicotinamide Adenine Dinucleotide reduced form
$NADP^+$	Nicotinamide Adenine Dinucleotide Phosphate
NADPH	Nicotinamide Adenine Dinucleotide Phosphate reduced form
NF-*k*B	Nuclear factor kappa-light-chain-enhancer of activated B cells
ORE	Osmotic response element
PIC	Protease inhibitor cocktails
pNO-FireflyLuc2P	pGL4.32/luc2p/NF-*k*B-RE/Hygro-vector without the gene for the expression of the gene for the Firefly Luciferase.
pNO-Renilla	pRL-SV40 without the gene for the expression of the Renilla Luciferase
pFireflyLuc2P	pGL4.32/luc2p/NF-*k*B-RE/Hygro-vector
PKC	Protein kinase C
pRenillaLuc	pRL-SV40
ROS	Reactive oxygen species
SDH	Sorbitol Dehydrogenase
*hr*TNF-alpha	human recombinant Tumor necrosis factor alpha
T1DM	Type 1 diabetes mellitus
T2DM	Type 2 diabetes mellitus
ΔA	Delta absorbance
ΔA/min	Delta absorbance in a minute

1. INTRODUCTION

1.1 Diabetes

Diabetes is a chronic condition caused by a lack or an ineffectiveness of insulin, characterized by increased glucose blood levels, which affects almost all organs. The prevalence of diabetes is continuously increasing and the International Diabetes Federation estimated that in the 2045 almost 6 million people will be suffering of diabetes (International Diabetes Federation, 2017).

The common symptom of diabetes is usually hyperglycemia, a high concentration of glucose in the blood. This condition is also associated with other symptoms that can develop later, such us weight loss, polyuria (excessive or abnormal production of urine), polydipsia (excessive thirst), reduction of the vision (American Diabetes Association, 2014) and cardiovascular diseases (Kovacic *et al.,* 2014; Petak and Sardhu, 2018).

Different types of diabetes have been identified. Type 1 diabetes (T1DM) is caused by a lack of insulin production caused by an autoimmune destruction of pancreatic β-cells. T1DM is usually diagnosed in early ages, generally children and adolescents are the most affected patients and the only therapy is based on exogenous insulin administration (World Health Organization, 2016).

Type 2 diabetes (T2M) is characterized by a deficiency of the organism to maintain a correct glucose homeostasis in the basal or postprandial state, usually associated with different causes such as abnormalities in insulin secretion, manifestation of insulin resistance in muscle, liver and adipocytes and also deficiencies in the glucose uptake from visceral organs (DeFronzo, 2004). The evolution of this disease is usually described by 5 stages, that if not kept under control may progress in more severe secondary complications that afflict different organs (Wu, 2015). Unlike patients afflicted by T1DM, patients with T2DM can prevent a more severe progression of the disease without the use of drugs in the very early stages. The first suggestion for those patients is changing their lifestyle introducing a correct diet and regular exercise. When those recommendations are insufficient, pharmacological treatment with the use of drugs such as metformin or insulin therapy, is introduced (Vijan, 2015).

Gestational diabetes is a disease that afflicts pregnant women usually during the second and third trimester of pregnancy, due to metabolic changes in maternal metabolism associated with hormones and other mediators secreted by the placenta. Usually the influence of pregnancy on glucose homeostasis of the mother is completely resolved within 6 to 12 weeks postpartum. If not kept under control, gestational diabetes can increase the risk of complications during the pregnancy

both for the mother and the child. Moreover, an insulin resistant state during the second semester may progress into T2DM even after childbirth. The therapy for women afflicted by gestational diabetes is a change of lifestyle with a correct diet and physical activity usually associated with the self-monitoring of blood glucose (Chiefari *et al*., 2017).

1.2 Diabetes secondary complications

Persistent hyperglycemia may progress to severe complications, some metabolic consequences even resulting in death. These metabolic disorders are usually associated either with diabetic ketoacidosis, due to an extremally high blood glucose concentration, or a coma caused by severe hypoglycemia.

The most common consequence of diabetes are the long-term vascular complications, which are characterized by damage to the structure and functionality mainly (even though not exclusively) of blood vessels. Usually the secondary complications are divided in two main categories based on the vessels that are afflicted: microvascular complications, when the small blood vessels are damaged, and macrovascular complications due to the damage of arteries (Forbes and Cooper, 2013).

The main microvascular complications include neuropathies that afflict the nervous system, and the renal system and the retinopathies, that afflict the eye. Macrovascular complications include severe cardiovascular diseases, stroke and peripheral vascular diseases which may progress and lead to gangrene and, in more severe cases, amputation (Deshpande *et al*., 2008).

Another complication of diabetes is the development of diabetic cataracts, which are characterized by a clouding of the crystallin lens which may progress in the loss of the vision.

Four molecular mechanisms have been suggested to converge in the development of the microvascular and macrovascular complications of diabetes (Brownlee, 2001). One is the formation of advanced glycation end-products (AGEs), generated by the auto-oxidation of glucose to glyoxal and its further decomposition/fragmentation to produce methylglyoxal and 3-deoxyglucosone. These compounds readily interact with the amino groups of proteins inside and outside the cells, resulting in the generation of AGEs. Those modified proteins induce cell damage because of altered function and altered ability to interact with matrix components. In addition, through the interaction with specific AGEs receptors, they induce the generation of reactive oxygen species (ROS) causing oxidative stress conditions. The interaction with the AGE receptors

is associated with the activation of nuclear factor-k binding protein (NF-*k*B), leading to changes in gene expression.

Another mechanism is the activation of protein kinase C (PKC), caused by an increase of the synthesis of the lipid second messenger diacylglycerol from dihydroxyacetone phosphate and subsequent acylation, which occur under hyperglycemic conditions.

Several experiments showed that the activation of PKC induced an accumulation of matrix proteins in vessel cells, which in turn induce abnormalities in blood flow and permeability, especially in the retina and in the renal glomeruli. Different PKC isoforms have been described and their activation under hyperglycemic conditions appeared to be tissue-specific. PCK activation may also be associated with AGEs formation, thus increasing ROS concentration inside the cells. PKC activation is considered responsible of the lower production of nitric oxide in renal glomeruli and in smooth muscle cells under hyperglycemic conditions and of the inhibition of the expression of the mRNA for endothelial nitric oxide synthase in cultured endothelial cells after stimulation with insulin. In addition to the modulation of blood flow and cell permeability, PKC activation is at the basis of microvascular matrix protein accumulation induced by the expression of TGF-β1, fibronectin and type IV collagen observed both in mesangial cells and glomeruli of diabetic rats. Diabetic animals treated with a PKC-β inhibitor showed a significant reduction of secondary complications improving, for example, the glomerular filtration rate and partial correction of the albumin excretion (Koya, *et al.,* 2000).

The third mechanism involved in the onset of diabetic complications is increased flux through the hexosamine pathway, in which fructose-6-phosphate is converted to glucosamine-6-phosphate, through a reaction catalyzed by fructose-6-phosphate amidotransferase (GFAT). The increased flux through this pathway induces several changes in gene expression and protein function of the cell; for example, activation of GFAT induces the activation of the plasminogen activator inhibitor-1 promoter in vascular smooth cells through the modification of the transcription factor Sp1.

The fourth mechanism involved is the increased flux through the polyol pathway whose roles in the development of secondary complications of diabetes will be discussed in detail in the following section.

1.3 The polyol pathway and secondary complications of diabetes

This pathway consists of two steps catalyzed by two enzymes: aldose reductase (E.C. 1.1.1.21) (AKR1B1), which converts glucose into sorbitol, and sorbitol dehydrogenase (E.C. 1.1.1.14) (SDH) an NAD^+ dependent enzyme which converts sorbitol into fructose (Fig. 1.1) (Clements, 1986).

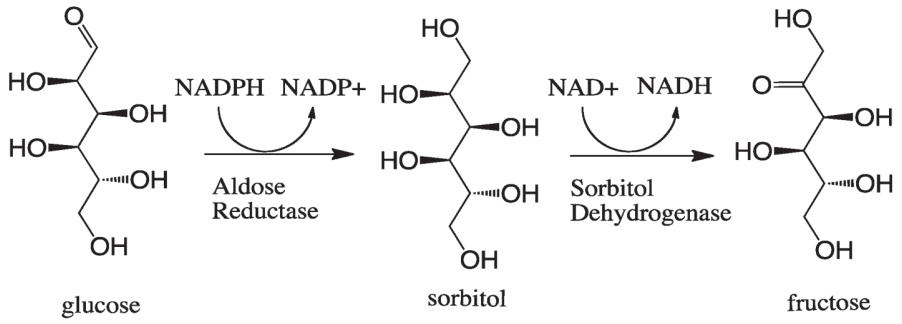

Figure 1. 1: Schematic representation of the polyol-pathway. AKR1B1, an NADPH dependent enzyme, converts glucose into sorbitol, which is then converted by SDH, an NAD^+ dependent enzyme, into fructose.

Under normoglycemic conditions only 3% of glucose enters the polyol pathway, since the AKR1B1 affinity for D-glucose, with a K_M around 50-100 mM (Ramana, 2011), is lower than the one observed for hexokinase, the first enzyme of glycolysis (K_M around 0.2-10 mM) (Nelson and Cox, 2018).

This percentage increases up to 30% under hyperglycemic conditions, such as occurs in diabetic patients (Ramana, 2011). Different metabolic alterations have been correlated to this increased flux through the polyol pathway. Since the limiting step of the pathway is the one catalyzed by the SDH, the increased glucose flux induces an accumulation of sorbitol inside the cells, which thus leads to an osmotic stress since sorbitol cannot permeate cell membranes (Lee and Chung, 1999). This osmotic unbalance, which may lead to the loss of membrane permeability, is considered the initial event in the formation of diabetic cataract (Kinoshita *et al.,* 1962).

Increased flux of the polyol pathway is also associated with an increased activity of SDH with the consequent reduction of NAD^+ concentration. Inside the cell, the $NADH/NAD^+$ ratio increases, resulting in the inhibition of glyceraldehyde-3-phosphate dehydrogenase and thus to increased methylglyoxal and diacylglycerol levels. As described above, this may contribute to increase in the level of AGEs and thus to induction of oxidative stress. Moreover, the observed activation of poly (ADP-ribose) polymerase, as a consequence of a higher production of ROS in hyperglycemic conditions, would contribute to the above described decrease of NAD^+ levels. The accumulation

of ROS inside the cells may cause cell damage since ROS chemically reacts with many macromolecules such as nucleic acids, proteins and lipids. Indeed, much evidence supports a marked increase of oxidative stress under hyperglycemic conditions.

In addition, the increase in AKR1B1 activity contributes to the generation of oxidative stress. In fact, AKR1B1 activity may result in a depletion of NADPH, which is the cofactor for glutathione reductase and is needed to regenerate antioxidant molecules such as reduced glutathione (GSH). (Brownlee, 2004) (Fig. 1.2). It is relevant that both oxidative stress and osmotic stress positively affect AKR1B1 expression. In fact, it was reported that the osmotic response element (ORE) is involved in the regulation of AKR1B1 expression in hyperosmotic conditions (Ferraris *et al.,* 1996; Ko *et al.,* 1997). Moreover, the high similarity between ORE and NF-*k*B binding sequences is the rationale behind the increased expression of AKR1B1 induced by TNF-alpha, which is indeed mediated by binding of NF-*k*B to ORE (Iwata *et al.,* 1999).

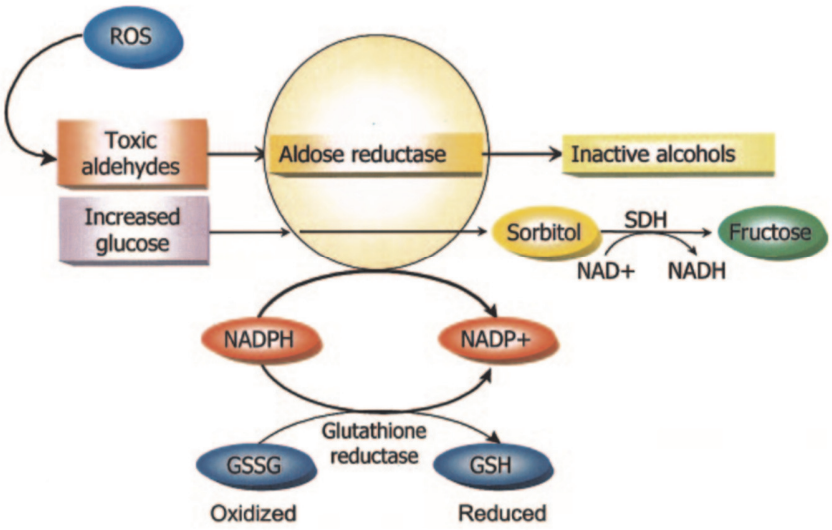

Figure 1. 2: Polyol Pathway flux under hyperglycemic conditions and correlation with oxidative stress. (taken from Brownlee, 2004)

All the consequences of an increased flux through the polyol pathway contribute to damage in different tissues, which as mentioned above include diabetic complications, i.e. retinopathies, cataract, nephropathies and neuropathies.

Diabetic retinopathy is one of the most common complications that afflicts diabetic patients and leads in almost 15-17% of the cases to total blindness (Stitt *et al.,* 2013). The involvement of the polyol pathway in the development of retinopathy may be associated with the localization of the enzyme in different retinal cells, such as endothelial cells, pigment epithelial cells, neurons and Muller cells. The increase of AKR1B1 activity in those cells induces changes in the retinal capillary basement membrane and leukocyte adhesion to endothelial cells, which are both the basis of the development of diabetic retinopathy (Tarr *et al.,* 2013).

It has been demonstrated that accumulation of sorbitol in lens cells activated apoptosis mechanisms which, in addition to osmotic stress, are the basis of the formation of diabetic cataract (Grewal *et al.,* 2016). In a recent study (Snow *et al.,* 2015) it was shown that over-expression of AKR1B1 under hyperglycemic conditions may be considered a risk factor that can lead to modification of the ERK and JNK pathways, altering the balance between cell growth and apoptosis, which is fundamental for the maintenance of homeostasis and thus of transparency of the lens.

Almost 40% of patients afflicted by diabetes develop nephropathies which may end up in most severe cases to kidney failure (Grewal *et al.,* 2016). It has been also demonstrated that AKR1B1 expression is increased in diabetic kidney compared to non-diabetic kidney (Kasajima *et al.*, 2001). An animal study (Hashimoto *et al.,* 2011) suggested a correlation between the early tubular changes and enhanced polyol pathway flux at the site of the juxtaglomerular area.

Another long-term complication that affects both type 1 and type 2 diabetic patients, is diabetic neuropathy. This pathology, caused by severe disorders that afflict both peripheral and autonomic nervous system, is usually associated with motor dysfunction, infections, gangrene and amputations. Some AKR1B1 inhibitors have been tested, using animal models, as drugs to counteract painful diabetic neuropathy; a 3-year clinical study with Epalrestat showed that it slowed down the progression of diabetic neuropathy (Hotta *et al.,* 2006).

1.4 Human Aldose Reductase

AKR1B1 belongs to the aldo-keto reductase (AKR) superfamily, which is composed of 16 families of NAD(P)H-dependent oxidoreductases expressed as 34-37 KDa polypeptides and conserved in both eukaryotes and prokaryotes. AKRs recognize different substrates such as hydrophobic aldehydes, monosaccharides, steroids, prostaglandins and xenobiotics (Jez *et al*., 1997).

1.4.1 AKR1B1 structure

AKR1B1 is a polypeptide composed of 315 amino acids, organized in an eight-stranded β/α-barrel with a small β-sheet capping at the N-terminal end (residues from 2 to 14) and a C-terminal extension (residues from 275 to 315). The enzyme is characterized by tight binding of the cofactor NADPH, which is maintained in position by a loop of residues which is located between β-strand 7 and α-helix 7 of the β/α-barrel. This loop, composed of residues from Gly213 to Ser226, is called the "*safety-belt*" (Fig. 1.3) and its movement is considered to be fundamental for both the binding and the release of the pyridine cofactor (Wilson *et al.,* 1992).

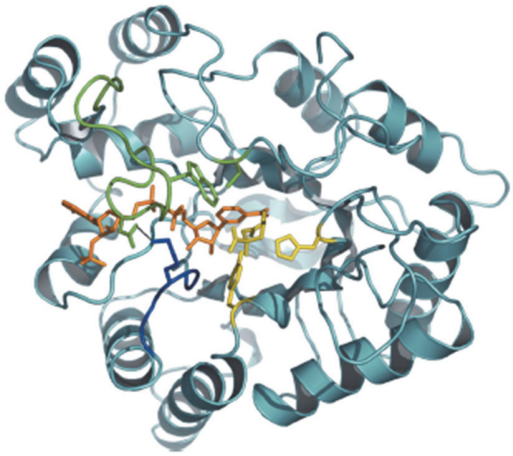

Figure 1. 3: Structure of human aldose reductase. The safety-belt loop is shown in green, the cofactor and the ligand (Citrate) are shown in orange and yellow, respectively (taken form Biadene *et al*., 2007).

The enzyme is characterized by an active site that can be divided in three parts: a rigid region called the "*anion-binding pocket*", composed of Trp20, Val47, Tyr48, Trp79 and His110, a more flexible part called the "*specificity pocket*", composed of Thr113, Phe115, Phe122, Cys303 and

Tyr309, and a mobile region, composed of the residues from Val297 to Leu300, which has been shown to change its position upon binding of specific ligands (Fig. 1.4) (Sotriffer *et al.,* 2004).

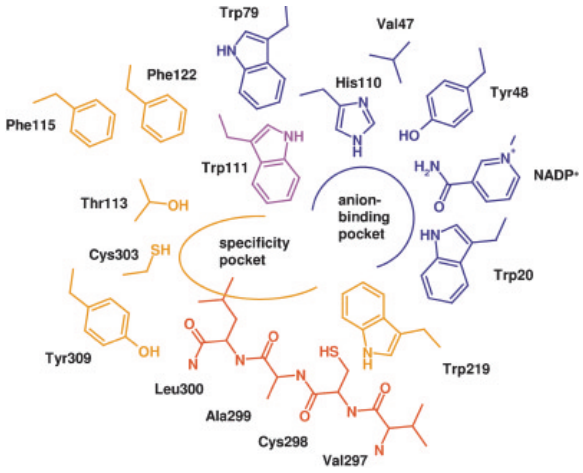

Figure 1. 4: Schematic drawing of the aldose reductase active site. In blue the "*anion-binding pocket*", in yellow the "*specificity pocket*" and in red the third mobile region (taken from Sotriffer *et al*., 2004).

The AKR1B1 reaction mechanism has been shown to involve a sequential ordered mechanism (Fig. 1.5). The binding of NADPH induces a conformational change of the enzyme structure, allowing the substrate to bind in the catalytic site. After the reduction of the aldehyde into the corresponding alcohol, the enzyme releases the alcohol before releasing the $NADP^+$. The release of the oxidized cofactor induces a further conformational change in the enzyme, which becomes ready to bind another molecule of NADPH.

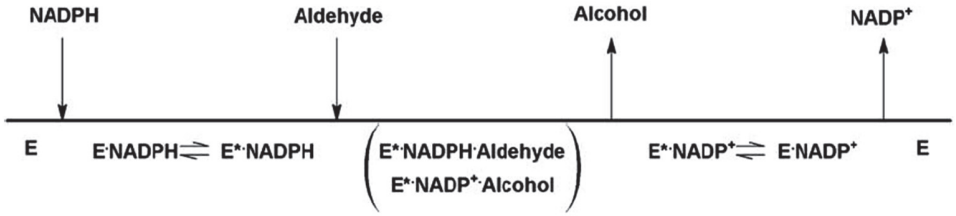

Figure 1. 5: AKR1B1 reaction mechanism. Sequential ordered mechanism model (taken from Del Corso A. *et al*., 2008).

In particular AKR1B1 catalyzes the stereospecific transfer of the 4-*pro*-*R*-hydride of the NADPH to the carbon of the carbonyl group of the substrate. This is followed by the protonation of carbonyl oxygen of the substrate by a proton donor group, which has been identified as Tyr48. This proton

release is strongly favored by the interaction of Tyr48 with Lys 77 (Fig. 1.6). Mutagenesis studies revealed also a relevant role for His110 in the interaction with different substrates (Bohren *et al.,* 1994).

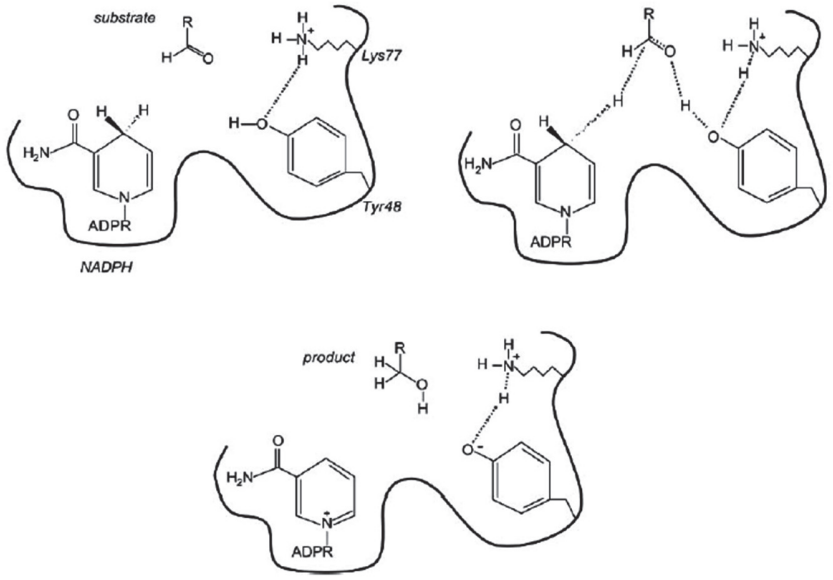

Figure 1. 6: Catalytic mechanism of the aldose reductase. (taken form Del Corso *et al*., 2008).

1.4.2 AKR1B1 Substrates

As outlined above, D-glucose can be considered the most relevant substrate for AKR1B1 in physio-pathological conditions. However, AKR1B1 is able to catalyze the reduction of several aldoses with 3 to 6 carbon atoms, so that it has long been considered an aspecific enzyme. However, the comparison of kinetic parameters displayed by AKR1B1 toward different aldoses (Balestri *et al.,* 2017) reveals that the enzyme is able in some cases to discriminate even between the D- and L-enantiomers of the same aldose. A prime example is the fact that L-glucose is not recognized at all as a substrate. As mentioned above, the K_M values for AKR1B1 toward D-glucose range from 50 to 100 mM. It is relevant that AKR1B1 acts on the open aldehydic form of the sugar (Inagaki *et al.,* 1982). This is the rationale for the use (Balestri *et al.,* 2015a) of L-idose as an alternative substrate to D-glucose for in vitro assay. In fact, for L-idose the concentration of the free aldehyde form present in solution is approximately 60–80-fold higher than that observed for glucose (Dworkin and Miller, 2000).

Another relevant class of AKR1B1 substrates is represented by hydrophobic toxic aldehydes, such as those produced from lipid peroxidation occurring under oxidative stress. The main substrate of this large group is 4-hydroxy-2-nonenal (HNE), which derives mainly from ϖ-6-polyunsaturated fatty acids (Fig. 1.7) (Zhang and Forman, 2017)

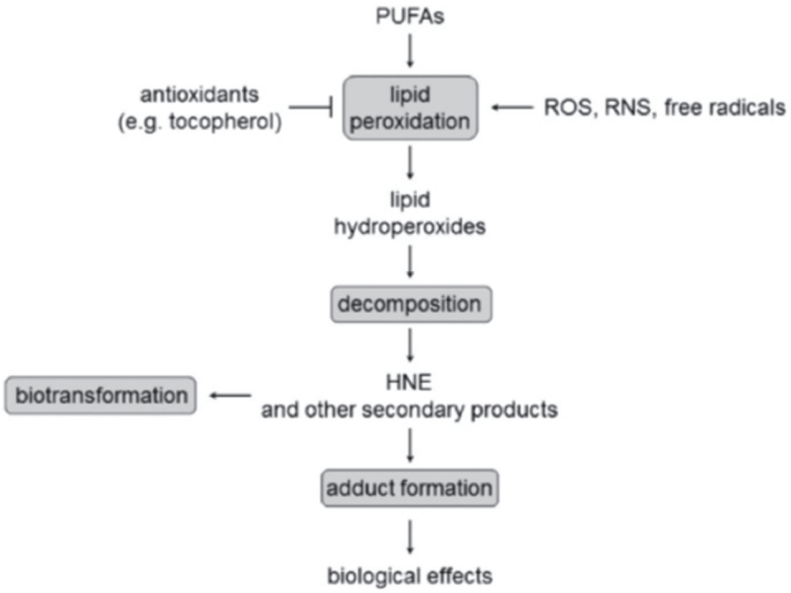

Figure 1. 7: Schematic representation of HNE metabolism. Schematic representation of HNE formation and removal pathways (taken from Csala *et al.,* 2015). Abbreviation: Polyunsaturated fatty acids (PUFAs).

Due to the presence of a conjugated carbonyl group and double bond between C2 and C3, HNE is a very reactive molecule. HNE is able to undergo Michael addition reactions, and Schiff base generation and thus it can react with molecules containing amino and thiol groups. It has been widely demonstrated that HNE can indeed modify lipids, nucleic acids and proteins (Fig. 1.8) increasing the damage caused by oxidative stress (Zhang and Forman, 2017).

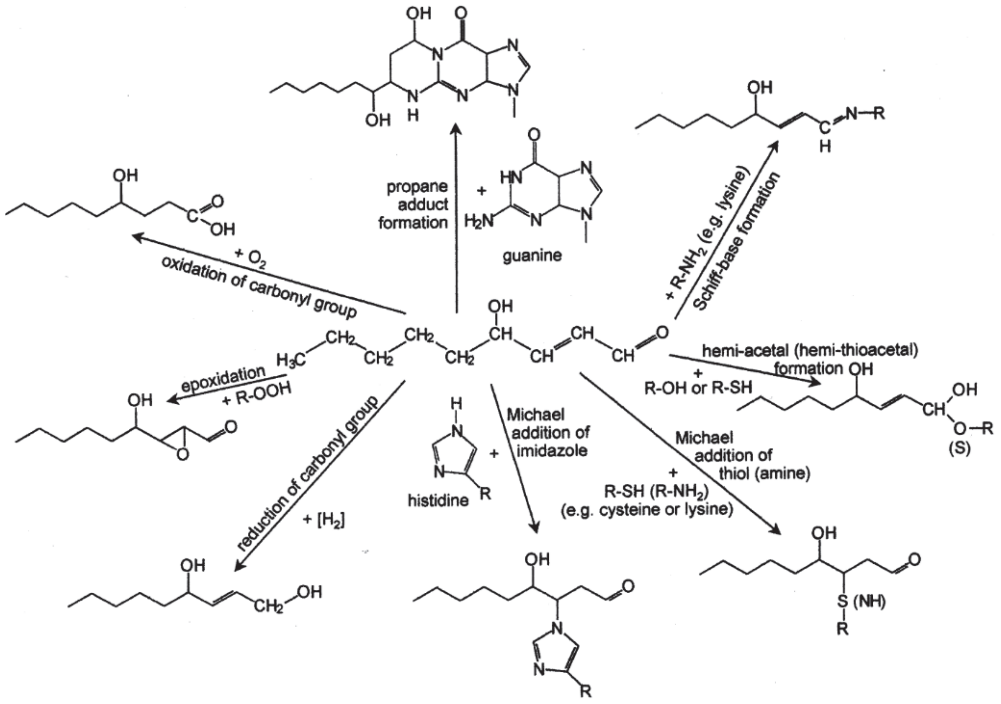

Figure 1. 8: HNE reactions with different biomolecules. (taken from Poli and Schaur, 2000).

Under physiological conditions, HNE concentration is well balanced between its production and degradation and is between 0.28 and 0.68μM in the plasma; this concentration rapidly increases under pathological and oxidative stress conditions (Zhang and Forman, 2017).

Higher concentrations of HNE are associated with cell damage; for that reason, cells have developed different mechanisms to metabolize HNE. The most relevant are:

- Oxidation of the carbonyl group with the formation of 4-hyroxy-2-nonenoic acid (HNA) by aldehyde dehydrogenases (Schaur *et al.*, 2015);
- Reduction of the carbonyl group to 1,4-dihydroxy-2-nonene (DHN) by alcohol dehydrogenase and aldo-keto reductases such as AKR1B1 and AKR1B10 (Zhang and Forman, 2017);
- Conjugation with GSH, catalyzed by several glutathione S-transferases, with the formation of 3-glutathionyl-4-hydroxynonane (GSHNE), which in turn can be reduced by AKR1B1 (Srivastava *et al.,* 1995), as discussed below.

HNE is not the only hydrophobic aldehyde recognized as substrate by AKR1B1. In fact, the enzyme is able to reduce a wide series of alkanals, alkenals and hydroxyalkenals (Srivastava *et al.,* 1999) and is more efficient in catalyzing the reduction of medium- to long-chain unbranched

saturated and unsaturated aldehydes with respect to short-chain aldehydes (Srivastava *et al.,* 1995). In addition, as stated above, AKR1B1 is able to catalyze the reduction of GSHNE and of other glutathionyl adducts of hydrophobic aldehydes.

It has been shown that the product of GSHNE reduction, glutathionyl-1,4-dihydroxynonane (GSDHN), activates NF-*k*B through the activation of phospholipase C/protein kinase C (PKC) to increase diacylglycerol (DAG) synthesis which occurs under hyperglycemic conditions. PKC activation induces the phosphorylation and activation of the I*k*B (Inhibitor of NF-*k*B) kinase complex, which leads to the phosphorylation, ubiquitination and subsequent degradation of I*k*B. Loss of I*k*B releases NF-*k*B heterodimer (p50 and p65) which can translocate to the nucleus and bind the DNA via its DNA binding subunits (Fig. 1.9) (Diaz-Meco *et al.,* 1994; Baeuerle and Baltimore, 1996; Bergmann *et al.,* 1998; Ramana *et al.,* 2005).

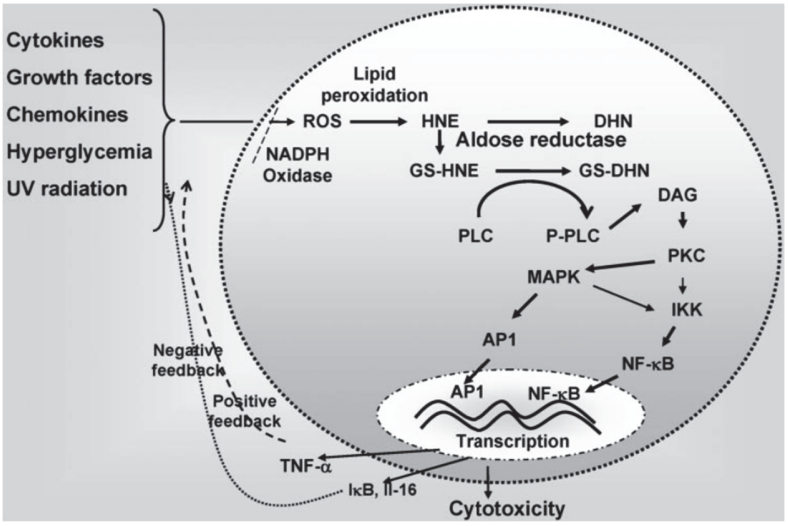

Figure 1. 9: Schematic representation of NF-kB activation. The increases of DAG concentration inside the cells, due to hyperglycemic conditions, leads to PKC activation. PKC inactivates IKK leading to NF-*k*B activation and migration into the nucleus where it binds the DNA (taken from Srivastava *et al.,* 2005). Abbreviation: IKK (I*k*B kinase).

Exposure of cultured vascular smooth muscle cells isolated from rat aorta to high glucose induces an increase of PKC activation and DAG formation. Treatment of these cells with AKR1B1 inhibitors (*Tolrestat* and *Sorbinil*) or AKR1B1 ablation decreases both PKC activation and DAG formation (Ramana *et al*., 2005). The same results were observed in the human lens epithelial cell line B-3, treated with both *Sorbinil* or *Tolrestat.* Inhibition of AKR1B1 attenuated TNF-alpha and hyperglycemia-induced PKC and NF-*k*B activation (Ramana *et al.,* 2003). The effect of AKR1B1

inhibition in the reduction of NF-*k*B activity was also recently demonstrated in human leukemic cells treated with artichoke leaf extract, containing AKR1B1 inhibitors (Milackova *et al.,* 2017).

1.5 "Classic" AKR1B1 inhibitors

Because of AKR1B1's implication in the onset of diabetic complications, it has for several years been a target for inhibition as a possible treatment (Grewal *et al.,* 2016).

The first AKR1B1 inhibitor (ARI) studied was 3,3-tetramethyleneglutaric acid, discovered due to the affinity of AKR1B1 for long-chain fatty acid substrates. The first inhibitor used in a clinical trial against the onset of diabetic neuropathy was *Alrestatin* in 1981. In the following years, other inhibitors were tested such as *Sorbinil*, *Ponalrestat* and *Tolrestat* (Krans, 1992). Today, the only ARI commercially available, and clinically used in Japan, is *Epalrestat* which has been shown to have positive long-term effects on the treatment of diabetic neuropathy (Hotta *et al.,* 2006). Despite the positive results obtained in *in vitro* experiments (Grewal *et al.,* 2016.), the use of these inhibitors in clinical trials was often associated with severe side effects, such as hypersensitivity reactions characterized by fever, skin rash and myalgia.

All the ARIs so far described can be divided in three groups; the first includes compounds containing cyclic imides such as the spirohydantoins, like *Sorbinil* and *Fiderestat* (Del-Corso *et al.,* 2008). *Sorbinil* is one of the most studied ARI that is used for clinical and *in vitro* studies. It was discovered in 1978 and subsequently its interaction with the enzyme was studied through crystallographic analysis of the enzyme-inhibitor complex (Urzhumtsev *et al.,* 1997). Another compound containing cyclic imides that has been tested as an ARI is *Fidarestat*, which unlike *Sorbinil* does not cause any side effects in patients and has an inhibitory potency ten times higher than *Sorbinil*. It counteracts the development of diabetic retinopathy and decreases the concentration of sorbitol in erythrocytes of diabetic patients (Asano *et al.,* 2002).

Carboxylic acid derivatives form a second group of ARIs. A problem with these compounds is their low bioavailability, meaning that despite the high affinity toward AKR1B1 observed in *in vitro* experiments, they have less efficacy as ARIs in *in vivo* experiments. One of the compounds of this group, *Ponalrestat,* is very effective *in vitro* but has not been promising in clinical trials for diabetic neuropathy. *Epalrestat,* previously mentioned, belongs to the carboxylic acid derivatives group.

The third group of ARIs includes molecules isolated from natural sources, which are not always as well characterized for their chemical structure, but only for their capability to inhibit the enzyme. Plants, flowers and vegetables are the most common sources of ARIs even though ARIs have been isolated even from marine organisms and microorganisms (De la Fuente and Manzanaro, 2003). Usually ARIs isolated from natural sources are flavonoids and other phenolic compounds, terpenoids, alkaloids, coumarins and tannins (Grewal *et al.,* 2016). Different compounds, such as phenolic compounds and anthocyanins were isolated from an ethanol extract of purple corn, *Zea mays* L. (Kim *et al*., 2013). Other two promising compounds, 2-(4-hydroxy-3-methoxyphenyl)ethanol and 2-(4-hydroxy-3methoxyphenyl)ethanoic acid, were isolated from a water extract of ginger (*Zingiber officinale* Roscoe) and tested not only *in vitro* as ARIs but also *in vivo* on the accumulation of sorbitol in human erythrocytes and of galactitol in the lens of galactose-fed rats with promising results (Kato *et al.,* 2006). From a methanolic extract of *Perilla frutescens,* rosmarinic acid was isolated and characterized as a potent ARI in *in vitro* experiment (Peak *et al*., 2013). More recently, the flavonoid quercetin 3-*O*-β-D-glucuronopyranoside, isolated from *Salsola soda* buds, has been identified and characterized as a potent ARI (Iannuzzi *et al.,* 2020).

1.6 Differential inhibitors of AKR1B1

The failure of ARIs in clinical trials may be at least partly due to the multiple functions that AKR1B1 has inside cells beside glucose reduction and generation of a pro-inflammatory signal. Other potential roles include involvement in osmoregulatory processes (Burg, 1995), in the metabolism of corticosteroids and tetrahydrobiopterin (Hirakawa *et al.,* 2009; Endo *et al.,* 2009) and, as outlined above, in the detoxification of hydrophobic aldehydes. ARIs so far described inhibit the activity of the enzyme towards multiple substrates, possibly causing the loss of its beneficial effects. Despite its ability to act on structurally very different substrates, such as aldoses and alkanals/alkenals, AKR1B1 cannot be considered a permissive enzyme (Del Corso et *al.*, 2013). This is clear from the comparison of specificity constants measured toward substrates belonging to different classes (i.e. hydrophylic aldoses and hydrophobic alkanals) (Balestri et *al.*, 2017). For both classes of substrates, significant differences were observed in the efficiency of the enzyme to catalyze their reduction, suggesting that a special recognition pattern must occur both for aldoses and for hydrophobic substrates. These patterns should be specific for each substrate

typology, thus making possible to hypothesyze the action of differential inhibitors. Indeed, recent molecular modeling evidence (Balestri et *al*., 2020) clearly indicate the occurrence of different modes of interactions for L-idose, HNE and GSHNE on the AKR1B1 active site.

Thus, development of differential AKR1B1 inhibitors (ARDIs) may be able to inhibit the enzyme activity towards hydrophilic, or partially hydrophilic substrates (i.e. aldoses and GSHNE), with no or limited inhibition of activity towards hydrophobic substrates (i.e. alkenals and alkanals) (Del-Corso et *al.*, 2013). Such ARDIs would block sorbitol accumulation and GSDHN formation, which are considered the damaging events for the cells, without affecting the detoxifying activity of the enzyme linked to HNE and other alkenals/alkanals reduction. The model represented in Fig. 1.10 shows the action of an ARDI (acting as a competitive inhibitor) which binds to free AKR1B1 competing with glucose. However, HNE may still bind and be reduced, even in the presence of the inhibitor (Cappiello *et al.,* 2020).

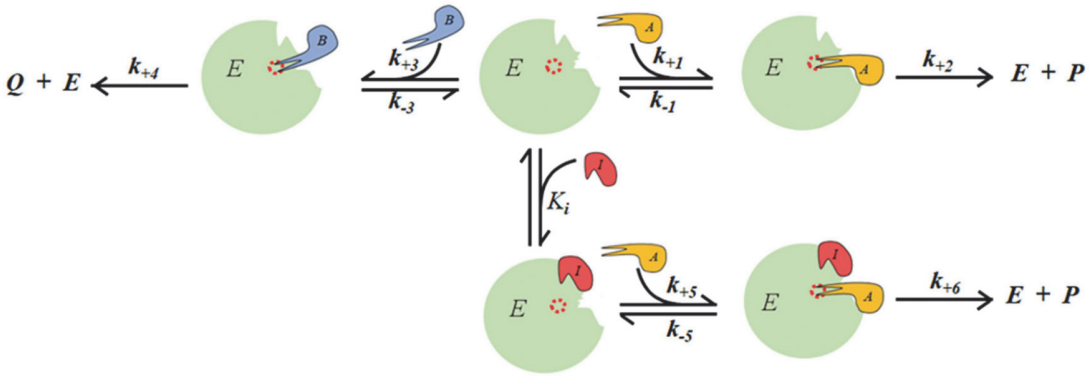

Figure 1. 10: Competitive model of action of an ARDI. The inhibitor I acts as an ARDI and binds to the free form of AKR1B1 competing with the substrate B (i.e. glucose) but not with the substrate A (i.e. HNE). When $k_{+6} = k_{+2}$ the inhibitor acts as "complete" ARDI. In this figure, different kinetic constants k_{+1}, k_{-1}, k_{+2} k_{+3}, k_{-3}, k_{+4}, k_{+5}, k_{-5} and k_{+6} are related to the formation and dissociation of all the complex EB and EA; K_i represent the dissociation constant of the EI complex. (taken from Cappiello *et al.,* 2020).

The relative rate equations and Hanes-Wolff plots for the reduction of glucose and HNE, when simultaneously present with the enzyme, are reported in Fig. 1.11A and 1.11B, respectively. It is predicted that the presence of an ARDI decreases the rate of reduction of glucose and increases the formation rate of HNE, due to the removal of the competing effect of glucose towards HNE. A decrease of the $^{app}K_M$ for HNE and the increase of the $^{app}K_M$ for glucose along with the increase of ARDI concentration is also shown.

The scheme of Fig. 10 also allows for the possibility that the inhibitor may act as an incomplete ARDI, i.e. that may be able to bind also to substrate A and the consequent ternary complex may evolve to product with $k_{+6} < k_{+2}$. In this case the differential effect is progressively reduced along with the increase in difference between k_{+2} and k_{+6}.

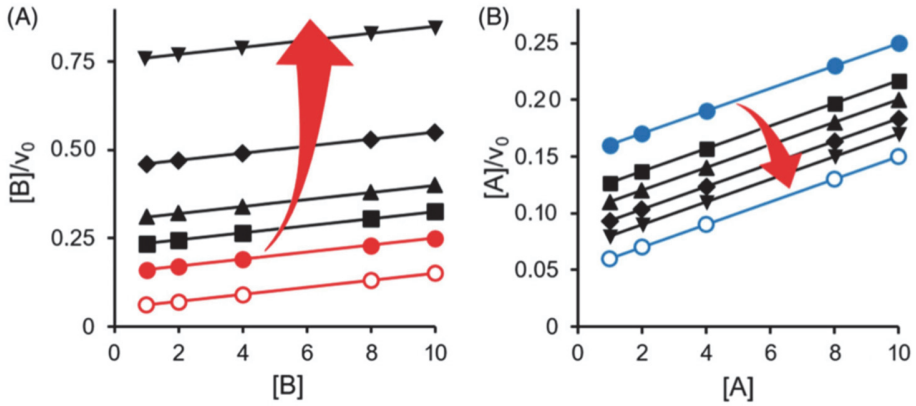

Figure 1. 11: Predictable effect of an ARDI on the transformation of glucose and HNE. The kinetic behavior is described by the model reported in Fig.10 with the two substrates displaying the same K_M and the same k_{cat} and is represented by the Hanes-Wolff plot. **Panel A:** the transformation of glucose (B) in the presence of both HNE (A) and an ARDI (I). The Hanes-Woolf plot indicates the dependence of the reaction rate on glucose concentration in the absence (red open circle) or in the presence (red closed circles) of HNE at a concentration equal to $2K_M$ respectively. Symbols ■, ▲, ♦ and ▼ refer to red closed circles in the presence of ARDI equal to 1,2,3 and 5 times the K_i value, respectively. The K_i value is considered as $K_M/10$. **Panel B:** the reduction of the HNE (A), which is not influenced by the presence of the inhibitor. Blue open and closed circles refer to HNE alone and in the presence of glucose (B) at a concentration equal to $2K_M$ value, respectively. Symbols ■, ▲, ♦ and ▼ refer to red closed circles in the presence of ARDI equal to 1,2,3 and 5 times the K_i value, respectively. The K_i value is considered as $K_M/10$. In panels A and B, the increase in [I] is emphasized by the red arrows (taken from Cappiello et al., 2020).

A model for ARDI acting on glucose with an uncompetitive mechanism of action (Fig. 1.12) indicates how incomplete ARDI action will result. In fact, even though the inhibitor does not affect the reduction of HNE, the formation of the ternary complex with glucose reduces the concentration of the free form of the enzyme and thus the velocity of product formation (v_p).

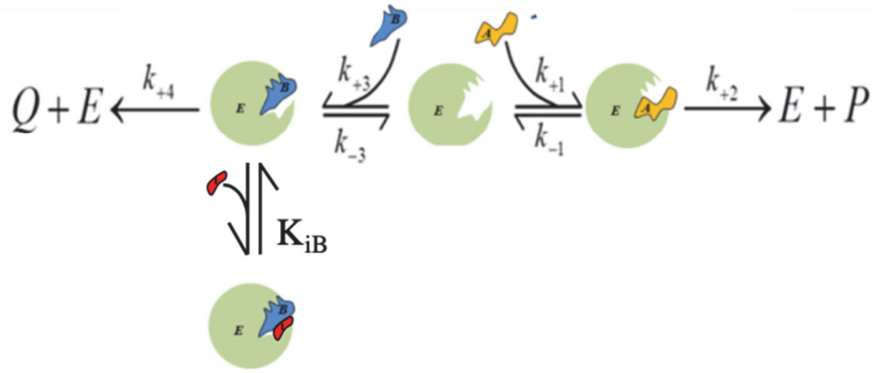

Figure 1. 12: Uncompetitive model of action of an ARDI. The inhibitor I acts as an ARDI and binds only to the enzyme-substrate B (i.e. glucose) complex. In this figure, different kinetic constants k_{+1}, k_{-1}, k_{+2} k_{+3}, k_{-3} and k_{+4}, are related to the formation and dissociation of all the complex. K_{iB} represent the dissociation constant of the EBI complex. (taken and modified from Cappiello *et al.,* 2020).

The relative rate equations for the reduction of glucose (substrate B) and HNE (substrate A), are shown in Fig. 1.13A and 1.13B. The resulting differential inhibition will depend on the different kinetic parameters of the reactions for the two substrates. In this case, the inhibitor can bind only the EB complex. The conversion of substrate B is affected both in terms of V_{max} as a result of the inhibitor action and in terms of apparent K_M as a result of the combined action of both the inhibitor and substrate A.

$$v_p = \frac{k_{+2}E_T[A]}{K_A\left[1+\frac{[B]}{K_B}\left(1+\frac{[I]}{K_{iB}}\right)\right]+[A]}$$

A

$$v_q = \frac{k_{+4}E_T[B]/\left(1+\frac{[I]}{K_{iB}}\right)}{K_B\left(1+\frac{[A]}{K_A}\right)/\left(1+\frac{[I]}{K_{iB}}\right)+[B]}$$

B

Figure 1. 13: Kinetic equations for the transformation of two substrates in the presence of an uncompetitive ARDI. Panel A. Kinetic equation of the transformation of substrate A (i.e. HNE) as represented in the scheme of Fig. 12. K_A is the Michaelis constant for substrate A, i.e. $(k_{-1} + k_{+2})/k_{+1}$. **Panel B.** Kinetic equation of the transformation of substrate B (i.e. glucose) as represented in the scheme of Fig. 12. K_B is the Michaelis constant for substrate B, i.e. $(k_{-3} + k_{+4})/k_{+3}$ and K_{iB} is the dissociation constant for the ternary complex EIB.

1.7 Aldose reductase differential inhibitors from natural and synthetic sources

Screening of known ARIs was performed to test their possible ability to act as ARDIs (Del Corso, 2013). This preliminary study, allowing the identification of compounds able to exert a differential effect, confirmed the feasibility of the differential inhibitory approach. Indeed, this screen, while showing the inability of classical ARIs to act as ARDIs, highlighted molecules preferentially affecting aldoses reduction but also molecules preferentially affecting alkenals reduction. On the basis of those results, pyrazolo[1,5-a]pyrimidine derivatives have been synthetized and characterized for their ability to act as ARDIs (Balestri *et al*., 2018). This study led to the identification of 4-(4-chlorobenzyl)-7-oxo-4,7-dihydropyrazolo[1,5-a]pyrimidine- 6-carboxylic acid as able to preferentially inhibit L-idose and GSHNE reduction with respect to HNE reduction, with an observed maximum differential inhibition of approximately 16%. At the same time indications of the presence of ARDIs in natural extracts were obtained (Balestri *et al*., 2017). In fact, the fractionation of methanolic extracts of "costoluto fiorentino" tomato (*Solanum lycopersicum*), "black" cabbage (*Brassica oleracea* var. *sabellica*) and Zolfino beans (*Phaseolus vulgaris*) revealed the presence of components with a significant differential inhibition. Further studies demonstrated that Soyasaponins Bb isolated from Zolfino beans contributed to the observed differential inhibitory effect (Balestri *et al.*, 2019). As for the synthetic ARDI studied to date, Soyasaponin Bb did not result a complete ARDI; indeed, the IC_{50} measured for HNE reduction was two-fold higher than that for L-idose reduction. Also, green tea appeared to be a promising source of ARDIs; its fractionation revealed the presence of several components able to preferentially affect L-idose reduction with respect to HNE (Balestri *et al.,* 2020). Indeed, epigallocatechin gallate and gallic acid, responsible at least in part for this effect, have been characterized through both kinetic and molecular modelling approaches.

2. AIM OF THE THESIS

The aim of this thesis is to identify, from both natural and synthetic sources, aldose reductase inhibitors that differentially inhibits towards various substrates, potentially useful to counteract polyol accumulation and inflammation associated to hyperglycemic conditions while leaving unaffected the ability of the enzyme to remove lipid peroxidation deriving toxic aldehydes.

3. EXPERIMENTAL PROCEDURES

3.1 Reagents

Sodium phosphate monobasic, ammonium sulfate, sodium hydroxide, sodium chloride (*J.T. Baker*); EDTA (*Juoro*); Protease inhibitor cocktails (PIC) (*ICN)*; NADPH, L-idose; 2-methoxyestradiol (*Carbosynth*); acetone, bovine serum albumin (BSA), D, L-glyceraldehyde (GAL), dithiothreitol (DTT), yeast extract, tryptone, phosphate buffered saline (PBS), kanamycin, polyethylenimine(*Sigma Aldrich*); acrylamide, N, N'-methylene-bis-acrylamide, Biorad protein solution (*Bio*R*AD Laboratories*); tris(hydroxymethyl)aminomethane, glycerol (*BDH*); DEAE Sepharose, DE-52 (*Whatman*); Matrex Orange A (*Millipore Amicon*); Sephadex G 75 (*GE Healthcare*); Bond Elut C18 (*UCT)*; pregnenolone sulfate sodium salt (*Cayman Chemical Company*); leucoside (*PhytoLab*); isopropyl ß-D-1-thiagalactopyranoside (IPTG) (*Inlac*); methanol (*Honewell I Riedel-de Haen*); puromycin dihydrocloride (Biochemica); human recombinant tumor necrosis factor alpha (*hr*TNF-alpha) (*R& D System Biotechne brand*); Minimum Essential Medium Eagle (MEM), fetal bovine serum (FBS), penicillin, streptomycin, gentamycin, hygromicyn (*Euroclone*); Bio-Glo™ Luciferase Assay reagent, Passive Lysis Buffer, FuGENE® HD Trasfection Reagent, pRL-SV40 (pRenillaLuc), Luciferase Assay System, Dual Luciferase Reporter Assay System, pGL4.32/luc2p/NF-*k*B-RE/Hygro-vector (pFireflyLuc2P), QuantiLum® Recombinant Lyciferase and BamHI (*Promega*); DNA Ladder (*Methabiom mi-E8201*); NheI, XbaI, NEBuffer 2 and BglII (*BioLabs*); T4 DNA ligase and T4 DNA Ligase Buffer (NEBiolabs); agarose powder (*RPI research products International*); Ro 61-8048, bicatulamide (CDX) (*MedChemExpress*). QIAEX II® Gel Extraction Kit (*QIAGEN*). *Human Recomunbinant* TNF-alpha (*hr*TNF-alpha) (*R&D System a biotechne brand)*; Hygromycin (*ThermoFisher*)*;* Duo-Luciferase Assay Kit 2.0 (*GeneCopoeia*). Dry seeds of yellow *Zolfino* beans were obtained from farm Agostinelli Mario in Leccio-Reggello (Florence, Italy) and authenticity was confirmed by comparing their features with those registered in the "Regione Toscana" germplasm data bank (access VE_027). The plasmid p5XIP10kB containing 5 copy of NF-*k*B response element was a gift from Professor Ronald Wek Indiana University School of Medicine. The plasmid pCDN3HA was a gift from Professor A. DePaoli-Roach, Indiana University School of Medicine, The Library of Pharmacologically Active Compounds (LOPAC). The Library of Pharmacologically Active

Compounds (LOPAC^{1280TM}, Lot # LO1280/LO3300) containing 1280 compounds was purchased from Chemical Genomics Facility at Purdue University, Indianapolis. K

3.2 AKR1B1 activity assay

The spectrophotometric measurements were performed with a Beckman DU-640 spectrophotometer. AKR1B1 activity was measured at 37°C, following the decrease in absorbance at 340 nm due to NADPH oxidation (ε_{340}=6.22 $mM^{-1}cm^{-1}$). The standard assay mixture (700 µl final volume) contained 0.25 M sodium phosphate buffer pH 6.8, 0.38 M ammonium sulfate, 0.47 mM EDTA, 0.18 mM NADPH, 4 mM GAL and proper amounts of the enzyme. The decrease in absorbance at 340 nm measured in the absence of the substrate was subtracted. One Unit of enzyme activity is the amount of enzyme able to convert 1 µmol of substrate/min under the above conditions.

These assay conditions were also adopted when L-idose, HNE and GSHNE were used as substrates. The kinetic analysis of the experimental rate measurements with different substrates in the presence of inhibitors was performed on the classical inhibition model of action. Data were analyzed by Hanes-Woolf plots. The apparent dissociation constants $^{app}K_i$' (for the ESI complex) and $^{app}K_i$ (for the EI complex) were determined from secondary plots of $1/^{app}V_{max}$ and $^{app}K_M/^{app}V_{max}$ as a function of the inhibitor concentration, respectively.

For the assay conditions adopted for the high throughput screen, see section 3.9.

3.3 Expression of Human Recombinant Aldose Reductase

The pET-30 vector, containing the sequence encoding human AKR1B1, was used to transform BL21 (DE3) pLysS *E. coli* cells. BL21 cells were incubated with the pET-30 vector for 1 h on ice, followed by heat shock treatment for 60 seconds at 42°C and then cooled on ice for 5 minutes. Luria-Bertani (LB) medium (10 g/l tryptone, 5 g/l yeast extract and 10 g/l NaCl) was added to the cells and further incubated at 37°C for 1 h. Transformed cells were grown overnight (O.N.) at 37°C in LB medium supplemented with 30 µg/ml kanamycin. When the culture had reached an absorbance of 0.8 at 600 nm, 4 mM IPTG was added and the cells were left to grow O.N. at 37°C under stirring. Cells were then centrifugated at 1880 *xg* for 30 min at 4°C. The resulting pellet

was resuspended with 10 mM sodium phosphate buffer pH 7 (standard buffer) supplemented with 0.1 mM EDTA, 2 mM DTT and 4 μg/ml of PIC. The suspension was frozen and thawed two times, sonicated for 30 sec with 1 min intervals for 10 times and then centrifuged at 10700 *xg* for 30 min at 4°C. The supernatant, which contained the expressed protein in soluble form, is referred to as the crude extract.

3.4 Purification of recombinant AKR1B1

The whole procedure was conducted at 4°C. An aliquot of the crude extract (22.5 ml, 13.7 mg/ml of protein) was applied to a DE52 column (22 x 3.5 cm), previously equilibrated with standard buffer containing 0.1 mM EDTA and 2 mM DTT, and eluted with the same buffer at a flow rate of 15 ml/h, collecting fractions of 3.7 ml. Once the absorbance at 280 nm reached baseline values, a linear gradient from 0 to 120 mM of NaCl in standard buffer containing 0.1 mM EDTA and 2 mM DTT was applied. Each fraction (3.7 ml) was tested for AKR1B1 activity; the ones showing enzymatic activity were pooled and dialyzed against standard buffer containing 0.1 mM EDTA, using a YM10 Amicon ultrafiltration membrane, in order to obtain final NaCl and DTT concentrations of 3 and 0.066 mM, respectively.

The pool (Pool DE52) was applied to an Orange Matrex column (17 x 3.5 cm) previously equilibrated with standard buffer containing 0.1 mM EDTA and eluted at 15 ml/h with the same buffer. Once the absorbance at 280 nm reached baseline values, the elution was performed with standard buffer containing 0.1 mM EDTA and 0.1 mM NADPH. Each fraction (3.7 ml) was tested for AKR1B1 activity; the ones showing enzymatic activity were collected in a pool and concentrated to approximately 6 ml with an YM10 membrane.

The resulting pool (Pool Matrex) was applied to a Sephadex G75 column (69 x 2.6 cm), previously equilibrated with standard buffer containing 2 mM DTT and eluted with the same buffer at a flow rate of 15 ml/h. The collected fractions (3.7 ml) were tested for the AKR1B1 activity and the ones showing enzymatic activity were pooled and concentrated to a final protein concentration of approximately 0.7 mg/ml using an YM10 membrane.

AKR1B1 activity and protein concentration of each pool are reported in Table 3.1.

The final protein preparation was electrophoretically homogeneous, as judged by SDS-PAGE with Coomassie blue-staining (Fig. 3.1). The purified enzyme was stored at -80°C in standard buffer containing 2 mM DTT, 0.1 mM EDTA and 33% (w/v) glycerol. Before enzymatic assays, if not

otherwise stated, the purified enzyme was extensively dialyzed at 4°C against standard buffer using an Amicon YM10 membrane and-stored at +4°C for no more than 5 days.

Step	Volume (ml)	Enzymatic concentration (U/ml)	Total Units	Protein concentrations (mg/ml)	Total protein	Specific Acitivity (U/mg)	Purification Factor	% yield
C. E.	22.5	17.5	393.9	13.2	296.3	1.3	1.0	100
DE-52 Pool	26.0	13.2	343.5	2.1	55.9	6.1	4.6	87.2
Matrex Pool	25.0	9.4	234.0	1.6	40.0	5.8	4.4	59.4
G75 Pool	47.0	4.0	188.9	0.7	31.0	6.1	4.6	47.9

Table 3. 1 AKR1B1 purification Table. For each purification step, starting from the crude extract (C.E.), volume (ml), enzymatic concentration (expressed as U/ml), total enzyme units, protein concentration (mg/ml), total protein (mg), AKR1B1 specific activity (U/mg), purification factor and percent yield are reported.

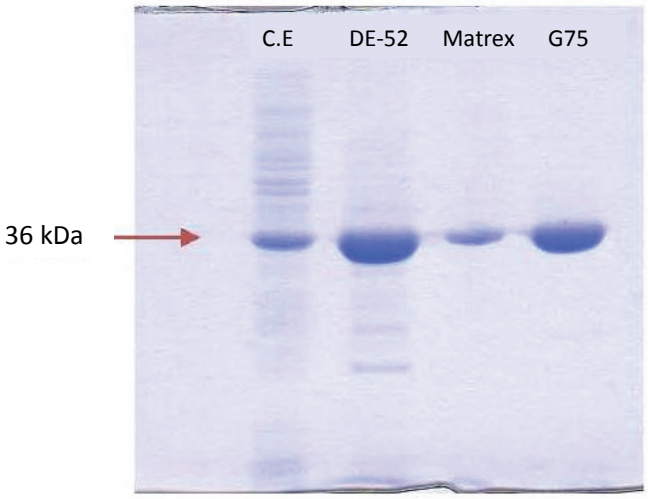

Fig. 3. 1: DISC-SDS-PAGE. Electrophoretic gel of the C.E., the DE-52 pool (DE-52), the Matrex Pool (Matrex) and the G75 Pool (G75). For each sample 10µg of protein was loaded.

3.5 Preparation of HNE and GSHNE

HNE was synthetized by Prof. F. Bellina, Department of Chemistry, University of Pisa as described (Balestri et al. 2019) and stored in hexane at -80°C in the form of dimethylacetal. Before use, HNE aliquots, after evaporation of hexane under nitrogen current, were dissolved in 1 mM

HCl and left under agitation on ice for 30 minutes. HNE concentration was evaluated measuring the absorbance at 224 nm, using an extinction coefficient of 13.75 mM^{-1} cm^{-1}.
GSHNE was prepared by incubating GSH and HNE (1.5:1 molar ratio) and monitoring the time course of GSH consumption.

3.6 Preparation of Zolfino beans extract

Zolfino beans were soaked (30 g/60 ml) overnight at 25°C in milliQ water under mild agitation. The supernatant was heated for 2 h at 100°C and then centrifugated at 142000 *xg* for 1 h at 4°C, with a Beckman L8 50 M/E ultracentrifuge. The supernatant was filtered through a 0.22 μm filter (*Stericup,* Millipore Amicon) under vacuum; filtration was repeated under sterile conditions. The resulting sample, referred to as "Zolfino beans extract" was stored at -20°C in sterile vials.

3.7 Chromatographic separation of Zolfino beans extract

3.7.1 Ionic exchange chromatography

An aliquot (20 ml) of *a Zolfino* extract was applied to a DEAE Sepharose column (12.5 x 3 cm) previously equilibrated with 20 mM TRIS HCl buffer pH 7.4. The elution was performed at a flow rate of 20 ml/h, collecting fractions of 2 ml and monitoring the absorbance at 254 nm. After elution of material that did not bind the chromatographic support, a linear NaCl gradient from 100 to 300 mM in the equilibration buffer was applied. Collected fractions were tested for their ability to inhibit AKR1B1 activity.

3.7.2 Hydrophobic interaction chromatography

An aliquot (20 ml) of a *Zolfino* extract was applied to a hydrophobic interaction *Bond Elut* C-18 column (10 g resin), previously activated with 100% acetone, 100% methanol and milli Q water. The elution was performed at a flow rate of 20 ml/h, collecting fractions of 2 ml and using milli Q water, 25%methanol and 50%methanol as consecutive eluents. The elution was monitored by measuring the absorbance at 254 and 265 nm. Eluted fractions were stored at 4°C and tested within 3 days from collection; fractions eluted with 25% and 50% methanol were dried, using a SpeedVac concentrator and resuspended in 2 ml of milli Q water before testing.
The same conditions were used for the analysis with 8 ml C18 column, except for the flow rate which was set at 10 ml/h.

3.8 Mass Spectrometry analysis

Mass spectrometry analysis was performed by Professor A. Braca and Professor M. De Leo, Department of Pharmacy, University of Pisa.

High-performance liquid chromatography (HPLC)-photodiode array (PDA)/UV-electrospray ionization (ESI) -tandem mass spectrometry (MS/MS) analyses were performed using a Surveyor LC pump, a Surveyor autosampler, coupled with a Surveyor PDA detector, and an LCQ Advantage ion trap mass spectrometer (Thermo/Finnigan, San Jose, CA, USA) equipped with Xcalibur 3.1 software. Analyses were performed on a Synerfi Fusion-RP column (4.6 x 150 mm, 4µm). The samples were dried, resuspended in 150 µl of methanol and injected in the LC-MS using an injection volume of 20 µl. Column elution was performed using a gradient of methanol in water from 5 to 100% in 90 min. After use, the column was cleaned with 100% methanol for 15 minutes and then equilibrated with 5% methanol for 10 minutes.

The elution was performed at 0.8 ml/min with a splitting system 2:8 to the MS (160 µl/min) and the PDA (640 µl/min) detectors, respectively.

Each mass spectrum was registered using the ESI interface in negative mode, using the following parameters: capillary temperature, 270°C; capillary voltage, -16.0 V; sheath gas flow rate, 60.00 arbitrary units; auxiliary gas flow rate, 3.00 arbitrary units; spray voltage, 4.50 kV: scan interval, *m/z* 150-2000. N_2 was used both as sheath gas and auxiliary gas. The data obtained for the PDA were registered in a lambda interval between 200 and 600nm. Data were then analyzed using Xcalibur 3.1 software.

3.9 High throughput screen pilot assay

The high throughput screen (HTS) was performed using 384 well plates and a final volume of 50 µl/well. The absorbance at 340 nm was measured at 37°C using a *Spectramax i3X* Plate Reader (Molecular Devices). The correlation between measured absorbance at 340 nm and NADPH concentration was evaluated. Fifty µl of different NADPH concentrations (evaluated from their absorbance at 340 nm measured using a spectrophotometer, 1 cm path length glass cuvettes, and considering an extinction coefficient of 6.22 mM^{-1} cm^{-1}) were added to different wells and the absorbance measured at 340 nm (Fig. 3.2).

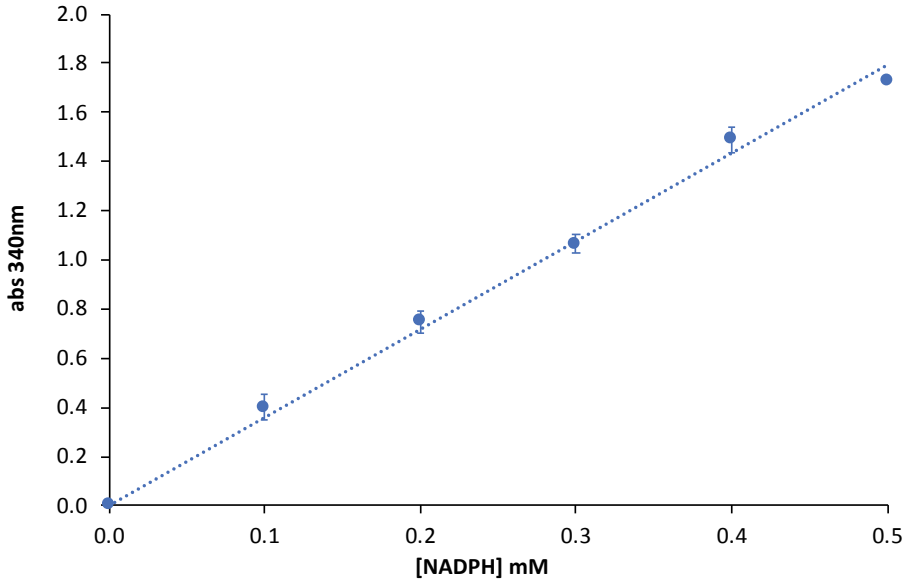

Fig. 3. 2: Correlation between NADPH concentration and absorbance at 340 nm in the 384 well plates. The absorbance at 340 nm of different concentration of NADPH was measured in a 384 well plate. Data are reported as the mean ± standard deviation (SD) of at least 3 measurements.

The NADPH concentration for measurements in the HTS was fixed at 0.3 mM (with a resulting absorbance around approximately 1.0); the concentrations of other assay components were the same as those used in the classical spectrophotometric assay, i.e. 0.25 M sodium phosphate buffer pH 6.8, 0.38 M ammonium sulfate and 0.47 mM EDTA. See Results Section (Paragraph 5.1) for the optimization of assay conditions in terms of both enzyme and substrate concentration. Kinetic measurements were performed collecting absorbance data every 90 sec for 22 min.

3.10 HTP screen of Library of Pharmacologically Active Compounds

The Library of Pharmacologically Active Compounds (LOPAC^{1280TM}) contains 1280 different molecules, including enzymes inhibitors, receptor ligands and approved drugs, which are known to exert different pharmacological actions. These compounds are reported to affect most signaling pathways and their classification on the basis of their targets is reported in Figure 3.3. The complete list of compounds included in LOPAC is reported in Appendix Table 1A.

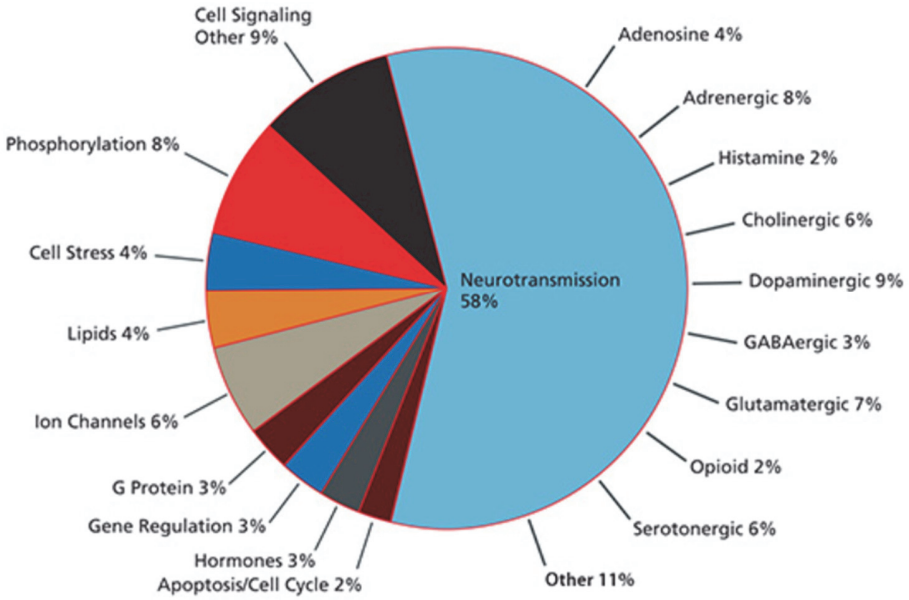

Fig. 3. 3: Classification of compounds present in LOPAC on the basis of the molecular target. (Imagine taken from https://www.sigmaaldrich.com/life-science/cell-biology/bioactive-small-molecules/lopac1280-navigator.html)

The four distinct 384 well plates (P1401, P1402, P1403 and P1404, for details see Appendix Table 1A) containing LOPAC were stored at -80°C. In each plate, wells of columns 1, 2 and 24 contained 10 µl of 2.5% DMSO; column 23 contained 10 µl of 5 µM Sorbinil in 2.5% DMSO; all other wells contained 10 µl of a 100 µM solution of different compounds in 2.5% DMSO.

The plates were thawed at room temperature for 20 min and then centrifuged at 1100*xg*, in a *Marathon 8K centrifuge (*Fisher Scientific*)*, for 1 min. The addition of the assay mixture (50 µl final volume) was performed using the liquid dispenser *Multiflo FX washer dispenser*. The optimization of assay conditions to define final concentration of each assay component is reported in Results Section paragraph 5.1.

After addition of the complete assay mixture the plate was centrifuged at 1100*xg*, for 30 seconds with the *Marathon 8K centrifuge* and then the absorbance at 340 nm was monitored. Kinetic measurements were performed collecting absorbance data every 90 sec for 22 min using the *Spectramax i3X* Plate Reader (Molecular Devices).

3.11 Evaluation of the quality of the HTS

The quality of the HTS was evaluated by measuring the Z' score, using the following equation (Zhang *et al*., 1999):

$$\mathbf{Z' = 1 - (3\sigma_1 + 3\sigma_2)/(|\mu_2 - \mu_1|)}$$

where σ_1 and μ_1 are the standard deviation and the average of the NADPH oxidation rate in the absence of the enzyme, respectively; σ_2 and μ_2 are the standard deviation and the average of the NADPH oxidation rate in the presence of the enzyme (i.e. 100% AKR1B1 activity), respectively.

3.12 Amplification of p5XIP10kB in DH5α cells

E. coli DH5α cells were thawed on ice and then incubated on ice for 2 min with 50 ng of the plasmid p5XIP10kB, which contains 5 copy of the NF-*k*B response element that controls the expression of Firefly Luciferase gene. Then 400 µl of Luria-Bertani (LB) medium (10 g/l tryptone, 5 g/l yeast extract and 10 g/l NaCl) was added and the suspension was incubated at 37°C for 45 minutes under shaking. The cells were quickly centrifuged, 200 µl of LB was removed and the cells were gently resuspended in the residual LB medium. Fifty and 100 µl of the cell suspension was transferred onto agar plates containing 30 ml of LB supplemented with 100 µg/ml ampicillin and 15 g/l agar and incubated overnight at 37°C. Isolated colony were picked and grown in a flask containing 10 ml of LB with 100 µg/ml ampicillin. The flasks were incubated O.N. at 37°C under agitation. The day after 850 µl of cell culture was supplemented with 150 µl of glycerol to create a glycerol stock and stored at -80°C. The rest of the 10 ml were used to isolate the plasmid using the miniprep kit QIAprep® Spin Miniprep Kit (250) form the QIAGEN. The obtained plasmid was digested using EcoRI (BioLabs, 20.000U/ml) and Buffer 2 (BioLabs) for 2h at 37°C and then run in a 1% agarose gel at 130V.

The purified plasmid was used for the transfection of the HEK-293 cells, see paragraph 13.

3.13 Transient transfection of Human embryonic kidney (HEK-293) cells and TNF-alpha effect

HEK-293 cells were plated in 12 well-plates (215,000 cells/well) and after 24 h at 37°C were transfected using the polyethylenimine and the proper plasmids. The pCDNA3HA (1 µg/well) was

used as an empty plasmid for transfect control cells; pRenillaLuc (0.35 μg/well), which express Renilla Luciferase under the control of a constitutive promoter, and p5XIP10kB(0.75 μg/well) were used for the expression of the Renilla and Firefly Luciferase, respectively. The cells were treated with three concentration (2 ng/ml, 5 ng/ml and 10 ng/ml) of rhTNF-α for 4h at 37°C.
Then the cells were lysate using the 1X Passive Lysis Buffer; the lysates were centrifuged at 14000*xg* at 4°C. The supernatant was analyzed for Renilla and Firefly Luciferase expression according to the manufacturing of the Duo-Luciferase Assay Kit 2.0 and the luminescence was measured using the Turner Biosystem 20/20^{n} Luminometer.
The statistical analysis was performed using a standard statistical software using the One-Way ANOVA (and Nonparametric or Mixed) carried out with Graphpad Prism Version 8.4.3.

3.14 Preparation of empty plasmid

The pRenillaLuc and the pFireflyLuc2P, which contains 5 copies of an NF-*k*B response element that drives transcription of the luciferase reporter gene *luc2P* (*Photinus pyralis*), plasmids were incubated with specific restriction enzymes in order to remove the Renilla Luciferase and the Firefly Luciferase genes from the corresponding plasmids. The digested plasmids were loaded on an 0.8% agarose gel, prepared in tris acetate buffer 0.04 M supplemented with 1mM EDTA (TAE Buffer), and then run at 90 V using as a running buffer the TAE Buffer with 2 mg/ml ethidium bromide. The bands in the agarose gel containing the empty plasmids were extracted using the QIAEX II® Gel Extraction Kit. The obtained linear plasmids were then ligated using the T4 DNA ligase and the T4 DNA Ligase buffer. The structure of both the original and empty plasmids (pNO-Renilla and pNO-FireflyLuc2P) are shown in Appendix A, Fig. 1A, 2A, 3A and 4A.

3.15 Amplification of pRenillaLuc, pFireflyLuc2P and empty plasmids in XL-1 cells

E. coli XL-1 cells were thawed on ice and then separately incubated with 50 ng of each of the following plasmids: pNO-Renilla, pNO-FireflyLuc2P, pRenillaLuc and pFireflyLuc2P. The cells were then left on ice for 1 hour and then incubated at 42°C for 1 min and then for 5 min on ice. Then 300 μl of LB medium was added and the cells were incubated for 1 hour at 37°C. The cells were spin down quickly, 200 μl of LB was removed and the cells were gently resuspended in the residual LB medium. Fifty μl and 100 μl of the cell suspension was transferred into plates

containing 15 ml of LB supplemented with 100 µg/ml ampicillin and 15 g/l agar and incubated overnight at 37°C. Isolated colony were collected and added to 10 ml of LB containing 100 µg/ml ampicillin. The tubes were left O.N. at 37°C under agitation. Then 850 µl of cell culture was supplemented with 150 µl of glycerol to create a glycerol stock of transformed cells and stored at -80°C. The residual suspension was centrifuged at 5000*xg* at 4°C. The pellet was used to isolate the plasmid using the miniprep kit EuroGOLD Plasmid Miniprepr Kit I. The concentration of the plasmids was evaluated using the absorbance at 260 nm, taking into account that a 50 µg DNA/ml solution has an absorbance of 1.0 at 260 nm. The ratio of $A_{260/280}$ was measured; values higher than 1.8 indicates plasmids purity > 90%.

3.16 Human Lens Epithelial cells (HLEC) transient transfection and TNF-alpha effect

HLEC were plated in 12 well-plates (80,000 cells/well) in MEM containing 20% FBS, 1% penicillin/streptomycin and 1% glutamine and incubated at 37°C with 5% CO_2 O.N. Then the medium was removed and replaced with MEM containing 0.5% FBS, 1% glutamine and 50 µg/ml of gentamycin. The cells were then transfected using the FuGENE® HD Transfection Reagent (in a 3:1 v:v ratio with respect to plasmid) and the following plasmids: the pRenillaLuc (0.35 µg/well) and the pFireflyLuc2P (0.75 µg/well) for the cells which express the Renilla and the Firefly luciferase, respectively. For the control cells two empty plasmids were used: pNO-Renilla (0.35 µg/well) and pNO-FireflyLuc2P (0.75 µg/well).

After 24 h the cells were treated with 0.2 nM of either hTNF-alpha or human serum albumin (HAS) for 24h. The cells were washed with a phosphate buffer solution containing 0.8 g/l monobasic sodium phosphate, 0.115 gr/l dibasic sodium phosphate and 0.02 gr/l potassium chloride, supplemented with 1 mM phenylmethylsulfonyl fluoride. Then the cells were lysate using the 1X Passive Lysis Buffer; the lysates were collected and centrifuge at 14000*xg* at 4°C. The supernatant was analyzed for Renilla and Firefly Luciferase expression using the Dual Luciferase® Reporter Assay System using the FluoSTAR Omega luminometer.

The statistical analysis was performed using a standard statistical software using the t- Tests (and Nonparametric tests) carried out with Graphpad Prism Version 8.4.3.

The correlation between measured luminescence and Firefly Luciferase concentration was evaluated. Different concentration of a commercially available Firefly Luciferase (QuantiLum®

Recombinant Lyciferase) were used to evaluate the linearity of the luminescence using the Luciferase Assay System and the FluoSTAR Omega luminometer (Fig. 3.4).

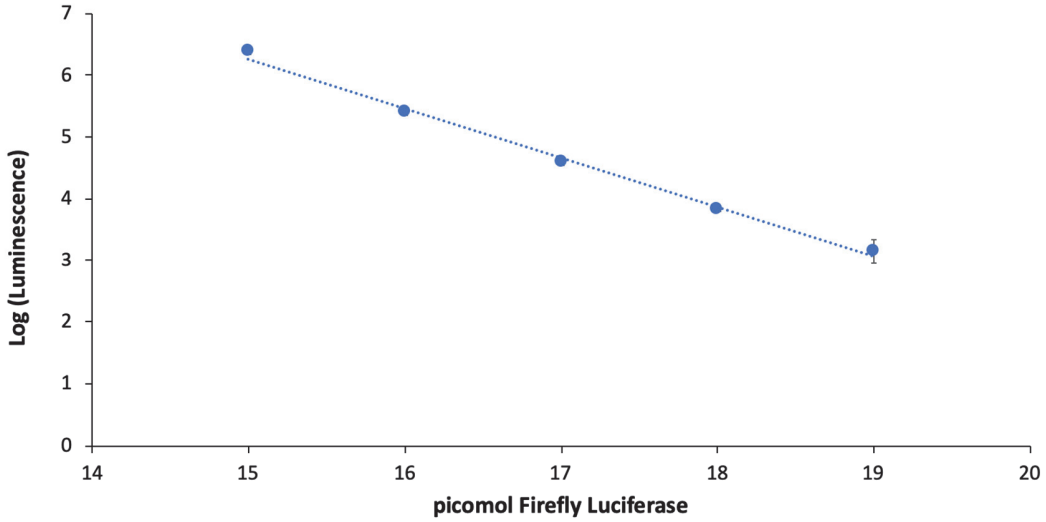

Fig. 3. 4: Correlation between mol of Firefly Luciferase and luminescence. The logarithm of the luminescence of different concentration of Firefly Luciferase was measured in a 384 well plate. Data are reported as the mean ± standard deviation (SD) of at least 3 measurements.

3.17 HLEC stable transfection and TNF-alpha experiment

HLEC were plated in 6 -35mm ($3.0x10^5$ cells/well) in MEM containing 20% FBS, 1% penicillin/streptomycin and 1% glutamine and incubated at 37°C with 5% CO_2 O.N. The cells were washed 2 times with MEM containing 10% FBS, 1% penicillin/streptomycin and 1% glutamine. Then 1 ml of the same medium was added in each plate. The cells were then transfected using the FuGENE® HD Transfection Reagent (in a 3:1 v:v ratio with respect to plasmid) and the following plasmids: the pRenillaLuc (0.4 µg/well) and the pFireflyLuc2P (2 µg/well) for the cells which express the Renilla and the Firefly luciferase, respectively. For the control cells the two empty plasmids were used: pNO-Renilla (0.4 µg/well) and pNO-FireflyLuc2P (2 µg/well).

After 48 h the cells were detached using 0.5 ml of a 0.05% trypsin/0.02% EDTA solution. The cells were then transferred in 6-60 mm plates and incubated at 37°C O.N. Then the mediium was replaced with MEM containing 20% FBS, 1% penicillin/streptomycin, 1% glutamine and 100µg/ml of hygromycin and incubated at 37°C. At this point all the cells that were not transfected started dying the only cells that kept growing were the transfected cells.

The obtained stably transfected cells were plated in 4-12 well-plates (80,000 cells/well) in MEM containing 20% FBS, 1% penicillin/streptomycin and 1% glutamine and incubated at 37°C O.N. Then the medium was replaced with MEM containing 0.5% FBS, 1% glutamine, 50 µg/ml of gentamycin and 100 µg/ml of hygromycin. Then cells were treated with 0.2 nM of either hTNF-alpha or HAS for 24 h. The cells were washed with a phosphate buffer solution containing 0.8 g/l monobasic sodium phosphate, 0.115 gr/l dibasic sodium phosphate and 0.02 gr/l potassium chloride, supplemented with 1 mM phenylmethylsulfonyl fluoride. Then the cells were lysate using the 1X Passive Lysis Buffer; the lysates were collected and centrifuged at 14000*xg* at 4°C. The supernatant was analyzed for Firefly Luciferase expression using the Luciferase Assay System using the FluoSTAR Omega luminometer.

The statistical analysis was performed using a standard statistical software using the t- Tests (and Nonparametric tests) carried out with Graphpad Prism Version 8.4.3.

3.18 Cells viability

HLEC were plated in 24 well-plates (40,000 cells/well) in MEM containing 20% FBS, 1% penicillin/streptomycin and 1% glutamine. The cells were incubated at 37°C with 5% CO_2 for 48 h. The medium was then removed and MEM containing 0.5% FBS, 1% glutamine and 50 µg/ml gentamycin was added. Different concentrations of the inhibitors, dissolved in DMSO were added to the plates in order to have a final DMSO concentration of 0.1% and left for 24 and 48 h. Cells viability was measured using crystal violet assay (Feoktistova *et. al.*, 2016).

The statistical analysis was performed using a standard statistical software using the One-Way ANOVA (and Nonparametric or Mixed) carried out with Graphpad Prism Version 8.4.3.

3.19 Other methods

Protein concentration was determined by the Bradford method (Bradford, 1976) using BSA as a standard protein. SDS-PAGE was performed according to Laemmli (Leammli, 1970) and gels were stained with Coomassie Blue.

4. RESULTS

4.1 Inhibitory effect of the *Zolfino* crude extract

A *Zolfino* bean extract was prepared as described in paragraph 3.6 of the Experimental procedures paragraph; its spectrum is shown in Fig. 4.1

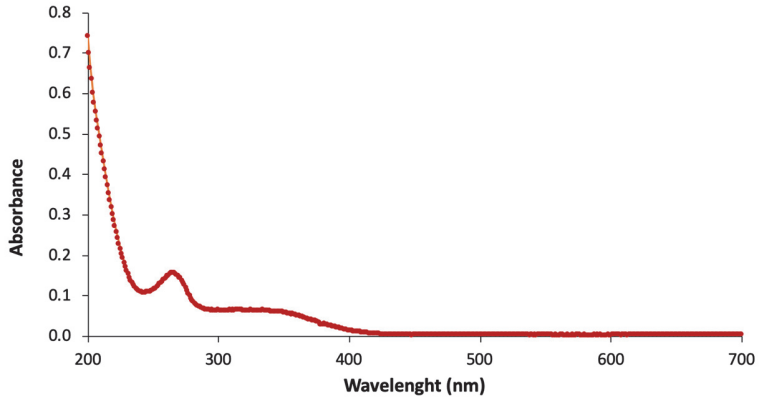

Figure 4. 1: Absorption spectrum of a thermally treated *Zolfino* beans extract. The spectrum was performed after diluting the extract 1:100 in milli Q eater and was recorded immediately after preparation.

As expected (Balestri et *al.,* 2016), the extract displayed a marked inhibitory effect on AKR1B1 (Fig. 4.2). However, no differences were observed in the inhibition measured using L-idose as substrate with respect to that observed with HNE. This result is not surprising since conventional inhibitors may mask the presence of differential inhibitors simultaneously present.

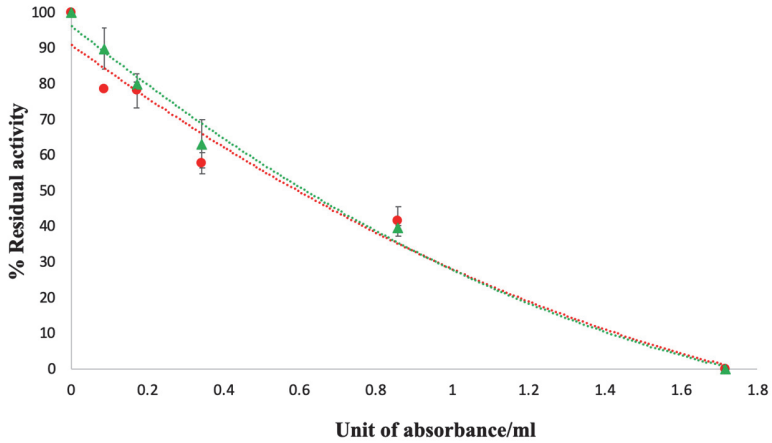

Figure 4. 2: Inhibitory effect of *Zolfino* extract on AKR1B1 activity. The percentage of AKR1B1 residual activity is rapresented in function of the concentration of *Zolfino* extract expressed as unit of absorbance at 265 nm per ml. The mean of percentage of inhibition measured using 0.8 mM L-idose (red circles) and 0.04 mM HNE (green triangles) from triplicate assays performed in the presence of 10 mU of AKR1B1 is reported. Bars represents the standard error of the measure.

4.2 Ionic exchange chromatography of *Zolfino* beans extract

The extract was processed through an ionic exchange chromatography step (see experimental procedure 3.7.1) obtaining the elution profile reported in Fig. 4.3.

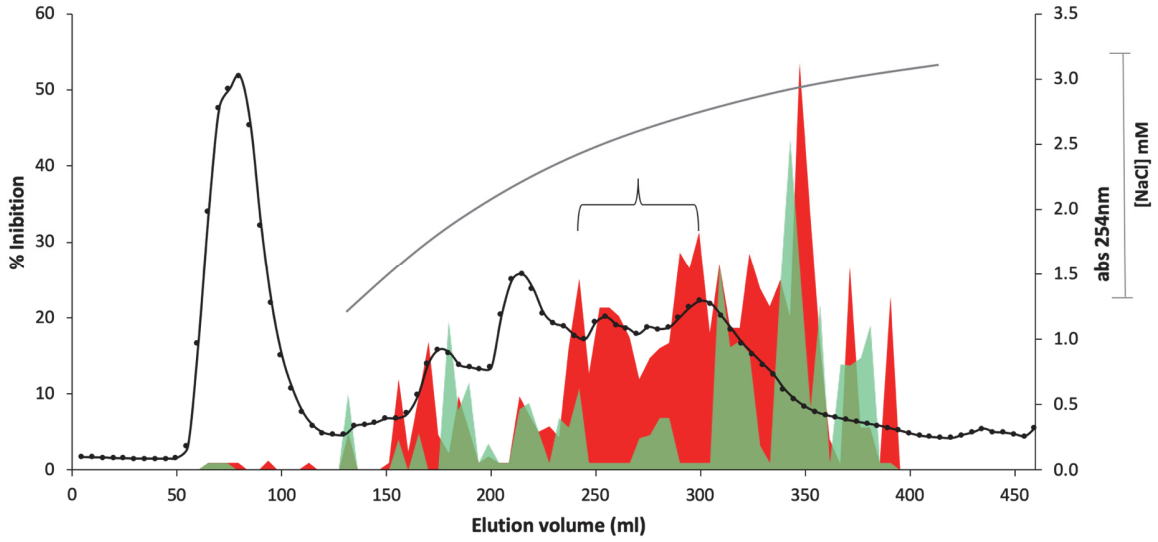

Figure 4. 3: Elution profile of an ionic exchange chromatography of a *Zolfino* extract. The chromatography has been performed as described in paragraph 3.7.1, using a DEAE-Sepharose resin loading 20 ml of *Zolfino* extract (corresponding to 30 gr of dried beans). The absorbance at 254 nm (black line) is reported as a function of elution volume. The grey line refers to the NaCl gradient. The elution was performed at flow rate of 20 ml/h and collecting fractions of 2 ml. The mean of percentage of inhibition measured using 0.8 mM L-idose (red area) and 0.04 mM HNE (green area) from triplicate assays using a fraction volume of 100 µl and 10 mU of AKR1B1 is reported.

The inhibitory ability of the extract appeared essentially associated to components able to interact with the support. In particular, fractions eluting in the range 250-320 ml showed significant differential inhibition between L-idose and HNE. Unfortunately, as observed in Fig. 4.4, the inhibitory effect exerted by the components included in this area resulted deeply affected by the storage of fractions. It is evident in fact that most of the differential inhibition measured immediately after fractions collection was lost after two weeks storage of isolated fractions.

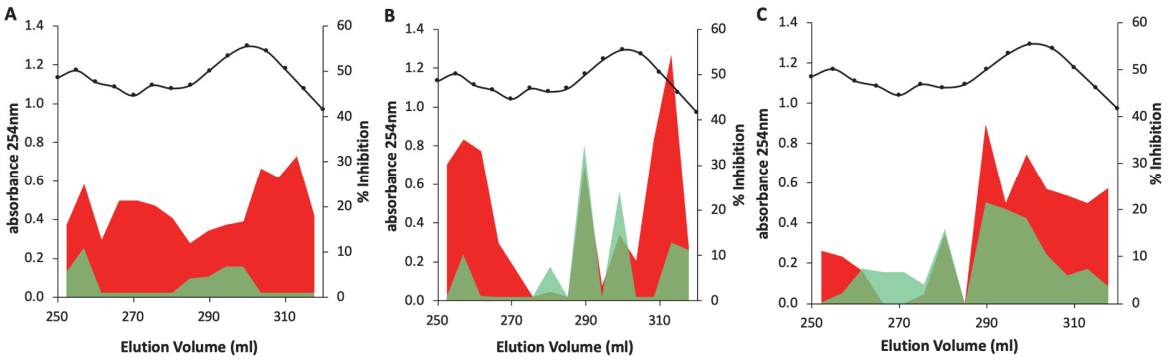

Figure 4. 4: Effect of storage on the inhibitory action of fractions eluted from ionic exchange chromatography. The absorbance at 254 nm (black line) and the percentage of inhibition of 0.8 mM L-idose (red area) and 0.04 mM HNE (green area) are reported as a function of the elution volume. Inhibition data are the mean from triplicate assays performed sing a fraction volume of 100 µL and 10 mU of AKR1B1 The inhibitory action of fraction eluting with a NaCl concentration between 135 and 150mM was evaluated immediately after collection of fractions (**Panel A**) and after 2 weeks storage either at +4°C (**Panel B**) or at -20°C (**Panel C**).

4.3 Hydrophobic interaction chromatography of *Zolfino* beans extract

A different separation approach was then adopted and the *Zolfino* extract was processed using a hydrophobic interaction chromatography (BondElut C18 column). The elution was performed increasing the hydrophobicity of the eluent by applying 25 and 50% (v/v) methanol solutions. A typical elution profile is reported in Fig. 4.5.

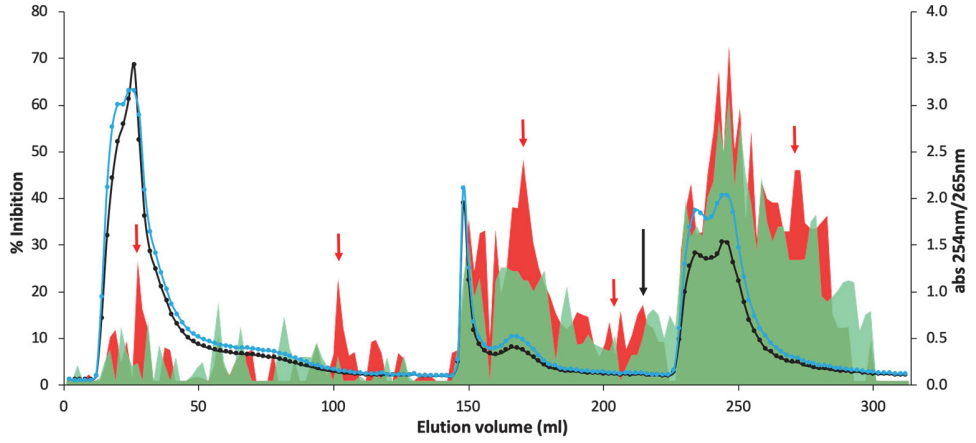

Figure 4. 5: Hydrophobic interaction chromatography of *Zolfino* extract on a BondElut C18 colum. The chromatography was performed using a BondElut C18 column (25 ml of resin) loading 10 ml of *Zolfino* extract (corresponding to 15 gr of dried beans). The elution was performed at 20 ml/h collecting fractions of 2 ml, using as consecutive eluents water, 25 % and 50% methanol. Blue and black lines refer to the absorbance at 254 and 265 nm, respectively. The percentage of inhibition measured with 0.8 mM L-idose (red area) and 0.04 mM HNE (green area) is also reported. Inhibition data are the mean from triplicate assays performed using a volume of 50 µl of the resuspended fraction (see Experimental Procedures 3.7.2) and 10 mU of AKR1B1. The red arrows indicate fractions with the highest differential inhibition.

All the adopted elution steps determined the release of materials displaying AKR1B1 inhibitory activity. The components not interacting with the support and eluted with water had a significantly lower inhibitory activity compared to the ones eluted with methanol. Overall, the highest AKR1B1 inhibitory ability was associated to fractions eluting with 50% methanol. Among all the eluted components, it was possible to detect the presence of fractions displaying a differential inhibition of L-idose with respect to HNE higher than 15%. These fractions are indicated with arrows in Fig. 4.5.

Our attention was focused on components eluting at the end of the 25% methanol step (i.e. approximately 70 ml after the application of 25% methanol). This region is characterized by absorbance values at 254 nm and 265 nm essentially comparable to baseline levels and by a lack of inhibitory effect on HNE reduction.

Chromatographic separations performed as described in Fig. 4.5 (30 samples analyzed) gave very reproducible results. As an example, Fig. 4.6 shows the elution of the fraction of interest referring to two among of the all analyzed samples. Results obtained allowed the identification of a fraction ("*Fraction X*") eluting at a volume of 75 ± 3 (mean ± SD) ml after the application of 25 % methanol and displaying a significant ($p>0.0001$) differential inhibition between L-idose and HNE of 16 ± 2 %. The obtained data are reported in Fig. 4.7; a comparison with fractions eluting in adjacent positions with respect to "*Fraction X*" is also shown.

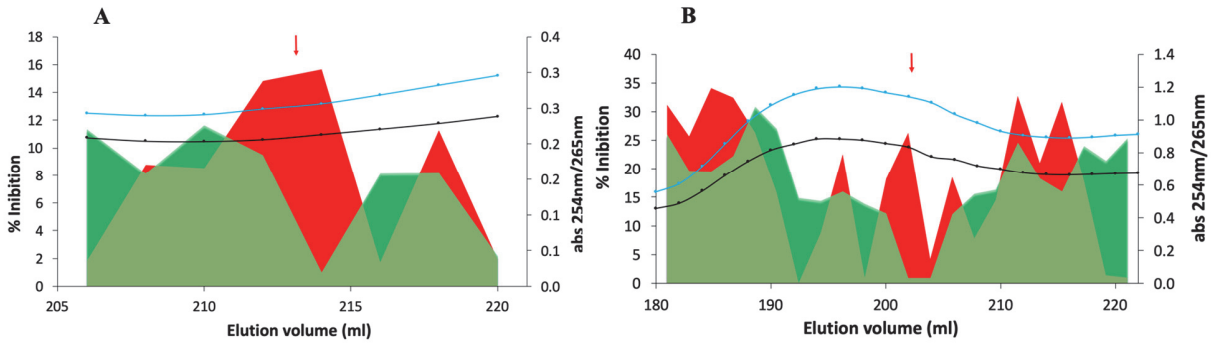

Figure 4. 6: Hydrophobic interaction chromatography of *Zolfino* extract on a BondElut C18 colum. Panel A and **Panel B** show the results of two chromatography performed using a BondElut C18 column (25 ml of resin) loading 20 ml of *Zolfino* extract (corresponding to 30gr of dried beans). Only the elution with 25% methanol in the range from 60 to 75 ml from the beginning of this step is reported. Black line refers to the absorbance at 254. The percentage of inhibition measured with 0.8 mM L-idose (red area) and 0.04 mM HNE (green area) is also reported. Inhibition data are the mean from triplicate assays performed using a volume of 50 µl of the resuspended fraction (see Experimental Procedures 3.7.2) and 10 mU of AKR1B1.

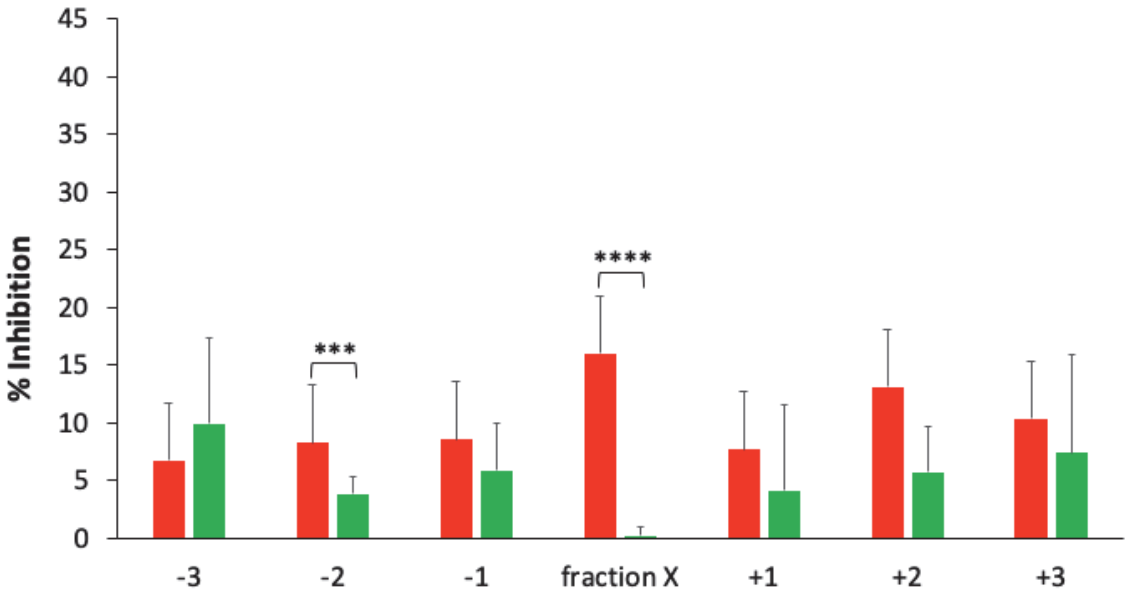

Figure 4. 7: Inhibitory effect of "*Fraction X*". The histograms represent the average of the percentage of inhibition of each fractions, obtained from different analyzed *Zolfino* extracts (n=12). For each extract triplicate assays of each fraction were performed using 0.8 mM L-idose (red) and 0.04 mM HNE (green) as substrates. Fractions eluting immediately before and after "*Fraction X*" in different chromatograms are indicated as "-" and "+", respectively. Bars represent the standard error of the measure. The statistical significance of the differential inhibition of each fraction was analyzed trough the t-test analysis with Dunn-Šidák correction (k=7) and is shown by the asterisks: (****): $p<0.0001$; (***): $p<0.001$.

The stability of "*Fraction X*" over time has been evaluated after storage of the dried fraction at +4°C up to 45 days. As shown in Fig. 4.8, the differential inhibitory effect appeared stable for up to a 30-day storage, despite a decrease of L-idose inhibition was observed. Further storage both affected the absolute level of inhibition and completely removed the differential inhibitory effect.

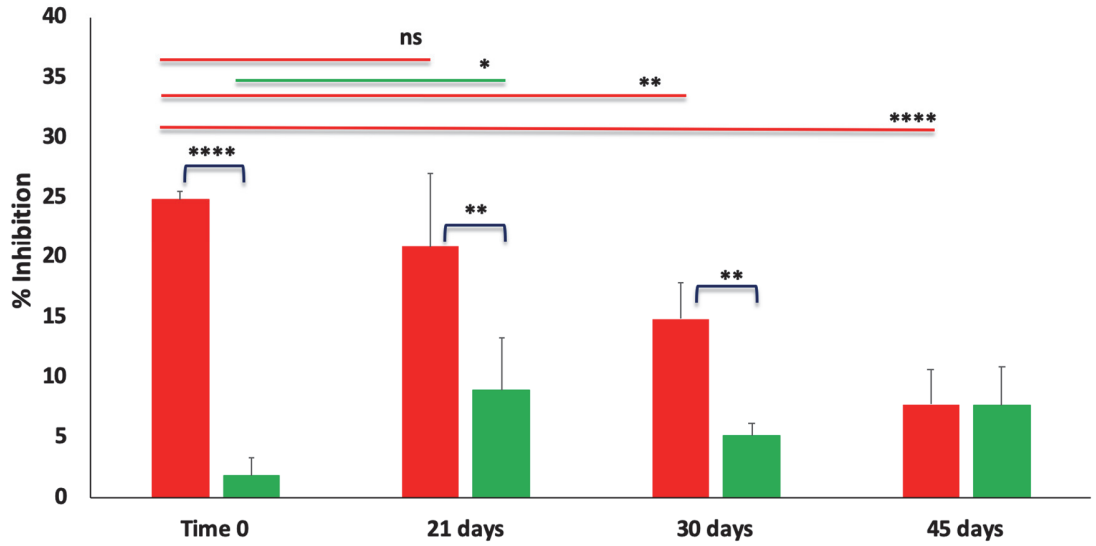

Figure 4. 8: Stability of the inhibitory activity of "*Fraction X*" over time. The inhibitory activity of "*Fraction X*" was tested at different times after it was collected and dried (time 0) and stored at +4°C. The fraction was tested for its inhibitory effect on the reduction of 0.8 mM L-idose (red histograms) and 0.04 mM HNE (green histograms). Each assay was done in triplicates, using 50 µl of the sample; data are reported as the mean of at least three measurements and bars indicate the standard error. The statistical analysis was performed trough the two ways ANOVA. The lines over the histograms indicate the groups of data that were analyzed and compared. The significance of the analysis is shown by the asterisks: (****): $p<0.0001$; (***): $p<0.001$; (**): $p<0.01$; (*): $p<0.05$; ns: not significant.

Once confirmed the stability of "*Fraction X*", a pool containing "*Fractions X*" collected from different C-18 chromatography was used for a dose-response curve. Figure 4.9 shows the percentage of inhibition of HNE and L-idose reduction in the presence of different concentrations of "*Fraction X*" (expressed as unit of absorbance at 265 nm/ml). The inhibitory effect on HNE reduction did not exceed 6%, while the effect on L-idose reduction progressively increased reaching a plateau up to 24%, measured in the presence of approximately 13 unit of absorbance/mL of fraction in the assay. No further increase in the inhibitory effect was observed for further increase in the concentration of "*Fraction X*" up to 27 unit of absorbance/ml in the assay.

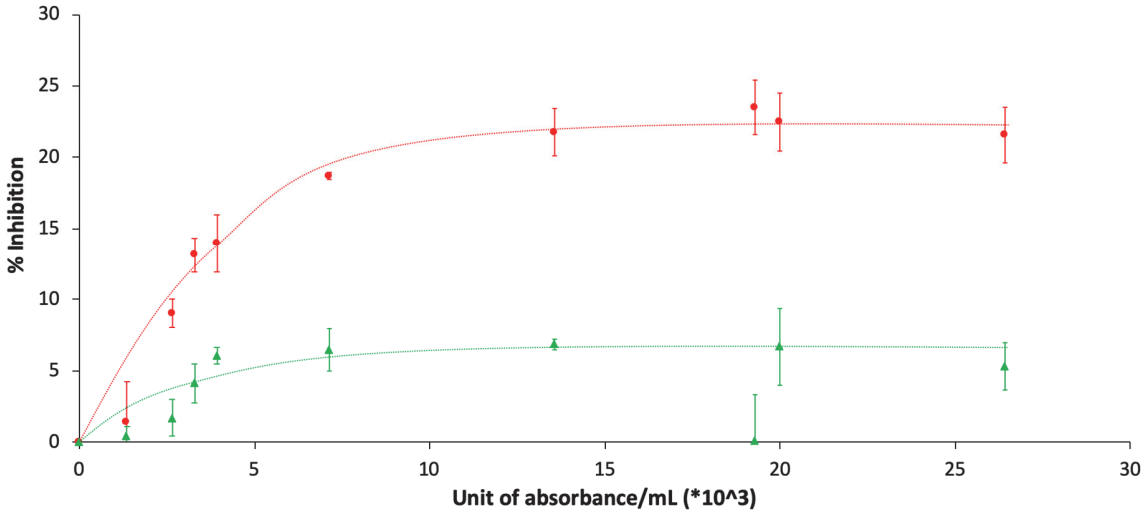

Figure 4. 9: Dose response of "*Fraction X*". The inhibitory effect of a pool of "*Fraction X*" collected from different C-18 columns was tested on the reduction of either 0.8 mM L-idose (red circles) or 0.04 mM HNE (green triangles). Sample concentration is expressed as unit of absorbance (λ = 265 nm) /ml. Each value represents the mean from at least three measurements; bars represent standard deviation.

Three "*Fraction X*" obtained from three different chromatographies were dried separately and then resuspended together in water using half volume of the original fractions. The pool was applied again to another C18 column (for details see section 3.7.2). The obtained elution profile is shown in Fig. 4.10; each fraction was tested for its capability to inhibit AKR1B1 activity acting on L-idose and HNE reduction. Results obtained allowed to identify a pool of fractions able to act as ARDIs eluting at a volume between 5 and 8 ml after the application of 25 % methanol.

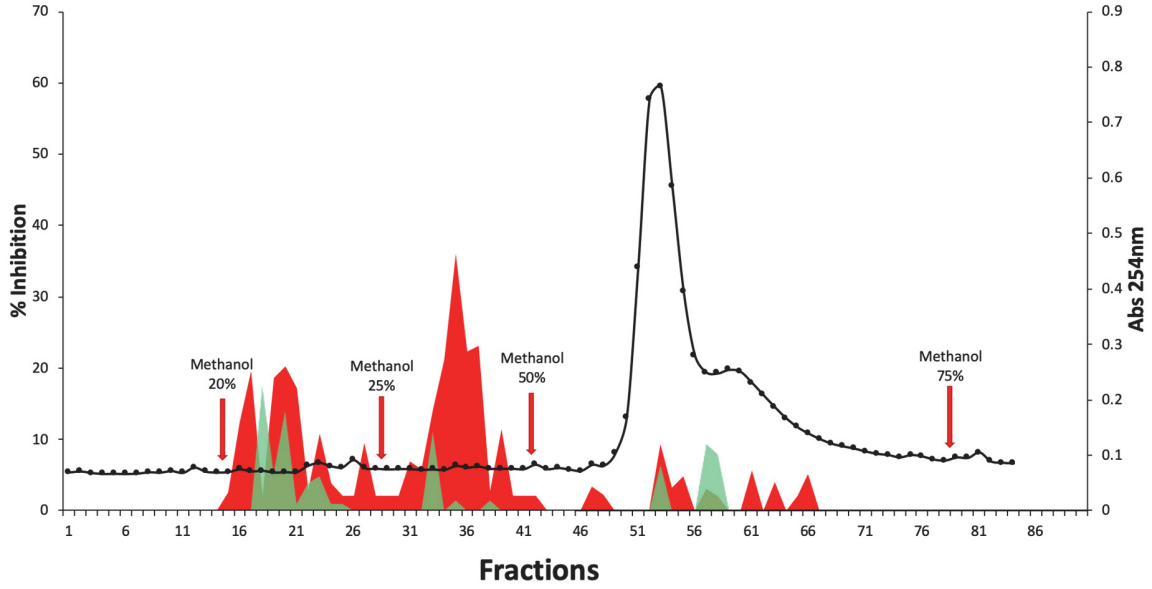

Figure 4. 10: Hydrophobic interaction chromatography of "*Fraction X*" on a BondElut C18 column. The chromatography was performed using a BondElut C18 column (8 ml of resin) loading 3.5 ml of a pool of "*Fraction X*" obtained from 3 different chromatographies . The elution was performed at 10 ml/h collecting fractions of 0.8 ml, using as consecutive eluents water, 25 %, 50% and 75% methanol. Black line refers to the absorbance at 254 nm. The percentage of inhibition measured with 0.8 mM L-idose (red area) and 0.04 mM HNE (green area) is also reported. Inhibition data are the mean from triplicate assays performed using a volume of 100 µl of the resuspended fraction (see Experimental Procedures 3.7.2) and 10 mU of AKR1B1.

4.4 Identification through HPLC-PDA/UV-ESI-MS/MS of compounds present in "*Fraction X*"

HPLC-PDA/UV-ESI-MS/MS analysis was performed on "*Fraction X*" and on the fractions eluted both immediately before and immediately after with respect to "*Fraction X*" ("Fraction -1" and "Fraction +1", respectively). The analysis underlined, in all the fractions, the presence of a single compound with a retention time of 43.0 min, as shown in the UV chromatograms (registered at 266 nm) (Fig. 4.12) and in the ESI-MS chromatograms (Fig. 4.13).

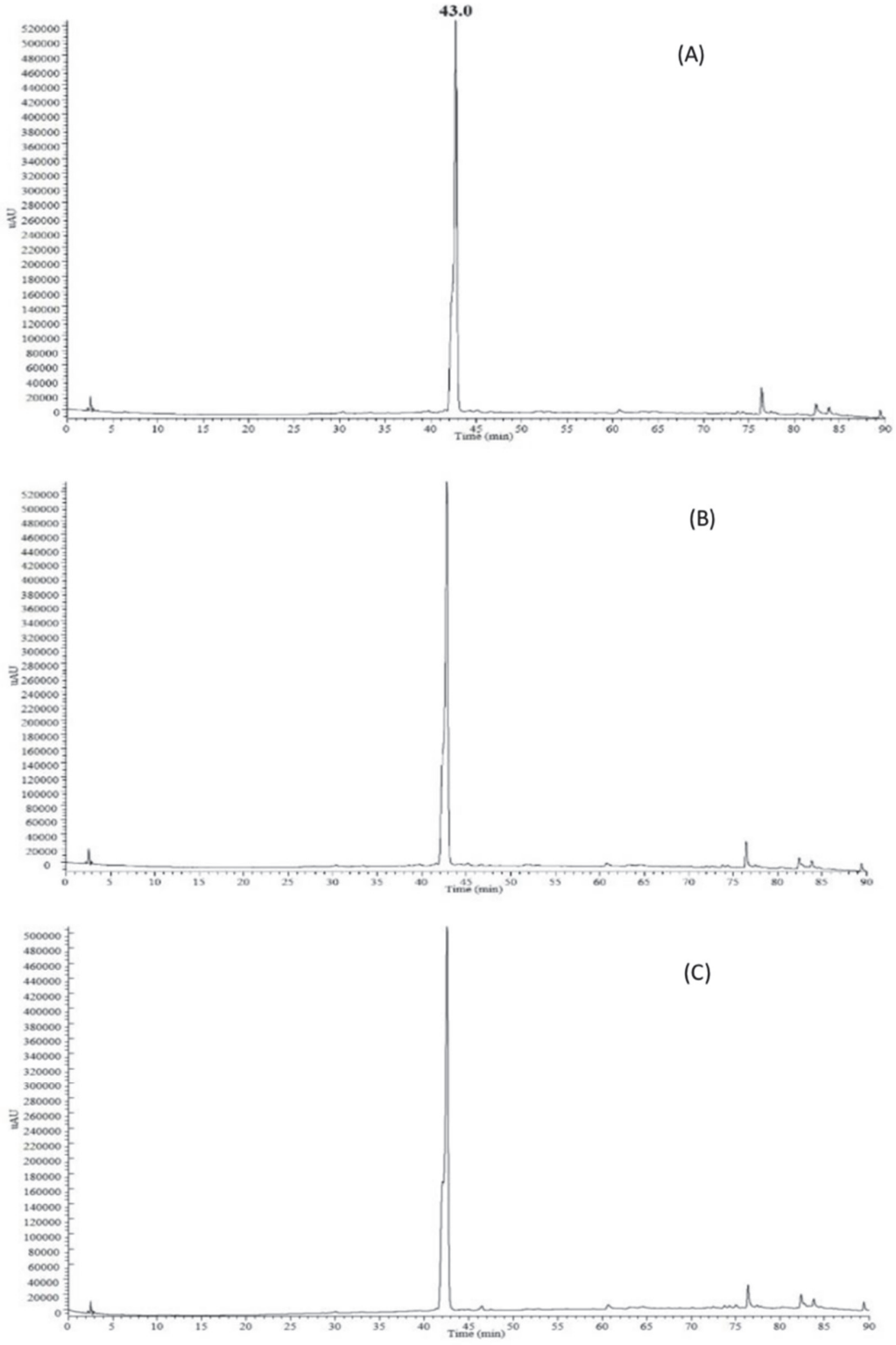

Figure 4. 11: UV Chromatograms. Panel A, B and C refer to the UV chromatograms registered at 266 nm for the analysis of "Fraction -1", "*Fraction X*" and "Fraction +1", respectively.

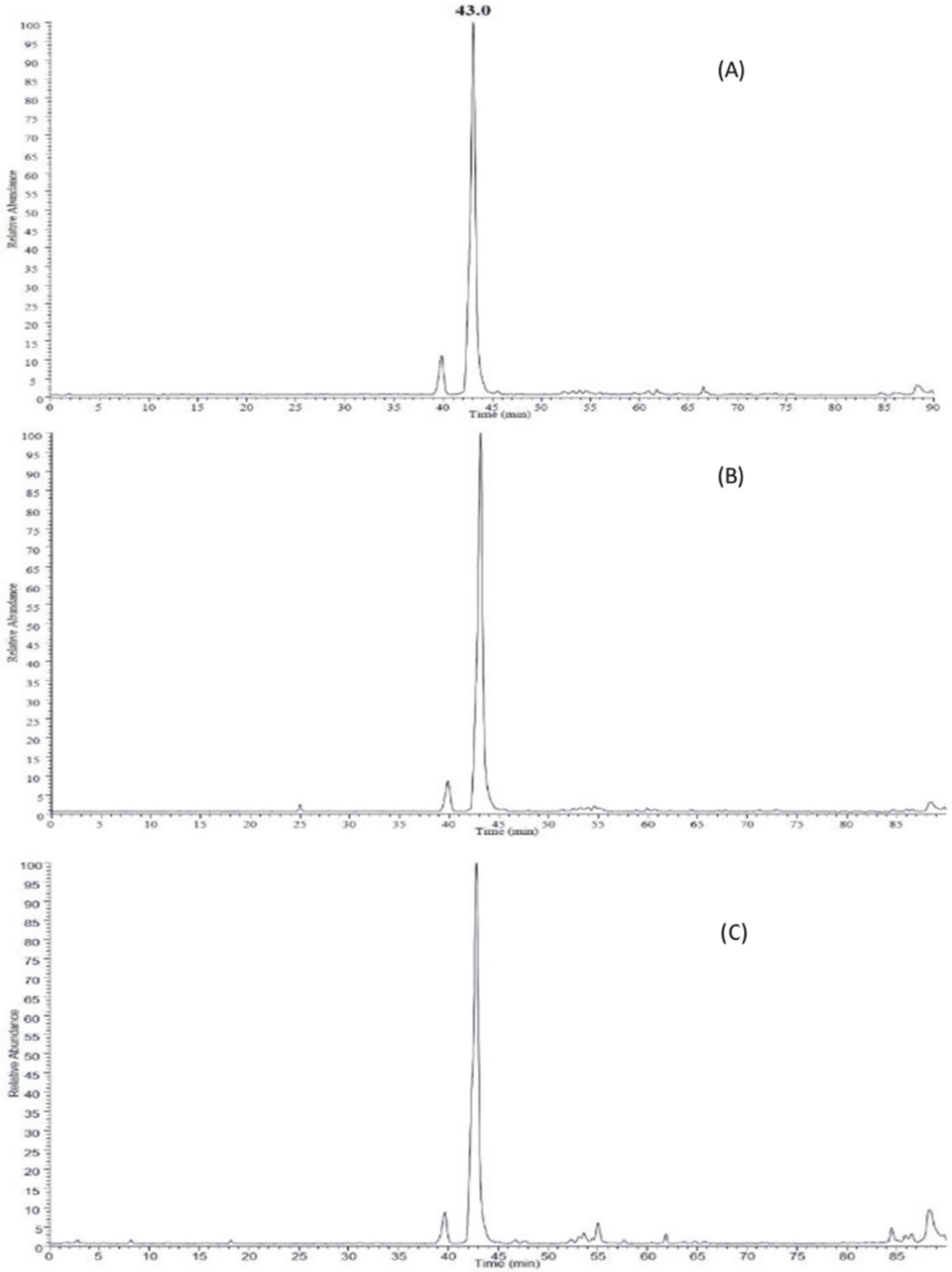

Figure 4. 12: ESI-MS Chromatograms. Panel A, B and C refer to the ESI-MS chromatograms registered in negative mode for the analysis of "Fraction -1", "*Fraction X*" and "Fraction +1", respectively.

Fig. 4.14 reports the UV spectrum of the analyzed sample; the spectrum showed the presence of two peaks of absorbance, at 266 nm and at 349 nm. These features are consistent with those of flavonoids (Tošović and Marković, 2015).

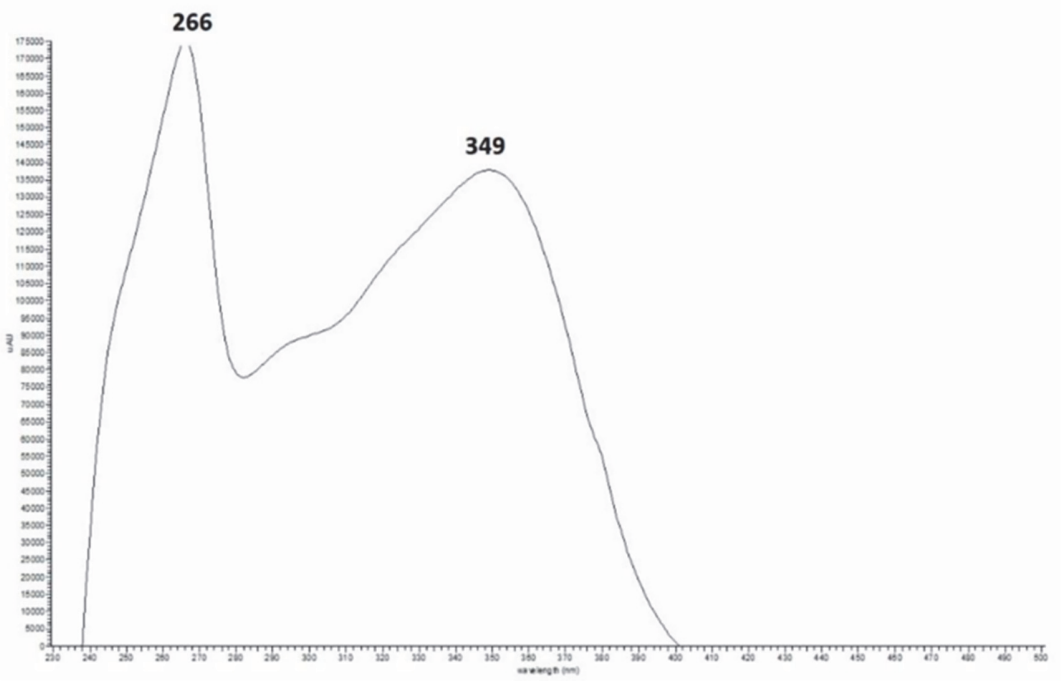

Figure 4. 13: UV Spectrum of "*Fraction X*". The wavelength of the maximal absorbance of the two peaks are evidenced.

Full ESI-MS spectrum acquired in negative mode (Fig. 4.15A) showed a peak at a *m/z* value of 579, corresponding to the deprotonated molecular ion $[M-H]^-$, and a peak at a *m/z* value of 625, corresponding to the adduct of the molecule with the formate ion [M+HCOO]. Moreover, a peak at a *m/z* value of 1159, corresponding to the dimeric ion, was also present. These results indicated for the component present in the sample a molecular weight of 580 uma.

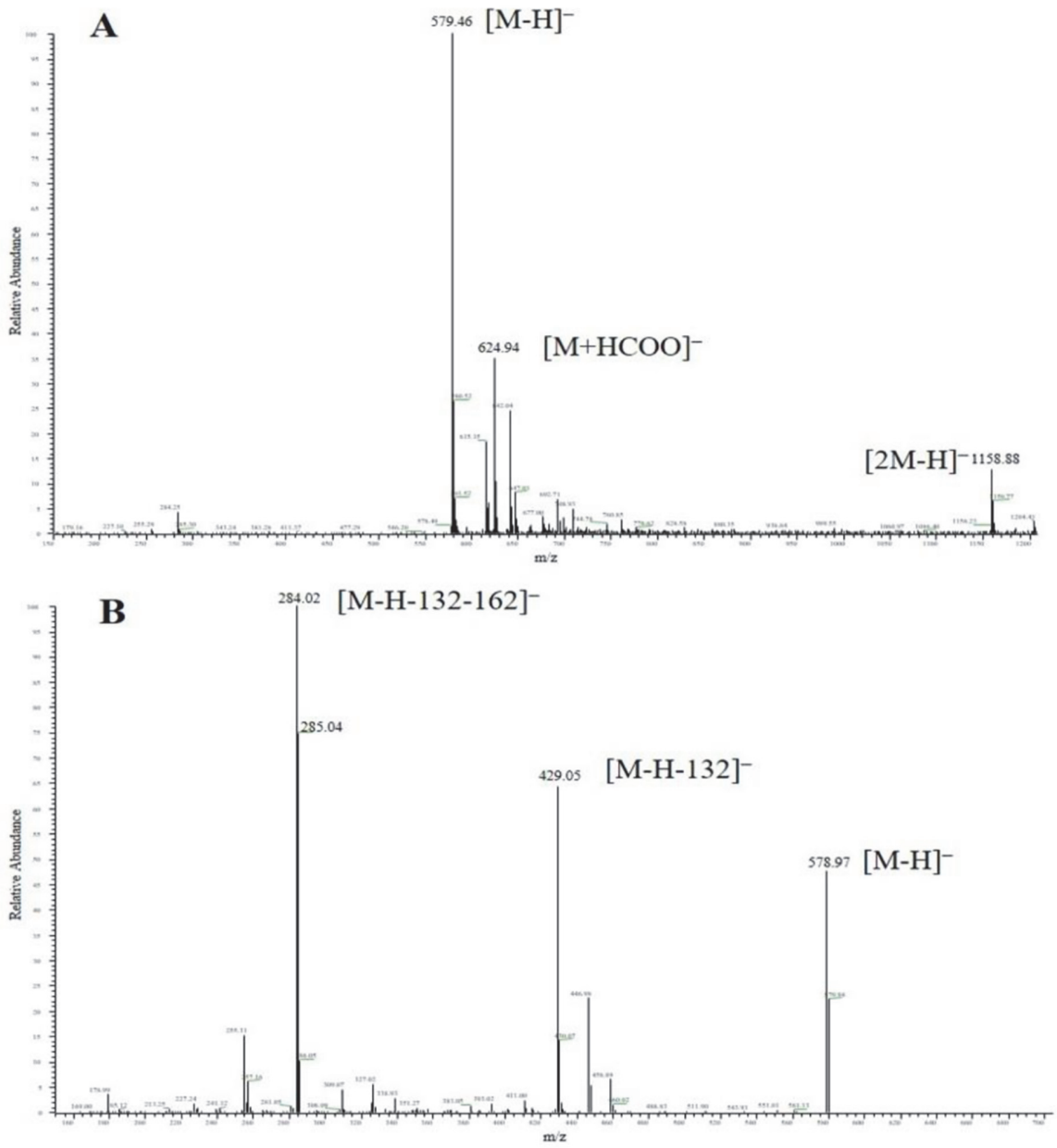

Figure 4. 14: ESI-MS Spectra of "*Fraction X*". Panel A refers to full ESI-MS spectrum acquired in negative mode; Panel B refers to the fragmentation spectrum.

The fragmentation ESI-MS spectrum of "*Fraction X*" (Fig. 4.15B) showed two additional peaks at *m/z* values of 429 and 285. These signals can be associated with the release from the initial compound of a pentose ($[M-H-132]^-$) and to the subsequent loss of a hexose ($[M-H-132-162]^-$), respectively, occurring upon hydrolysis of glycosidic bonds. The ion at *m/z* 285 can be associated

with the flavonoid kaempferol (M=286). Previous studies on *Phaeosolus vulgaris* have reported the presence of a kaempferol diglycoside, i.e kaempferol 3-O-β-D-glucopyranoside-(2→1)-O-β-D-xylopyranoside (whose structure is shown in Fig. 4.16), known as leucoside (Beninger *et al.,* 1999; Dinelli *et al.,* 2006), whose molecular weight was consistent with our results. A commercially available standard of leucoside was analyzed through HPLC-PDA/UV-ESI-MS/MS under the conditions adopted for "*Fraction X*" analysis. Results, reported in Fig. 4.17, are in complete agreement with those obtained from the analysis of "*Fraction X*".

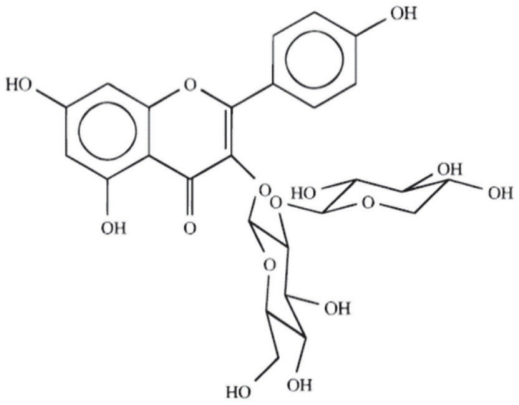

Figure 4. 15: Structure of leucoside.

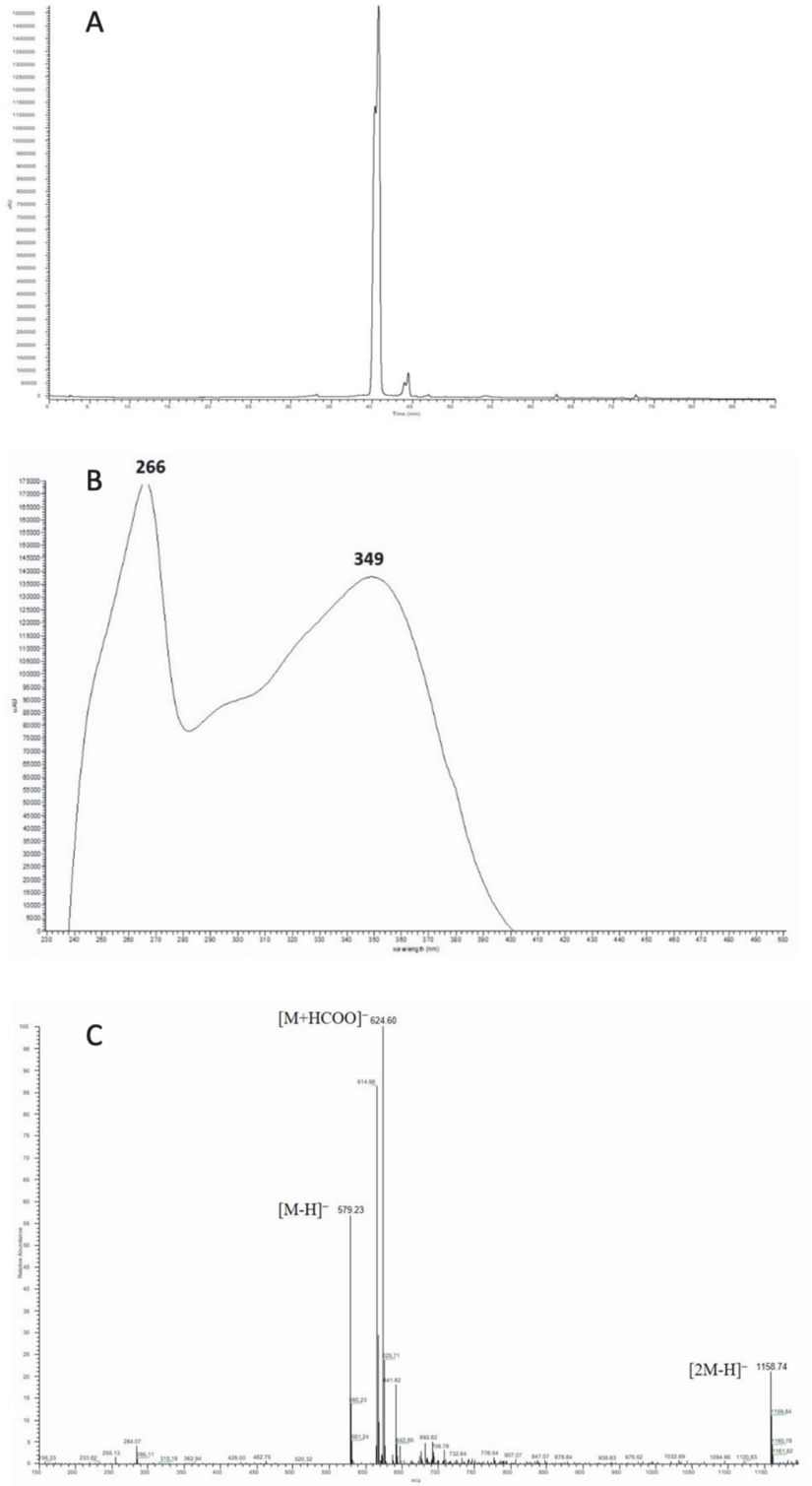

Figure 4. 16: Analysis of commercial leucoside. A solution of the commercial leucoside was analyzed under the conditions adopted for the analysis of "*Fraction X*". Panel A: UV chromatograms registered at 266 nm; Panel B: UV spectrum; The wavelength of the maximal absorbance of the two peaks are evidenced. Panel C: Full ESI-MS spectrum acquired in negative mode.

4.5 Inhibitory effect of commercial leucoside on AKR1B1

The commercial leucoside was tested as a differential inhibitor of AKR1B1, using L-idose and HNE as substrates. The compound resulted to affect AKR1B1 activity. Approximately 70% of residual activity was observed in the presence of 19 µM leucoside, using either 4 mM L-idose or 0.04mM HNE as substrates, dose no significant differential inhibition was observed, as suggested by the t-test analysis of data in Fig. 4.18.

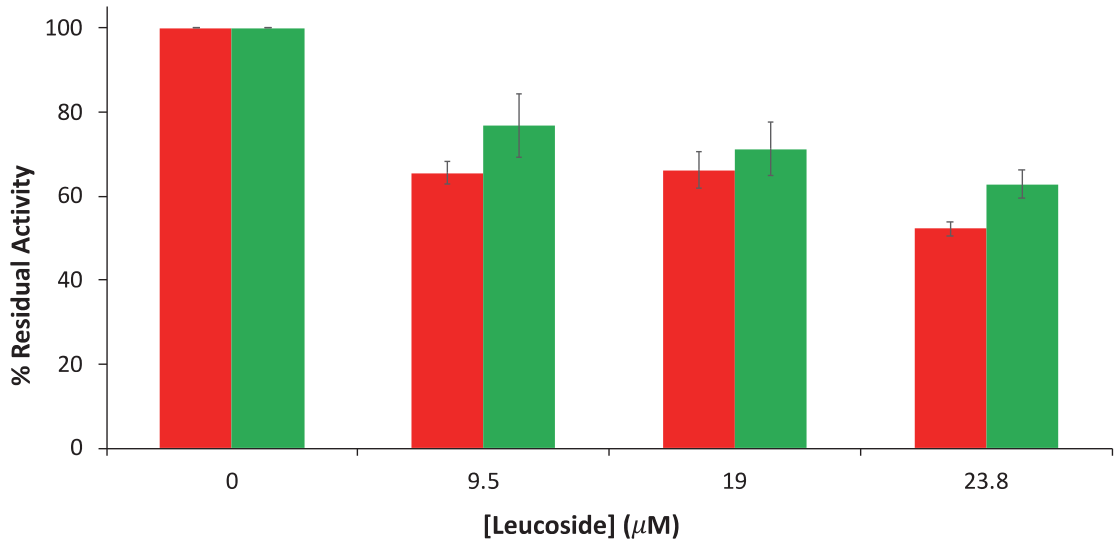

Figure 4. 17: Inhibitory effect of the leucoside of AKR1B1 activity. The inhibitory effected of commercial leucoside was tested on the reduction of 4 mM L-idose (red histograms) and 0.04 mM HNE (green histograms). Data are reported as the mean of at least three measurements and bars indicate the standard error. N significant differential inhibition was observed by a statistical analysis performed trough the t-test analysis with Welch's test correction.

4.6 High throughput screen pilot assay

4.6.1 Determination of assay conditions

In order to screen the 1280 compounds in the LOPAC library as ARDIs, it was necessary to optimize the conditions for the AKR1B1 assay in the 384 well plate.

A preliminary evaluation of the conditions to set up a reliable AKR1B1 assay in the 384 well plates was performed using GAL as substrate.

Data reported in Fig. 4.19 refer to the absorbance measured when different amounts of AKR1B1 (0.8, 1.6 and 3.3 mU) were used in assay in the presence of 0.07 mM GAL as substrate. The

differences in both the absorbance values measured at the end of the incubation (ΔA) and in the rate of absorbance decrease in the interval time 0-5 min (ΔA/min) between the assay in the absence (blank values) and in the presence of the enzyme were evaluated. Essentially no differences were observed between the measurements in the absence and in the presence of 0.8 mU of AKR1B1. The presence of both 1.6 and 3.3 mU of enzyme showed a significant difference with respect to the absence of AKR1B1. In fact, values of (0.12 ± 0.01) ΔA, and (-0.004 ± 0.0012) vs (-0.011 ± 0.0006) ΔA/min and (0.17 ± 0.02) ΔA, and (-0.004 ± 0.0017) vs (-0.014 ± 0.0012) ΔA/min were calculated for 1.6 and 3.3 mU, respectively.

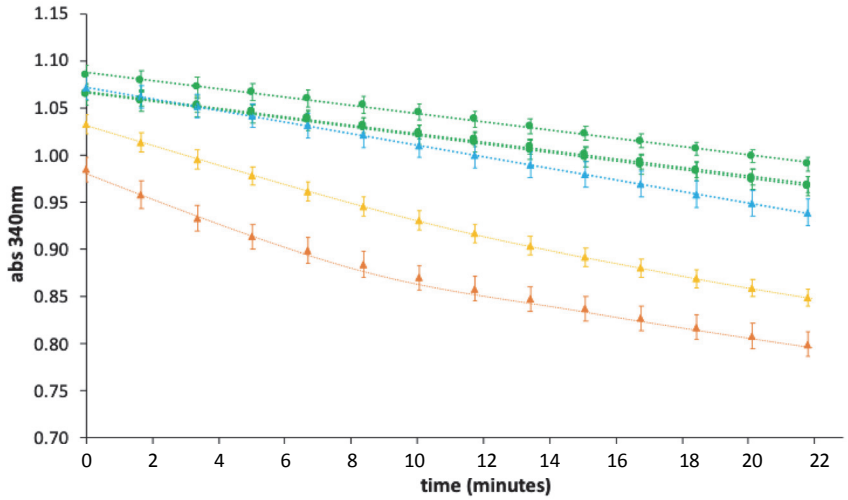

Figure 4. 18: Optimization of HTS assay conditions: effect of enzyme concentration in the presence of sub-saturating GAL concentrations. The absorbance at 340 nm was monitored over time in different wells. The assay mixture contained 0.3 mM NADPH, 0.38 M ammonium sulphate, 0.5% DMSO, 0.07 mM GAL and the following AKR1B1 amounts: 0.8 mU (blue), 1.6 mU (yellow) and 3.3 mU (orange). Circles refer to assays in the absence of the enzyme. Bars represent the standard deviations of the mean from 8 independent measurements.

A further increase in GAL concentration up to 4 mM made the differences with respect to blank values more evident, as observed in Fig. 4.20, which refers to the presence of 1.6 mU of AKR1B1. In fact, ΔA and ΔA/min values of (0.5 ± 0.03) and (-0.0035 ± 0.0001) vs (-0.021 ± 0.001), respectively were measured.

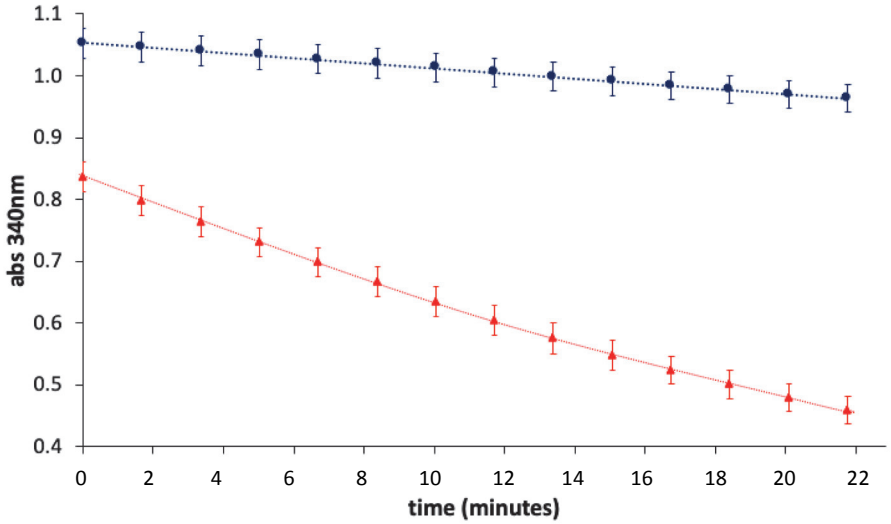

Figure 4. 19: Optimization of HTS assay conditions: enzyme activity in the presence of saturating GAL concentrations. The absorbance at 340 nm was measured in the presence of an assay mixture containing 0.3 mM NADPH, 0.38 M ammonium sulphate, 0.5% DMSO, 4 mM GAL in the absence (circles) and in the presence of 1.6 mU of AKR1B1 (triangles). Bars represent the standard deviations of the mean from 96 independent measurements.

These conditions were adopted for the calculation of Z' score using a number of replicates of 96 for both the blank and the enzyme activity determination (Fig. 4.21); the resulting Z' score of 0.73 indicates a good quality assay. The Z' score was calculated as reported below:

$$Z' = 1 - [3x(0.02)+3(0.02)]/(|0.46-0.96|) = 0.73$$

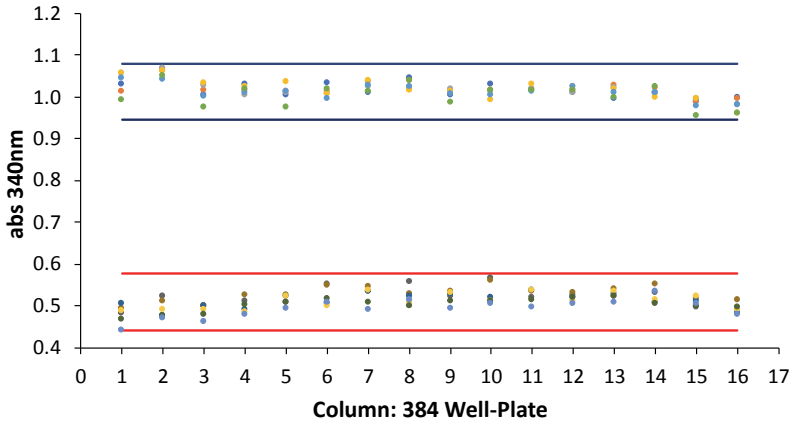

Figure 4. 20: Assay replicates for calculation of Z' score using GAL as substrate. Each point represents the absorbance at 340 nm measured in different wells of the indicated columns of the 384well-plate after 22 min, under the conditions described in Fig. 4.20. Points between blue and red lines refer to blank and activity values, respectively. The intervals delimited by blue and red lines represent 3-fold the standard deviation of blank and activity measurements, respectively.

Assay conditions were then optimized to detect AKR1B1 activity using L-idose as substrate. The enzyme activity was measured in the presence of different concentrations of L-idose (from 0.8 to 8 mM), as shown in Fig. 4.22, using both 1.6 and 3.3 mU of AKR1B1. On the basis of these results, 3.3 mU of enzyme and a sub-saturating substrate concentration for L-idose of 2.5 mM were adopted in following tests.

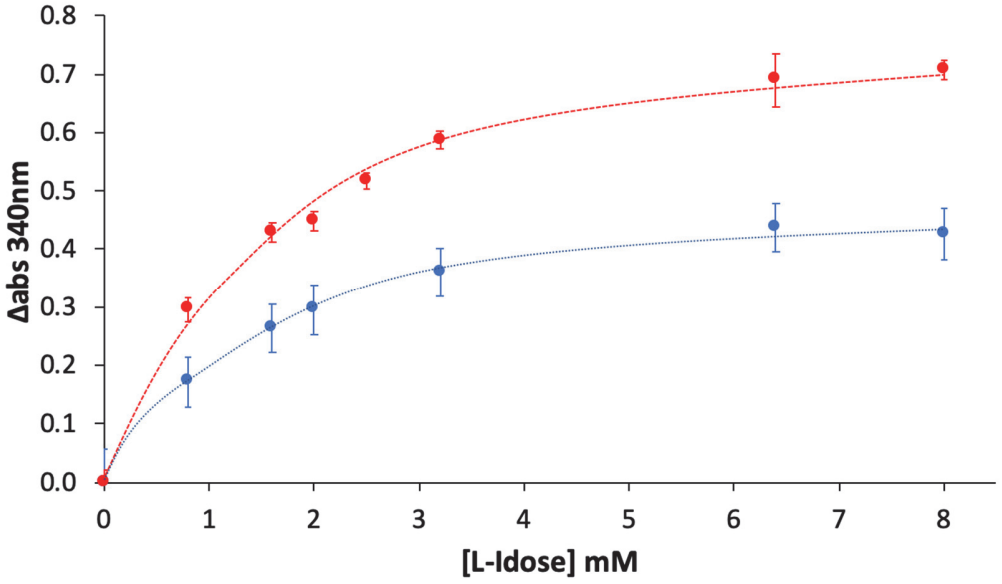

Figure 4. 21: Effect of L-idose concentration on AKR1B1 activity. The *ΔA* at 340 nm was measured in different wells after 22 min at the indicated L-idose concentrations, in the presence of 1.6 (blue) or 3.3 (red) mU of AKR1B1. From each reported value the ΔA measured under the same conditions in the absence of the substrate is subtracted. Bars (when not visible are within the symbol size) represent the standard deviations of the mean from at least 6 independent measurements.

Under these conditions, as observed in Fig. 4.23, also an appreciable ΔA/min value was observed in the presence of the enzyme (-0.019 $\pm$ 0.0006) with respect to blank values (-0.003 $\pm$ 0.0001). In addition, to test the sensitivity of the assay to inhibition, the effect on enzyme activity of 1 µM Sorbinil (here used as reference inhibitor) was evaluated (Fig. 4.23). An inhibition of 47% both in terms of ΔA (0.45 $\pm$ 0.01 vs 0.23 $\pm$ 0.02) and ΔA/min (-0.019 $\pm$ 0.0006 vs -0.009 $\pm$ 0.0003) with respect to control assay in the absence of the inhibitor was observed.

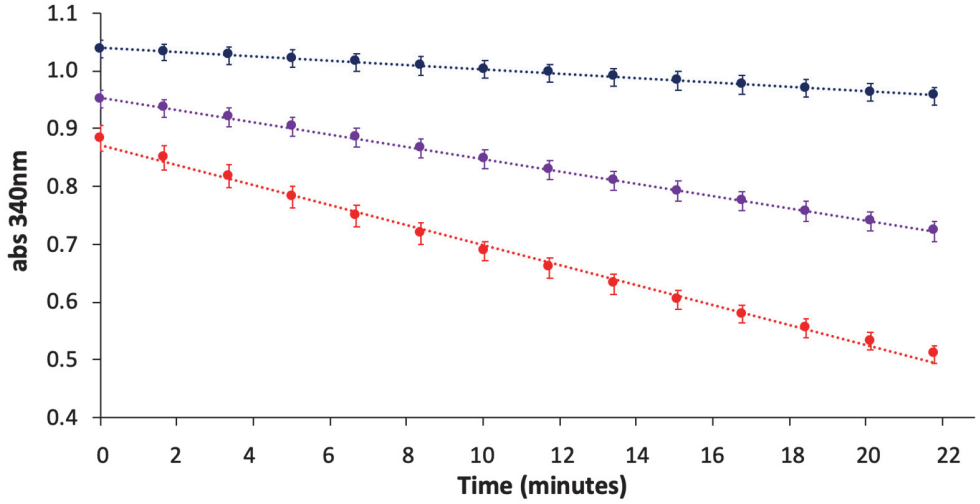

Figure 4. 22: Effect of Sorbinil. The absorbance at 340 nm was measured in a reaction containing 0.3 mM NADPH, 0.38 M ammonium sulphate, 0.5% DMSO, 2.5 mM L-idose in the absence (blue), in the presence of 3.3 mU of AKR1B1 (red) and in the presence of 1µM Sorbinil (purple). Bars represent the standard deviations of the mean from 32 independent measurements.

These conditions were adopted for the calculation of Z' score using a number of replicates of 32 for both the blank and the enzyme activity determination (Fig. 4.24); the resulting Z' score of 0.79 indicates a very good quality assay. Moreover, the effect of Sorbinil resulted well evident.

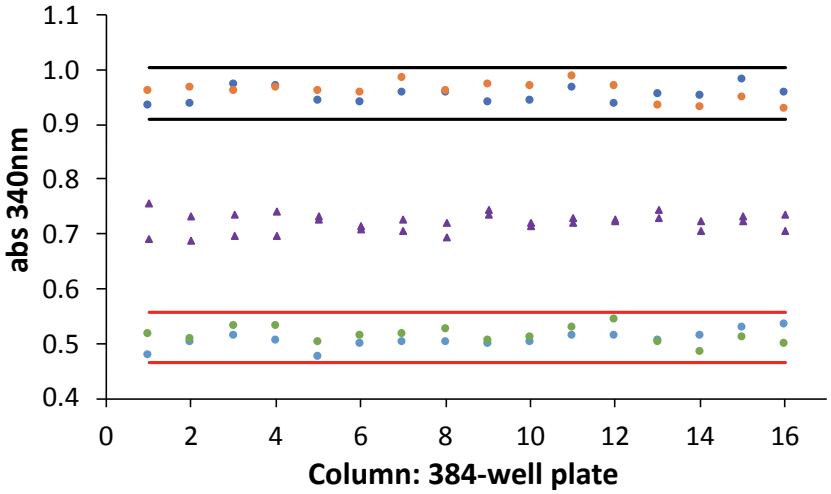

Figure 4. 23: Assay replicates for calculation of Z factor using L-idose as substrate. Each point represents the absorbance at 340 nm measured in different wells of the indicated columns after 22 min, under the conditions described in Fig. 4.23. Points between blue and red lines refer to blank and activity values, respectively. The intervals delimited by blue and red lines represent 3-fold the standard deviation of blank and activity measurements, respectively. Triangles refer to assays performed in the presence of 1µM Sorbinil.

Similarly, assay conditions were optimized using HNE as substrate. Figure 4.25 reports results from assays conducted in the presence of 3.3 mU of AKR1B1 and 100, 150 or 200 µM HNE.

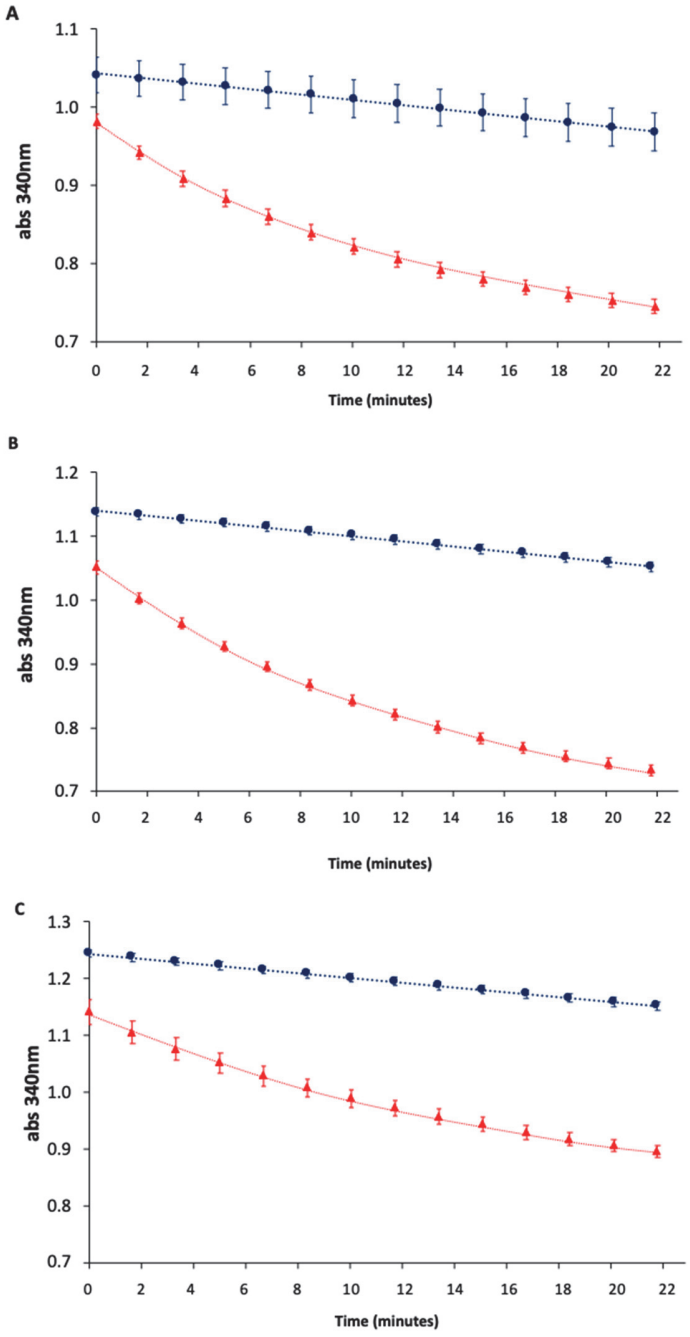

Figure 4. 24: **Optimization of HTS assay conditions using HNE as substrate.** The absorbance at 340 nm was measured at different times in assay mixtures containing 0.3 mM NADPH, 0.5% DMSO, 0.38 M ammonium sulphate in the absence (circles) or in the presence (triangles) of 3.3 mU of AKR1B1, using as substrate HNE at the following concentrations: 100 µM (**Panel A**), 150 µM (**Panel B**) and 200 µM (**Panel C**). Bars (when not visible are within the symbol size) represent the standard deviations of the mean from 5 independent measurements.

When HNE concentration was raised from 100 to 150 µM, an increase in both ΔA and ΔA/min from 0.22 ± 0.03 to 0.32 ± 0.01 and from -0.019 ± 0.002 to -0.024 ± 0.002, respectively was observed. On the other hand, when 200 µM HNE was used as substrate, a lower activity (0.25 ± 0.01 ΔA and -0.02 ± 0.0018 ΔA/min) was detected, probably as a consequence of the enzyme saturation effect and/or of the inactivating effect reported for the aldehyde (Del Corso *et al.,* 1998, Srivastava *et al.,* 1999). Thus, 150 µM was adopted as HNE concentration to perform assays for the calculation of Z' score using a number of replicates of 5 for both the blank and the enzyme activity determination (Fig. 4.26); a resulting Z' score of 0.67 was calculated.

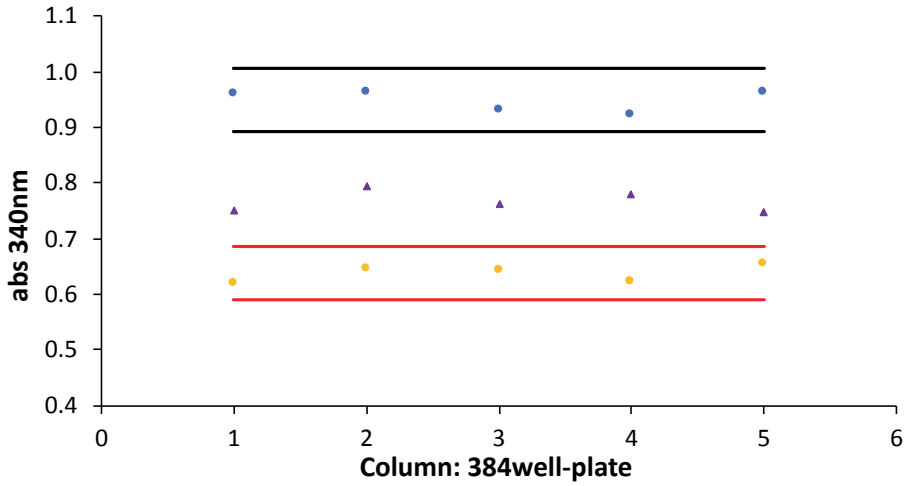

Figure 4. 25: **Assay replicates for calculation of Z factor using HNE as substrate.** Each point represents the absorbance at 340 nm measured in different wells of the indicated columns after 22 min, in assay mixtures containing 0.3 mM NADPH, 0.5% DMSO, 0.38 M ammonium sulphate, 3.3 mU AKR1B1 and 150 µM HNE. Points between blue and red lines refer to blank and activity values, respectively. The intervals delimited by blue and red lines represent 3-fold the standard deviation of blank and activity measurements, respectively. Triangles refer to assays performed in the presence of 1 µM Sorbinil.

Thus, Table 4.1 summarizes assay conditions selected to perform the HTS of LOPAC.

Table 4.1. Assay conditions for HTS
❖ 0.25 mM sodium phosphate buffer pH 6.8 ❖ 0.47 mM EDTA ❖ 0.5% DMSO ❖ 0.38 M Ammonium Sulfate ❖ 0.3 mM NADPH ❖ 3.3 mU AKR1B1 ❖ 2.5 mM L-Idose or 150 µM HNE

Table 4. 1: Assay condition for the HTS. The Table summarizes the assay conditions adopted for the screening of the LOPAC with L-Idose and HNE as substrates.

Under the conditions defined above we did not observe any appreciable effect on the AKR1B1 activity either by the presence of 0.5% DMSO, or by the use of non-dialyzed enzyme preparations (data not shown). Therefore, the screen was performed in the presence of 0.5% DMSO and non-dialyzed enzyme was used.

4.6.2 Screening of the LOPAC library

The LOPAC contains 1280 compounds, including enzymes inhibitors, receptor ligands and approved drugs, which are known to exert different pharmacological actions, was thus screened under the conditions described above; the ability of the compounds to affect L-idose reduction was initially evaluated. Fig. 4.27 reports the results of the analysis of the 4 plates containing the LOPAC. Blank values (i.e. blue symbols in each Panel of Fig. 4.27) and 100% AKR1B1 activity values (i.e. red symbols in each Panel of Fig. 4.27) were determined for each plate (n=16 and n=32, respectively). The relative delta absorbance values between blank and activity and the derived Z' score (reported in Table 4.2) were consistent with those measured for the optimization of the HTS conditions.

	P1401	P1402	P1403	P1404
ΔA	0.41 ± 0.03	0.46 ± 0.02	0.42 ± 0.01	0.44 ± 0.02
Z' score	0.66	0.77	0.84	0.79

Table 4. 2: LOPAC plates value. For each plate, the delta absorbance between the blank and the activity observed at 22 minutes and the related Z' score is reported.

As is the case for the reference AKR1B1 inhibitor Sorbinil (i.e. violet symbols in each Panel of Fig. 4.27), the compounds whose absorbance values at 340 nm measured at 22 min were higher than that observed for control activity (i.e. symbols that are above the region delimited by red lines in each Panel of Fig. 4.27), exerted an inhibitory action on AKR1B1. Among them, 89 compounds were selected displaying an inhibitory effect ranging from 25 to 94 %. It is conceivable that an ARDI, in order to exert its effect should not be characterized by an extremely potent inhibitory action. On this basis, compounds able to completely inhibit AKR1B1 activity were not selected for further studies. Details on the selected 89 compounds (position on the plate, CAS number and % inhibitory effect) are reported in Appendix Table 2B. In support of the validity of the HTS to identified AKR1B1 inhibitors was the ability to pick up compounds already shown to be AKR1B1 inhibitors such as: *Epalrestat* (Grewal *et al.,* 2016; Ramirez and Borja, 2008), *apigenin* (Choi *et al.,* 2014; Hwang *et al.,* 2019), *colchicine* (Gabbay and Tze, 1972), *daidzein* (Kim *et al.,* 2017), *genistein* (Kim *et al.,* 2008; Kim *et al.,* 2017), *emodin* (Chang *et al.,* 2016; Jang *et al.,* 2007), *hispidin* (Lee *et al.,* 2008), *myricetin* (Comahli *et al.,* 2020), *indomethacin* (Chaudhry *et al.,* 1983), *Sulindac* (Chaudry *et al.,* 1983; Zheng *et al.,* 2012), *phloretin* (Sampath *et al.,* 2016).

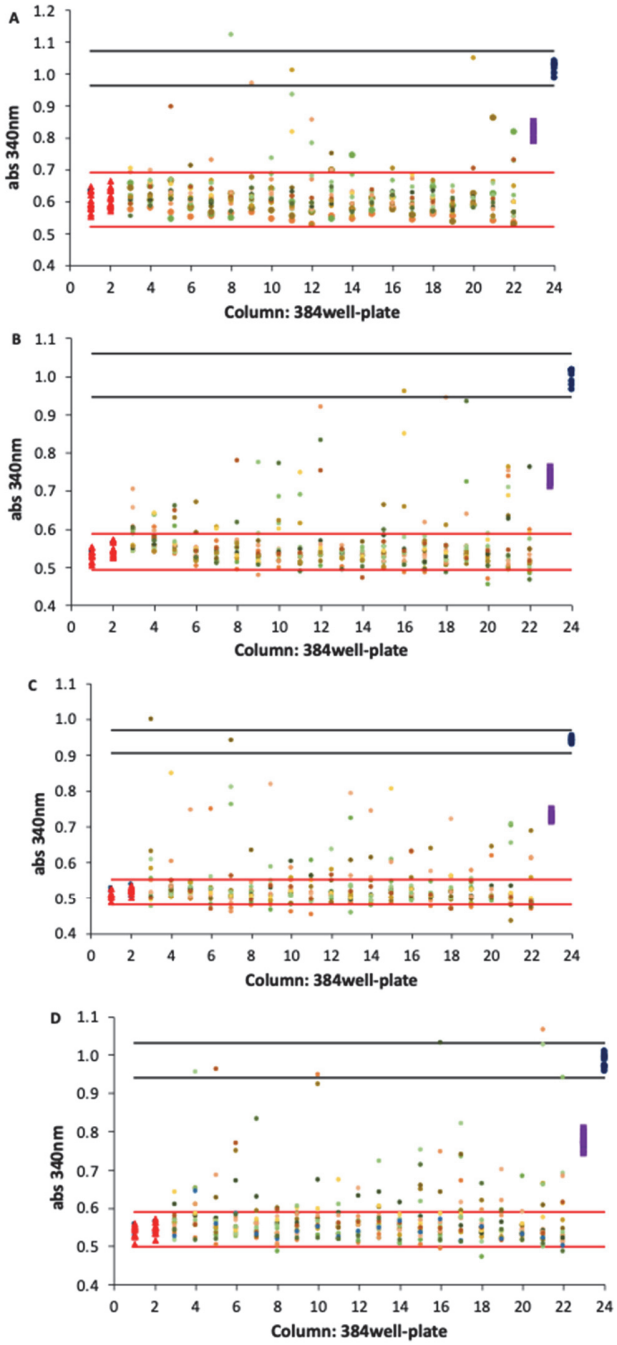

Figure 4. 26: HTS of LOPAC. The absorbance at 340 nm measured after 22 min is reported for each well for the four LOPAC plates (**Panel A**, plate P1401; **Panel B**, plate P1402; **Panel C**, plate P1403; **Panel D**, plate P1404). Each column includes 16 wells. For each panel, wells from columns 1 and 2 (red symbols) refer to enzyme activity in the absence of inhibitor; wells from column 24 refer to blank values (blue symbols); wells from colum 23 refer to the AKR1B1 activity measured in the presence of 1µM Sorbinil (purple). Each well of all other columns refers to a single different compound of LOPAC present at a final concentration in the assay of 20 µM. The intervals delimited by black and red lines represent 3-fold the standard deviation of blank and activity measurements, respectively. These two intervals are defined by assay values calculated from the mean of columns 1 and 2 and from colum 24, respectively.

The 89 compounds selected were then tested again towards L-idose and HNE. Two plates contained, in addition to the 89 HITS to be validated, 16 wells for blank measurements, 32 wells for AKR1B1 activity measurements and 8 wells for 1 µM Sorbinil effect evaluation. Results are reported in Fig. 4.28 and in Appendix, Table 2B. For L-idose, data obtained in the initial screen were essentially confirmed. In fact, a difference in the inhibitory effect not higher than 15%, with respect to the first measurement was observed, except for 8 compounds which showed a difference in the inhibitory effect of approximately 20%. Among the 89 compounds, 8 did not show a significant differential inhibitory effect (lower than 10%) between L-idose and HNE, 14 appeared to inhibit HNE reduction more than L-idose reduction. The remaining 13 compounds displayed a differential inhibition of L-idose reduction with respect to HNE reduction between 15% and 44%.

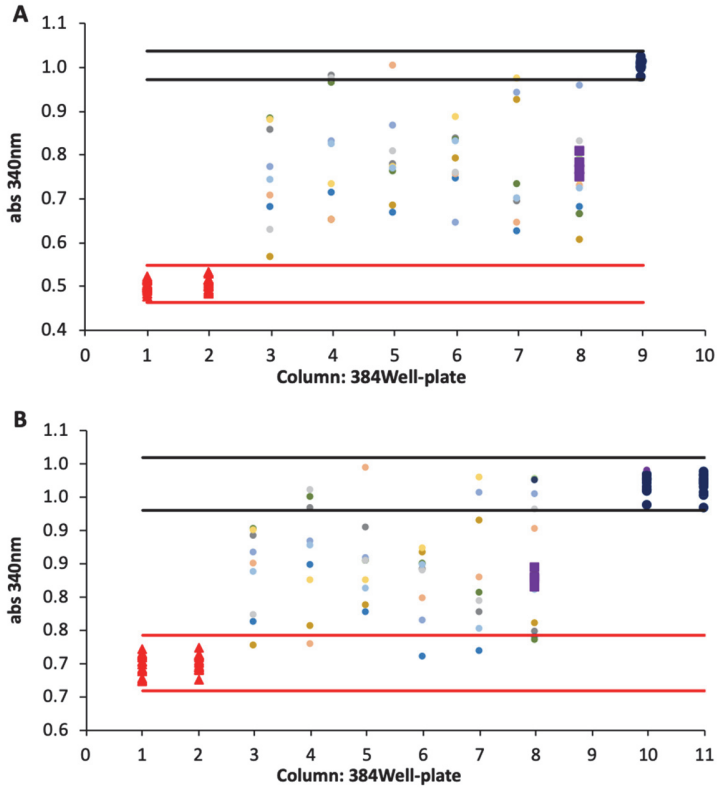

Figure 4. 27:Evaluation of differential inhibitory action of selected compounds. The absorbance at 340 nm measured after 22 min is reported for each well for the 89 compounds (**Panel A**, plate tested with L-idose as substrate; **Panel B**, plate tested with HNE as substrate). Each column includes 16 wells. For each panel, wells from columns 1 and 2 (red symbols) refer to enzyme activity in the absence of inhibitor; wells from column 9, 10 and 11 refer to blank values (blue symbols); wells from colum 8 refer to the AKR1B1 activity measured in the presence of 1µM Sorbinil (purple symbols). Each well of all other columns refers to a single different compound of the 89 selected at a final concentration in the assay of 20 µM. The intervals delimited by black and red lines represent 3-fold the standard deviation of blank and activity measurements, respectively. These two intervals are defined by assay values calculated from the mean of columns 1 and 2 and from colum 9, 10 and 11, respectively.

Of the nine compounds with the highest differential inhibitory activity between L-idose and HNE (Table 4.3), four were selected for further characterization.

Compound	CAS number	% Inhibition L-Idose	% Inhibition HNE	Delta %L-Idose - %HNE
1	362-07-2	46.61	23.13	15.31
2	199666-03-0	47.87	3.79	44.31
3	1852-38-6	30.85	8.70	21.09
4	90357-06-5	34.91	14.80	22.76
5	136790-76-6	29.23	10.45	16.53
6	426834-69-7	40.83	25.32	10.83
7	567-02-2	40.85	18.26	15.28
8	138091-43-7	25.55	3.20	25.29
9	145040-37-5	31.45	12.57	16.34

Table 4. 3: Percent inhibition of the 9 compounds with the best differential inhibition. The Table indicates the percent inhibition of the 9 compounds identified by the HTS with L-Idose and HNE calculated at 22 minutes. For each compound the delta of inhibition between L-Idose and HNE was calculated. The compounds selected for further characterization are shown in red.

4.7 Kinetic characterization of ARDIs HITS identified in the LOPAC.

4.7.1 Evidence for differential inhibition of AKR1B1-dependent reactions

Four of the nine compounds emerging from LOPAC-HTS as ARDIs, displaying a differential inhibition of at least 11% (red items in Table 4.3) were selected for further kinetic characterization. The compounds, namely: 2-methoxyestradiol (**Compound 1**) 3,4-dimethoxy-N-(4-(3-nitrophenyl)thiazol-2-yl)benzenesulfonamide (**Compound 2**), pregnenolone-sulfate (**Compound 3**) and bicalutamide (CDX) (**Compound 4**), all commercially available, were chosen essentially taking into account the effectiveness as ARDIs (as reported in Tab.4.3) over the item cost. The structures of these compounds are shown in Fig. 4.29.

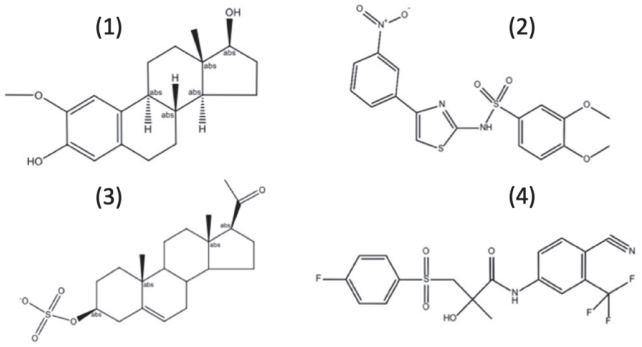

Figure 4. 28: Structure representation of the selected inhibitors. Structure representation of compounds **1** to **4** undergoing kinetic characterization.

All these molecules have already been highlighted to be involved in different physio pathological situations. Compound **1** is a natural derivative of estradiol generated by sequential hydroxylation and O-methylation at the 2-position (Ba *et al.,* 2019). It is an inhibitor of angiogenesis (Fotsis *et al.,* 1994) and endothelial cells proliferation (Pribluda *et al.,* 2000) and was investigated as an anticancer drug in the hepatocellular carcinoma (Tao *et al.,* 2019).

Compound **2** was reported as an inhibitor of kynurenine 3-monooxygenase. This enzyme, which catalyzes the insertion of molecular oxygen into the aromatic ring of kynurenine to produce 3-hydroxy-L-kynurenine, is a potential target for the development of immunological, neurodegenerative and neuroinflammatory diseases, such as Huntington's, Alzheimer's and Parkinson's diseases (Gao *et al.,* 2018; Smith *et al.,* 2016). Compound **3** is a neurosteroid that antagonizes the GABA-A receptor chloride channels (Harteneck, 2013) and is used for its neuropharmacological actions in memory enhancement (Lee *et al.,* 2010). Finally, compound **4,** is a synthetic, non-steroidal androgen, which competitively binds to cytosolic androgen receptors in target tissues. It is commonly used for the treatment of prostate cancer (Schellhammer and Davis, 2004; Wellington and Keam, 2006) and, more recently, also to treat androgen receptor - positive, estrogen receptor and progesterone receptor-negative metastatic breast cancer (Gucalp *et al.,* 2013).

The characterization of these molecules as inhibitors of human recombinant AKR1B1 was conducted through a preliminary dose response evaluation of the initial reduction rate of L-idose, HNE and GSHNE catalyzed by the enzyme at different concentrations of the inhibitor, performed by spectrophotometric determinations. A steady state analytical approach of the enzyme inhibition

was then performed. The inhibitory effect of the selected compounds towards L-idose, HNE and GSHNE reduction is reported in Fig. 4.30.

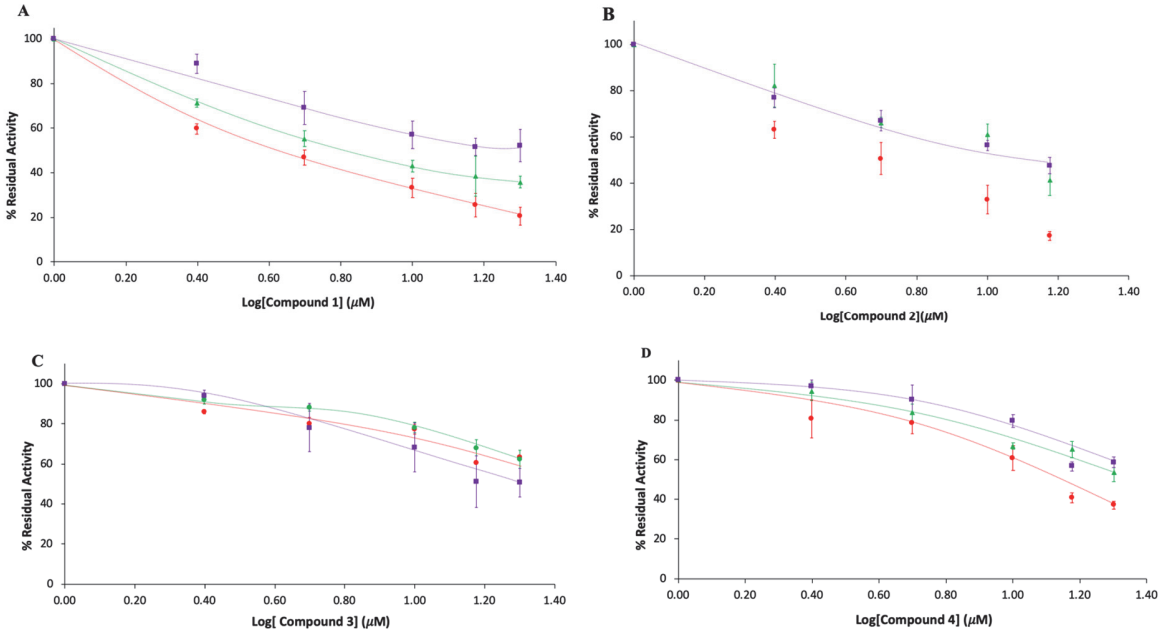

Figure 4. 29: Inhibitory effect of selected compounds on human recombinant AKR1B1 activity. The inhibitory effect at different concentrations was evaluated using 0.8 mM L-idose (red circles), or 40 µM HNE (green triangles) or 100 µM GSHNE (purple squares) as substrates. **Panels A**, **B**, **C** and **D**, refer to compounds **1**, **2**, **3** and **4**, respectively. The percent residual activity is presented ias a function of the concentration of the inhibitor (µM). Bars (when not visible are within the symbol size) represent the standard deviations of the mean from at least 3 independent measurements.

The resulting IC_{50} values are reported in Table 4.4.

Substrate	**IC_{50} (µM)**			
	Compound 1	**Compound 2**	**Compound 3**	**Compound 4**
L-idose	5.0 (3.3-7.6)	5.0 (2.9-8.6)	27.9 (20.7-39.0)	12.1 (10.1-14.4)
HNE	8.2 (5.7-11.9)	12.3 (8.6-17.8)	33.5 (30.1-37.4)	24.4 (19.9-30.4)
GSHNE	16.1 (11.8-22.4)	12.1 (8.6-17.5)	19.5 (15.5-24.9)	28.6 (19.2-45.6)

Table 4. 4: IC_{50} value of the 4 compounds. The Table shows the IC_{50} value of the 4 compounds tested with L-idose, HNE and GSHNE. In parenthesis intervals of confidence of the mean are reported. IC_{50} determination was performed using standard statistical software using the One site- Fit logIC_{50} carried out with Graphpad Prism Version 8.4.3.

These results confirmed, except for compound **3**, the ability of the tested compounds to differentially inhibit the reduction of L-idose compared to HNE as observed in the HTS. Here, while compounds **1** and **2** displayed the same effectiveness on L-idose reduction, compound **2**

appeared more effective as ARDI with a differential inhibition (L-idose *versus* HNE reduction) of 28 %. Compound **4**, despite less efficient toward all substrates compared to compounds **1** and **2**, resulted in a differential action on L-idose versus HNE. Finally, for all these compounds the inhibitory effect on GSHNE appeared significantly less potent than what observed for L-idose.

Concerning compound **3,** it was identified by the HTS as a differential inhibitor between L-idose and HNE reduction (Table 4.4); however, no evidence of this feature resulted from the IC_{50} evaluation data (Fig 4.30). Indeed, for this compound a modest, but significant preferential inhibition of GSHNE compared to both L-idose and HNE ($p<0.05$) was observed.

4.7.2 Inhibition kinetic analysis

The inhibitory features of the four selected compounds (**1-4**) towards L-idose, HNE and GSHNE reduction were evaluated by measuring the initial rate of reduction at different substrate concentrations and at different inhibitors concentrations. The rate measurements were analyzed by the Hanes-Wolff plot. The apparent kinetic constants K_i and K'_i (which refer to the dissociation constant of EI and ESI complexes, respectively) were determined by secondary plots in which ${}^{app}K_M/{}^{app}V_{max}$ and $1/{}^{app}V_{max}$ values, resulting from the primary Hanes plot, were analyzed as a function of the inhibitor concentration. The results for compounds **1**, **2**, **3** and **4** are shown in Figs. 4.31, 4.32, 4.33 and 4.34, respectively.

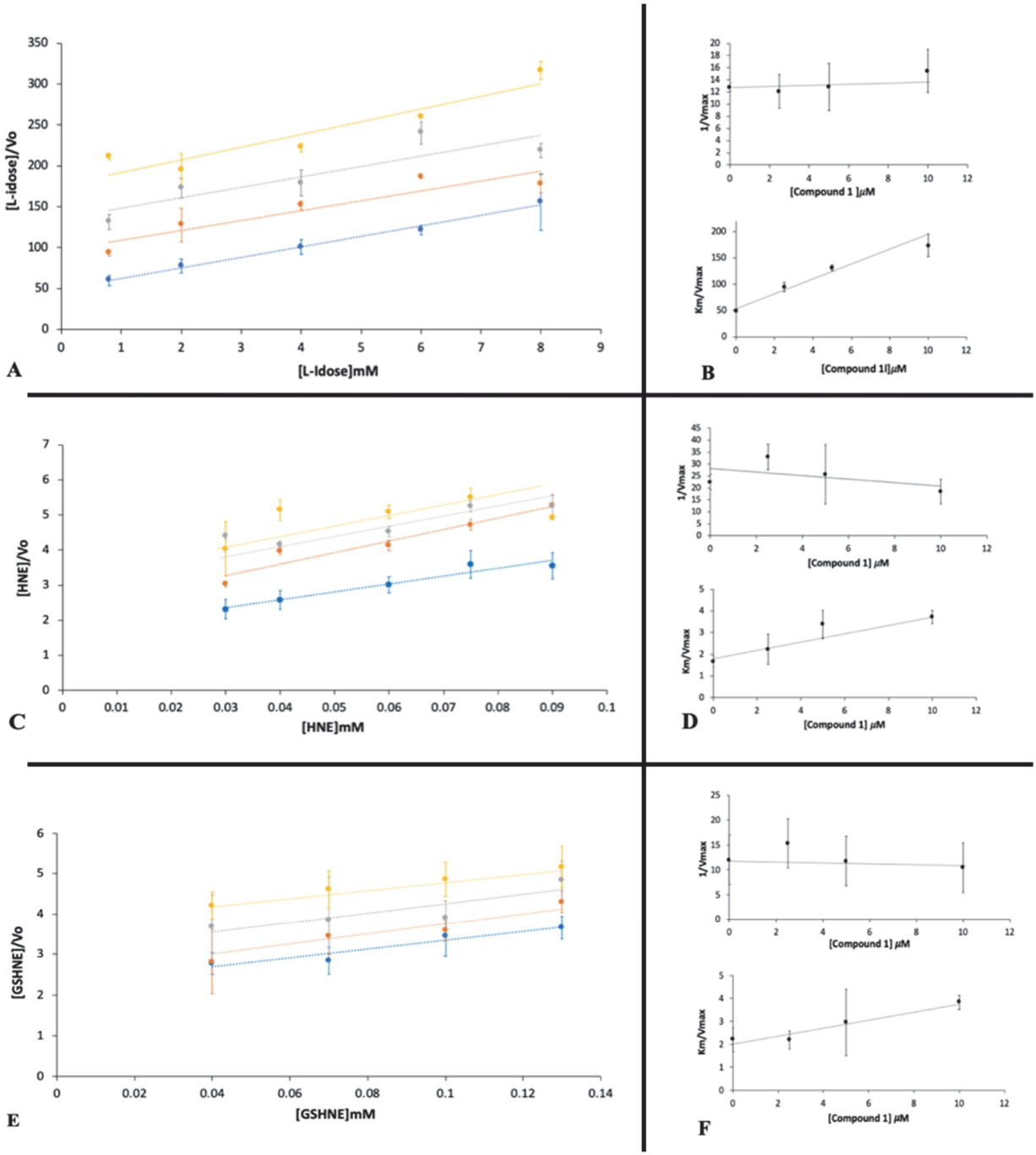

Figure 4. 30: Kinetic characterization of compound 1 as an AKR1B1 inhibitor. Panel A, **Panel C** and **Panel E** are the Hanes-Woolf plots obtained when the activity of the purified enzyme (10 mU) was measured at the indicated concentrations of L-idose, HNE and GSHNE as substrates, in the absence (blue) or in the presence of the following inhibitor concentrations: 2.5 µM (orange), 5 µM (grey) and 10 µM (yellow). **Panel B**, **Panel D** and **Panel F** refer to the secondary plots of the slopes ($1/^{app}Vmax$) and the ordinate intercept ($^{(app}K_M/^{app}V_{max}$) of the relative primary plot, as a function of the inhibitor concentration. Panel A and Panel B refer to L-idose; **Panel C** and **Panel D** refer to HNE; **Panel E** and **Panel F** refer to GSHNE. Bars (when not visible are within the symbol size) represent the standard deviations of the mean from at least three independent measurements.

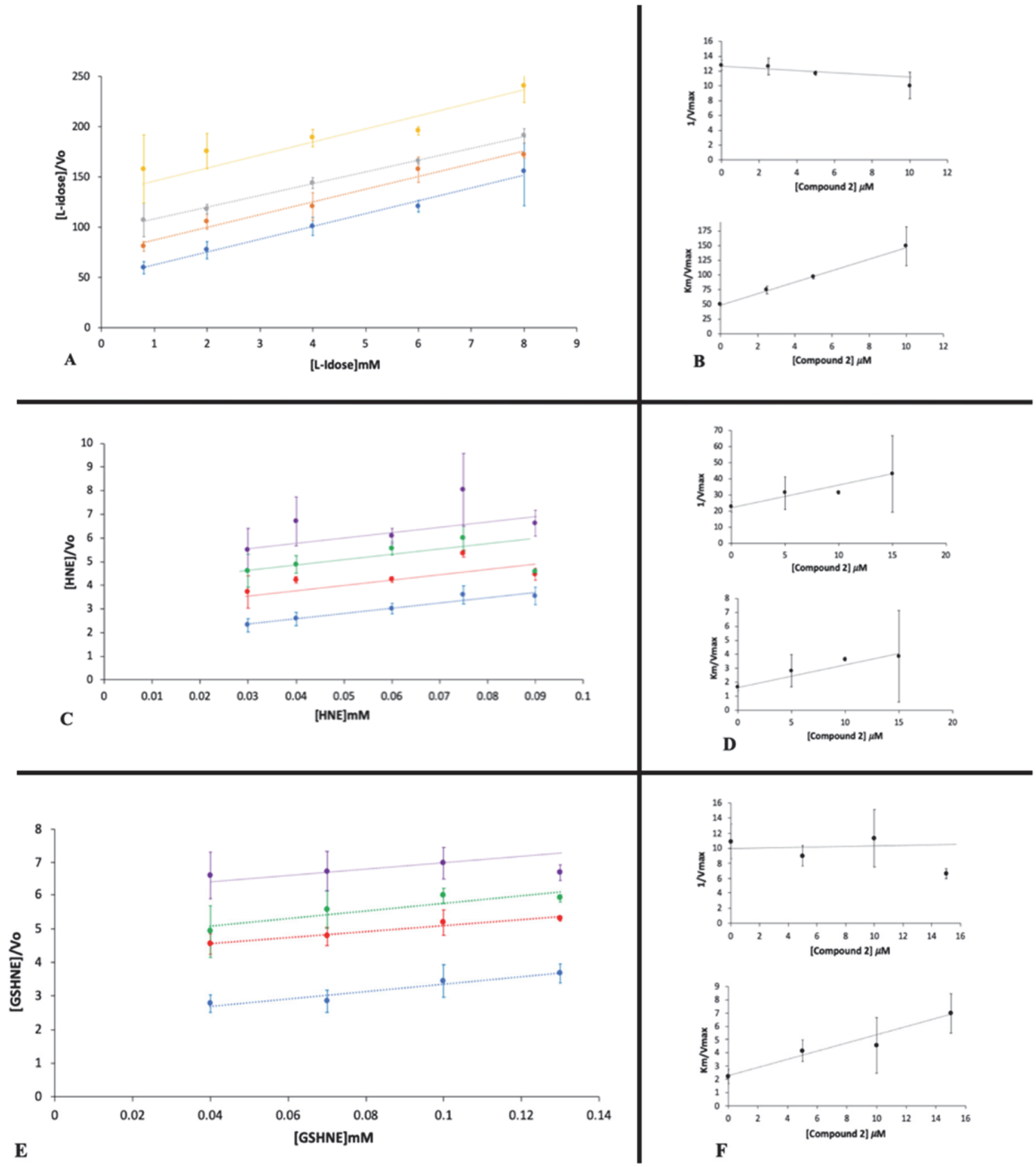

Figure 4. 31: Kinetic characterization of compound 2 as an AKR1B1 inhibitor. Panel A, **Panel C** and **Panel E** are the Hanes-Woolf plots obtained when the activity of the purified enzyme (10 mU) was measured at the indicated concentrations of L-idose, HNE and GSHNE as substrates, in the absence (blue) or in the presence of the following inhibitor concentrations: 2.5 µM (orange), 5 µM (grey) and 10 µM (yellow) for **Panel A**; 5µM (red), 10 µM (green) and 15 µM (purple) **Panel C** and **E** . **Panel B**, **Panel D** and **Panel F** refer to the secondary plots of the slopes (1/appVmax) and the ordinate intercept ($^{app}K_M/^{app}V_{max}$) of the relative primary plot, as a function of the inhibitor concentration. **Panel A** and **Panel B** refer to L-idose; **Panel C** and **Panel D** refer to HNE; **Panel E** and **Panel F** refer to GSHNE. Bars (when not visible are within the symbol size) represent the standard deviations of the mean from at least three independent measurements.

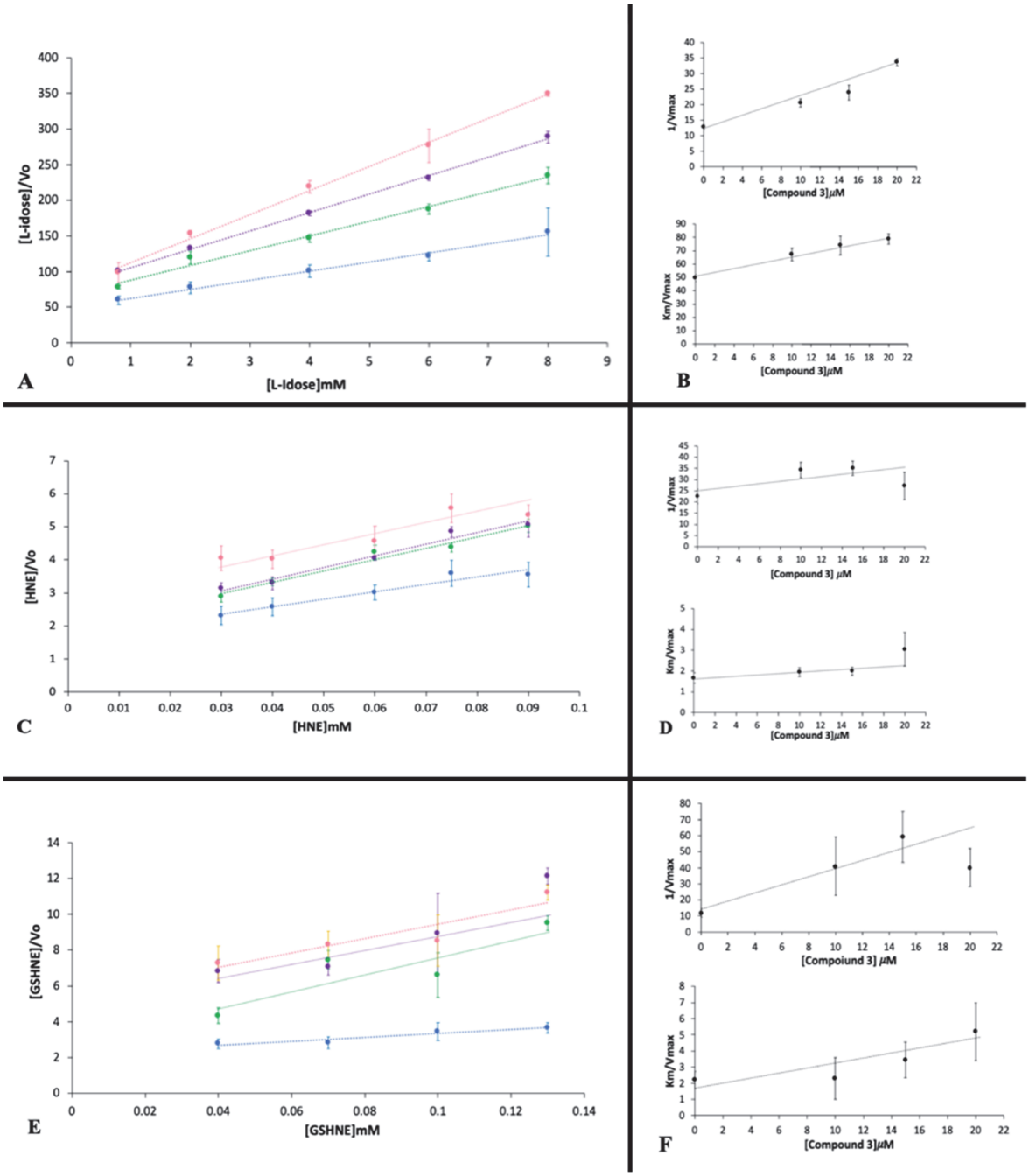

Figure 4. 32: Kinetic characterization of compound 3 as an AKR1B1 inhibitor. Panel A, **Panel C** and **Panel E** are the Hanes-Woolf plots obtained when the activity of the purified enzyme (10 mU) was measured at the indicated concentrations of L-idose, HNE and GSHNE as substrates, in the absence (blue) or in the presence of the following inhibitor concentrations: 10 µM (green), 15 µM (purple) and 20 µM (pink) for **Panel A**, **C** and **E**. **Panel B**, **Panel D** and **Panel F** refer to the secondary plots of the slopes ($1/^{app}V_{max}$) and the ordinate intercept ($^{app}K_M/^{app}V_{max}$) of the relative primary plot, as a function of the inhibitor concentration. **Panel A** and **Panel B** refer to L-idose; **Panel C** and **Panel D** refer to HNE; **Panel E** and **Panel F** refer to GSHNE. Bars (when not visible are within the symbol size) represent the standard deviations of the mean from at least three independent measurements.

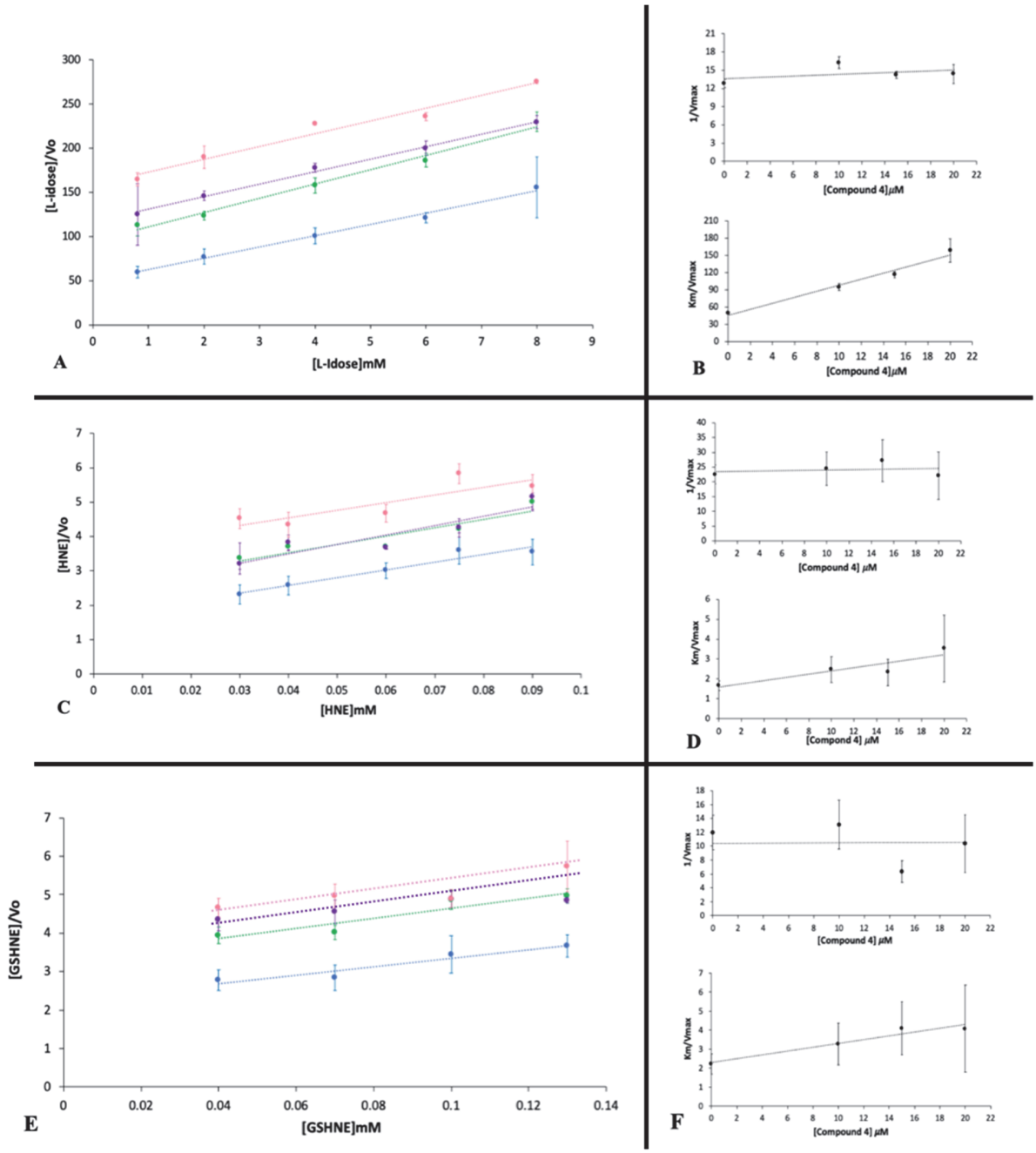

Figure 4. 33: Kinetic characterization of compound 4 as an AKR1B1 inhibitor. Panel A, **Panel C** and **Panel E** are the Hanes-Woolf plots obtained when the activity of the purified enzyme (10 mU) was measured at the indicated concentrations of L-idose, HNE and GSHNE as substrates, in the absence (blue) or in the presence of the following inhibitor concentrations: 10 μM (green), 15 μM (purple) and 20 μM (pink) for **Panel A**, **C** and **E**. **Panel B**, **Panel D** and **Panel F** refer to the secondary plots of the slopes ($1/^{app}V_{max}$) and the ordinate intercept ($^{app}K_M/^{app}V_{max}$) of the relative primary plot, as a function of the inhibitor concentration. **Panel A** and **Panel B** refer to L-idose; **Panel C** and **Panel D** refer to HNE; **Panel E** and **Panel F** refer to GSHNE. Bars (when not visible are within the symbol size) represent the standard deviations of the mean from at least three independent measurements.

The results of the kinetic analysis are summarized in Table 4.5.

Substrate	Compound 1		Compound 2		Compound 3		Compound 4	
	K_i	K'_i	K_i	K'_i	K_i	K'_i	K_i	K'_i
L-idose	5±0.1	n.d.	5 ± 0.1	n.d.	34±2	12±1	9 ± 0.5	n.d.
HNE	13±0.2	n.d.	13 ± 0.7	19 +2	28± 8	n.d.	20±2	24 ± 3
GSHNE	12±1	n.d.	9 ± 2	n.d.	12±1	9+3	23±2	n.d.

Table 4. 5: Apparent inhibition constants of AKR1B1 inhibitors selected by LOPAC-HTS. Abbreviation n.d: not determined.

Despite their marked structural differences, compounds **1**, **2** and **4** displayed a competitive type of inhibition towards the reduction of both L-idose and GSHNE, with apparent kinetic constants in line with the preferential targeting of L-idose reduction ($^{app}K_i$ two to three fold lower than the $^{app}K_i$ for GSHNE reduction). For these compounds, HNE resulted to be the substrate less affected (inhibition constants 2.5 fold higher than those measured for L-idose), with a mixed (compounds **2** and **4**) or competitive (compound **1**) mechanism of action. Compound **3** was confirmed as the least potent among the four compounds, acting as mixed inhibitor toward L-idose and GSHNE and as competitive inhibitor toward HNE.

4.8 HLEC viability with LOPAC HITS

The cytotoxicity of the four selected inhibitors was tested on HLEC, as described in the Section 3.18. Figure 4.35 reports the effect on HLEC viability of both 24 and 48 h incubation in the presence of different concentrations of compounds **1-4**. No significant effects were observed, except for compounds **1** and **2**, which appeared to significantly affect cell viability. In fact, for compound **1** and **2** a decrease of approximately 31 % and 16 % of cell viability, respectively was observed after 48 h of incubation with respect to control cells.

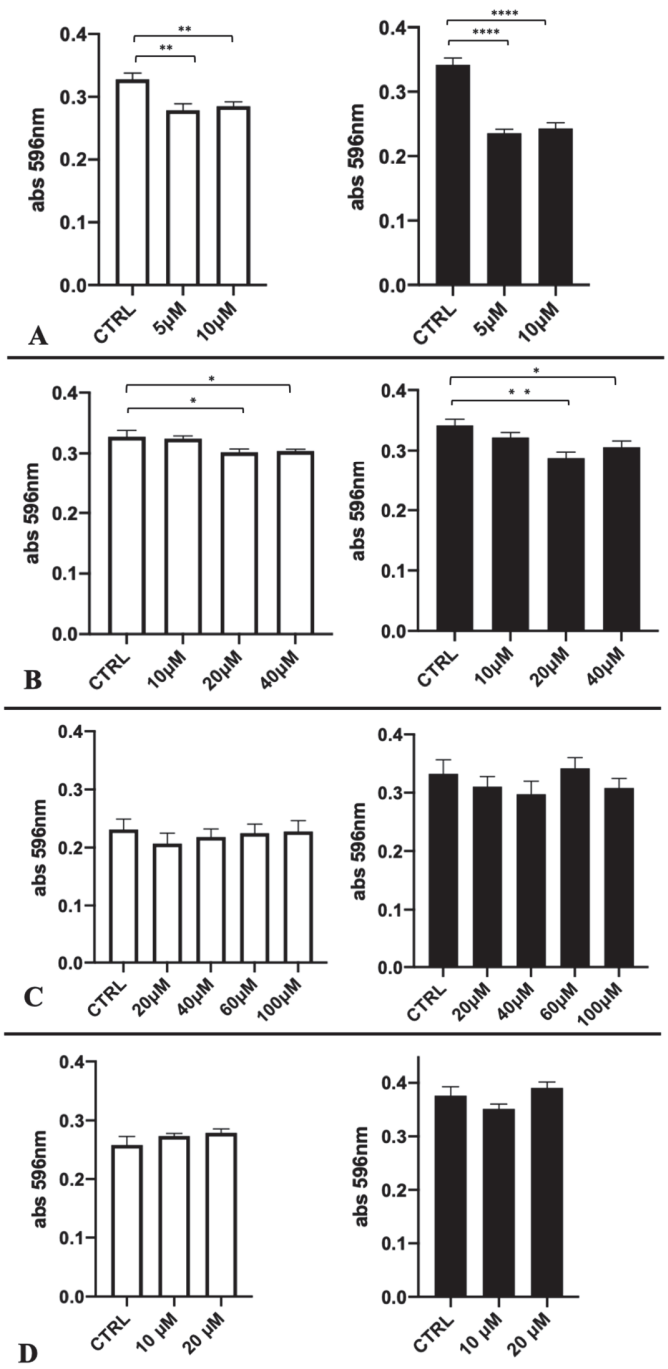

Figure 4. 35: Effect of compounds 1-4 on HLEC. HLEC were incubated alone (CTRL) or in the presence of the indicated concentrations of the following compounds: **1** (Panel A), **2** (Panel B), **3** (Panel C), **4** (Panel D). The incubation was performed **f**or 24 (white histograms) or 48 h (black histograms)**. T**he absorbance at 596 nm is reported as a measure of cell viability (see Section 3.18 for details). Bars refer to the standard error of the mean from at least 4 independent experiments. The statistical significance is shown by the asterisks: (****): p<0.0001; (**): p<0.01; (*): p<0.05;

4.9 HEK-293 cells transient transfection and TNF-alpha stimulation

HEK-293 cells were transiently transfected with the pRenilla and p5XIP10KB plasmid (see Section 3.13) and treated with TNF-alpha. The NF-*k*B expression as a consequence of the treatment was evaluated by a Dual-Luciferase assay kit 2.0 (see Section 3.13). Results are reported di in Fig. 4.36. A statistically significant increase of the ratio Firefly/Renilla Luciferase luminescence of 1.7, 2.2 and 2.4 fold for treated cells with respect to control cells was observed along with the increase in the TNF-alpha concentration used.

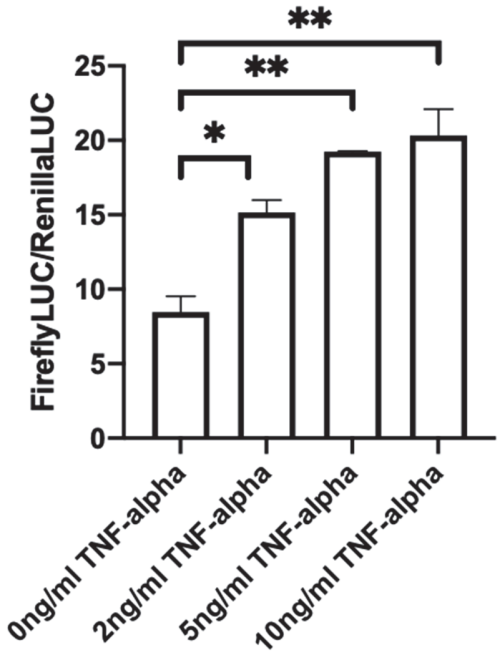

Figure 4. 36: Ratio of Firefly Luciferase over Renilla Luciferase activity in HEK-293 cells stimulated with TNF-alpha. The histograms represent the ratio between the luminescence product by the Firefly Luciferase over the Renilla Luciferase in HEK293 cells stably transfected with pRenillaLuc and p5XIP10kB (see section 3.13) and treated with different concentration of TNF-alpha. Bars (when not visible are within the symbol size) represent the standard error of the mean of two independent measurements. The significance of the analysis is shown by the asterisks: (**): $p<0.01$; (*): $p<0.05$.

4.10 Effect of TNF-alpha on transfected HLEC

HLEC were transiently transfected with the pRenilla and pFireflyLuc2P plasmid (see Section 3.16) and treated with TNF-alpha. The NF-kB expression as a consequence of the treatment was evaluated by a Dual-Luciferase assay (see Section 3.16). Results are reported di in Fig. 4.37. A statistically significant ($p<0.0001$) increase of the ratio Firefly/Renilla Luciferase luminescence of 1.6 for treated cells with respect to control cells was observed.

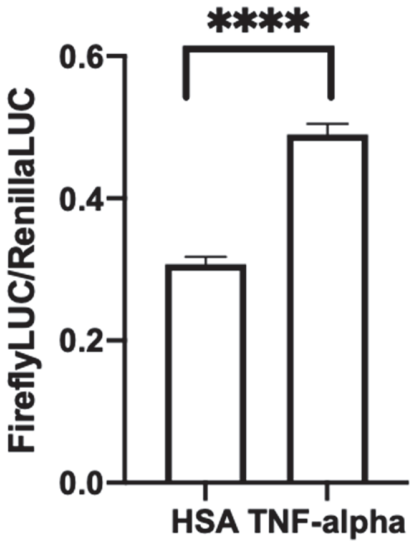

Figure 4. 34: Effect of TNF-alpha on transiently transfected HLEC. The histograms represent the ratio between the luminescence product by the Firefly Luciferase over the Renilla Luciferase in HLEC transiently transfected with pRenillaLuc and pFireflyLuc2P (see Section 3.16) and treated with either 0.2nM of HAS or TNF-alpha. Bars (when not visible are within the symbol size) represent the standard error of the mean of four independent experiments. The significance of the analysis is shown by the asterisks: (****): $p<0.0001$.

The same experiment was performed using the HLEC stably transfected with pFireflyLuc2P plasmid (see Section 3.17). The NF-*k*B expression as a consequence of the treatment was evaluated by a Luciferase assay System assay (see Section 3.17). Results are reported in Fig. 4.38. A statistically significant ($p<0.0001$) increase of the mol of Firefly Luciferase l/mg of total protein of 1.7 for treated cells with respect to control cells was observed.

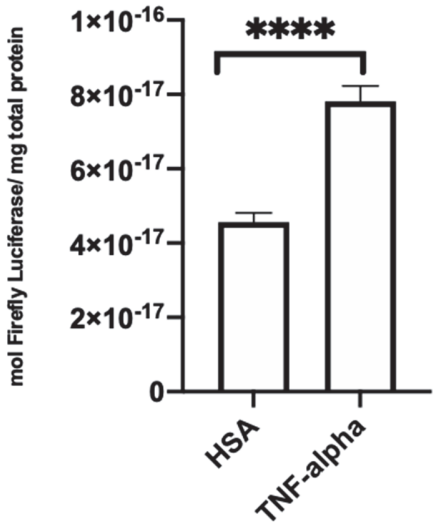

Figure 4. 35: Effect of TNF-alpha on HLEC stably transfected with pRenilla and pFireflyLuc2P. HLEC stably transfected with pRenilla and pFireflyLuc2P (see Section 3.17) were the histograms represent the ratio between the mol of Firefly Luciferase over the mg of total proteins in cells treated either with 0.2nM of HSA or TNF-alpha. Bars represent the standard error of the mean. The significance of the analysis is shown by the asterisks: (****): $p<0.0001$.

6. DISCUSSION AND CONCLUSION

Aldose reductase (AKR1B1), a NADPH-dependent reductase, is the first enzyme of the so-called "*polyol pathway*", in which glucose is converted into sorbitol, and then to fructose by sorbitol dehydrogenase, a NAD^+-dependent enzyme. The increased polyol flux occurring in hyperglycemic conditions is considered a relevant co-causative factor for the onset of secondary complications of diabetes. For this reason, AKR1B1 has been studied for decades a potential target of drugs able to inhibit its activity and counteract or delay the development of secondary diabetes complications. The partial failure of the clinical trials of potent AKR1B1 inhibitors, together with the evidence of multiple metabolic functions of the enzyme, raised the question of the real relevance of a complete inhibition of the enzyme. Thus, a new approach for AKR1B1 inhibition has been proposed (Del Corso *et al.,* 2013), aimed at inhibiting the enzyme depending on the substrate undergoing reduction. This type of inhibitors, defined as differential inhibitors of AKR1B1 (ARDIs), should be able to inhibit the enzyme when acting on glucose, thus reducing the accumulation of sorbitol in the cell, leaving unaffected the detoxifying ability of the enzyme.

Analysis of hydrophobic components of *Zolfino* beans, as those present in a methanolic extract, recently revealed the presence of Soyasaponins, able to act as ARDIs (Balestri *et al.,* 2019). In this thesis the presence of molecules able to act as ARDIs in a water extract of *Zolfino* beans was investigated. Zolfino bean has been described as a source of compounds, such as flavonoids, known to affect AKR1B1 activity (Dinelli *et al.,* 2006). Indeed, the water extract of Zolfino appeared to efficiently impair AKR1B1 activity, despite, when evaluating a differential effect, no detection of differences of inhibitory effect measured on the reduction of L-idose compared to the reduction of HNE (Fig.4.2). The requirement of a fractionation step of the extract in order to reveal the presence of ARDIs has been already demonstrated in the case of green tea (Balestri *et al*., 2020) and it may be considered common for extracts in which the high abundance of canonical and potent AKR1B1 inhibitors may mask the presence of lower abundance of ARDIs.

Indeed, aqueous *Zolfino* extract fractionation by both an anionic exchange approach and a hydrophobic interaction approach resulted useful in revealing several components able to exert an AKR1B1 differential inhibition. However, because of the high instability in terms of inhibitory activity of the components separated by anionic exchange chromatographic fractionation, only components isolated by hydrophobic chromatography were further investigated. The analysis through the hydrophobic C18 interactive support revealed that, despite the use of an aqueous

extract, components with appreciable hydrophobic features (i.e. eluting with 25 to 50% methanol) can be underlined. This is consistent with the abundance of partially hydrophilic species, such as glycosylated flavonoids, reported for beans extracts (Lin *et al.,* 2008).

In particular, components collected as the very last species eluting with 25 % methanol ("*Fraction X*" Fig.4.6), were characterized by a complete ineffectiveness on HNE reduction and by a significant (16 + 2%) differential inhibition of L-idose reduction. The stability of "*Fraction* X" upon storage made these components valuable for further characterization.

The dose-response curve obtained for a pool of "*Fraction X*" derived from different chromatographies revealed that the inhibitory effect on HNE reduction did not exceed 6%, while the effect on L-Idose reduction progressively increased, reaching a plateau of approximately 24%. No further increase in inhibition was observed at higher concentrations. of "*Fraction X*". These data are consistent with "*Fraction X*" being an incomplete AKR1B1 inhibitor, a feature already reported for the hemiacetalic form of aldoses (Balestri *et. al.,* 2015b). A preliminary analysis, conducted through an additional C18 step performed on "*Fraction X*" (Fig. 4.10), clearly indicated that components possessing ARDI features can be successfully further separated from non-ARDI components. Therefore, an attempt to identify molecular species present in "*Fraction X*" was conducted through a mass spectrometry approach, together with a comparative analysis of components present in the two adjacent (in terms of elution volume) fractions with respect to "*Fraction X*" (Fig 4.12 and 4.13). Unexpectedly, the analysis revealed the presence in "*Fraction X*" of a single molecular component and no differences were observed with respect to adjacent fractions. This result hardly fitted with the completely different inhibitory pattern observed for adjacent fractions (i.e. the absence of differential action), unless the presence of trace amounts of components, acting as classical AKR1B1 inhibitors, were not detected by the mass spectrum analysis. The compound present in "*Fraction X*" was tentatively identified as leucoside (kaempferol 3-O-β-D-glucopyranoside-(2→1)-O-β-D-xylopyranoside) a glycosylated kaempferol whose presence in Zolfino has been reported (Dinelli et *al.* 2006). Other molecules with different glycosidic moieties still compatible with the same mass of leucoside may account as the "*Fraction X*". Indeed, the possibility of arabinose as pentose representing the glycosyl portion of glycosylated flavonoids exits. For example the presence of a quercetin arabino-(1-6)glucoside has been reported (Abu-Reidah *et al.,* 2013). An attempt to univocally determine the chemical structure of the compound present in "*Fraction X*" through NMR failed, due to the very low amount of sample.

The analysis performed on the leucoside, the unique kaempferol derivative commercially available with features fitting the MS analysis, did not reveal any appreciable differential inhibitory activity (Fig 4.18). This left open the problem of structure attribution to the disclosed ARDI; this problem may find a solution, beside through chemical synthesis, by scaling up the preparative isolation approach of the compound. The clarification of the molecular structure will obviously shed light on the specific structural requirements leading the classical inhibitory action of the aglycone scaffold of a flavonoid as kaempferol to become a differential inhibitor.

The section of this thesis work devoted to set up an effective approach to reveal ARDIs among known compounds of chemical synthesis and eventually available on the market, was mainly realized during the 6 months abroad period spent in the Department of Biochemistry and Molecular Biology at Indiana University, under the supervision of Professor Anna DePaoli-Roach and Professor Peter J. Roach. An HTS was performed of a library (LOPAC) of 1280 small molecules known to affect several signaling pathway and to exert different pharmacological actions through their ability to interact with different molecular targets. In order to test the ability of LOPAC molecules to affect AKR1B1 activity, an optimization of the enzyme assay under conditions suitable for the HTS was necessary. In fact, the HTS was conducted with an automatic system making use of 384-well plates, which implied a 14-fold reduction of the assay volume and a 5-fold increase of the duration compared to the conditions used in the classical spectrophotometric assay. Thus, enzyme, cofactor and substrates concentrations were defined in order to guarantee the optimal responsiveness of the assay to different components (Figs. 4.20, 4.23, 4.25). Once assay conditions for the HTS had been established, the quality of the measurements was assessed through the evaluation of Z' score; for all the measurements a Z' score never lower than 0.67 was obtained. A first screening of the inhibitory effect of the 1280 compounds of LOPAC was conducted using L-idose as substrate. This allowed the selection of 89 compounds (see Appendix Table 2B), with an inhibitory effect on L-idose reduction ranging from 25 to 95% (Fig. 4.27). Among them, compounds already shown to be AKR1B1 inhibitors were present; this undoubtedly confirmed the validity of the HTS to identify AKR1B1 inhibitors. The 89 compounds were validated through a further assay of their effect on L-idose reduction and then tested for their effect on HNE reduction (Fig. 4.28). For approximately 90% of the 89 selected hits, the results obtained in the initial screen, in terms of L-idose inhibition, were essentially confirmed; in fact, the observed differences in the inhibition values were within 15%. When the differential effect between L-idose and HNE

reduction was considered, it turned out that for 13 out of the 89 compounds a differential inhibition of L-idose reduction with respect to HNE reduction between 15% and 44% was observed. The remaining compounds were either ineffective as ARDIs (i.e. the differential effect was lower than 15%) or even more active on HNE reduction compared to L-idose. The latter compounds did not fit with the feature required for an ARDI with potential pharmacological relevance; however future work might be focused on a deep analysis of their structural features to obtain useful information to facilitate future ARDIs selection. Among the nine compounds showing the highest differential inhibitory activity between L-idose and HNE (Table 4.3), four were selected (compounds **1-4)** on the basis of both their effectiveness and cost and further characterized, through classical spectrophotometric measurements (section 3.2) in order to evaluate their potency and their mechanisms of action. In this case, in addition to L-idose and HNE, also GSHNE was used as substrate (figs. 4.30; Table 4.4). Preliminary evidence confirming for the four hits, except for compound **3**, the ability to act as ARDIs, came from the IC_{50} evaluation (Table 4.4). However more relevant considerations could be derived from the comparison of ES and ESI dissociation constants measured for different substrates Thus, it resulted that compounds **1**, **2** and **4** were able to differentially inhibit L-idose reduction compare to HNE, with inhibition constants for the latter substrate approximately 2.5-fold higher than the former. Among them, compound **2** is the most effective toward GSHNE reduction, thus the most relevant in terms of a potential anti-inflammatory action. Interestingly, compounds **1**, **2**, and **4**, despite their marked structural differences, all acted as competitive inhibitors in the reduction of both L-idose and GSHNE. Finally, compound **3** not only was the least potent among the four compounds, but also was devoid of any differential action between L-idose and HNE, being even less potent in inhibiting the reduction of the aldose than the hydrophobic aldehyde. Compound **3** is the only inhibitor, among the four selected, that acts on L-idose as a mixed non-competitive inhibitor, with a prevailing affinity toward the ESI complex ($^{app}K'_i$ approximately 3 fold lower than $^{app}K_i$). Thus, it is possible that the HTS assay conditions, that compared to the classical assay had a comparable substrate concentration but a ratio enzyme/substrate at least 4.5-fold higher, might have favored L-idose inhibition, through an increased level of the ES complex. In any case, compound **3** displayed an appreciable ability to inhibit GSHNE reduction, thus possessing potential anti-inflammatory features.

The final specific aim to verify the potential of the selected inhibitor in an *ex vivo* cell system could not be accomplished because the lack of time. Nevertheless, the tools necessary to accomplish this aspect of the study have been optimized. In particular, a preliminary evaluation of the ability of compounds **1-4** to affect cell viability was performed, using cultured Human Lens Epithelial Cells as cellular model (Fig. 4.35). No significant effect was observed for compounds **3** and **4**, at least for inhibitor concentrations of approximately three-fold and two-fold their $^{app}K_i$ values measured for L-idose, respectively. Compound **2** significantly impaired HLEC viability only when present in the culture medium at a concentration higher than two-fold the $^{app}K_i$ value measured for L-idose. Compound **1** appeared to reduce cell viability by 31 % when present for 48h at a concentration equal to the $^{app}K_i$ value measured for L-idose. Thus, on the basis of these results and the ARDIs characteristics of the selected hits, compound **2** appeared as the most promising for its effect on cell systems.

In order to test this effect, two cellular models suitable to test the ability of molecules to impair AKR1B1 activity in cultured cells and the consequent NF-*k*B activation were set up. Specifically, a transient transfection of both HEK-293 cells and HLCE with plasmids containing the Renilla Luciferase as constitutive gene and the Firefly Luciferase as reporter gene for the activation of NF-*k*B was performed. A stable transfection of HLCE with a plasmid containing the Firefly Luciferase as reporter gene for the activation of NF-kB was also performed.

Using TNF-alpha as pro-inflammatory stimulus, all the transfected cell models showed an increase of luciferase ranging from 1.6-fold to 2.4-fold, confirming the activation of the NF-*k*B signaling pathway. Both cell systems are thus available to evaluate the cellular effect of compounds, including those selected from HTS, acting as ARDIs in vitro

5. APPENDIX

APPENDIX A

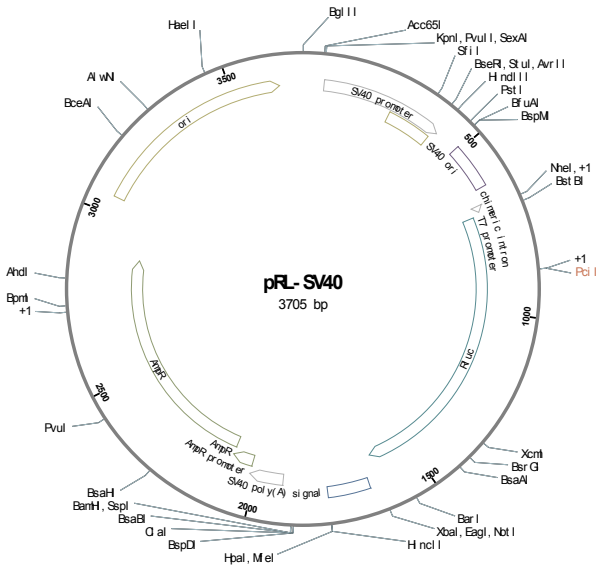

Figure 1A: pRL-SV40 maps. The plasmid contains the sequence for the Renilla Luciferas. A T7 promoter is located immediately upstream of Rluc for in vitro synthesis of Renilla luciferase. The SV40 late poly(A) signal sequence is positioned downstream of Rluc to provide efficient transcription termination and mRNA polyadenylation. A prokaryotic origin of replication and β-lactamase gene allow selected propagation of pRL-SV40 vector in *E. coli* host strains.

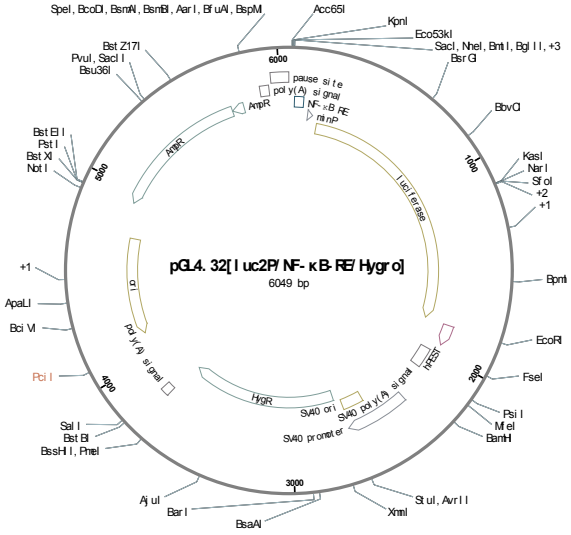

Figure 2A: pGL4.32[luc2P/NF-kB-RE/Hygro] maps. The plasmid contains 5 copies of NFkB response element (NF-kB-RE) that drives transcription of the luciferase reporter gene luc2P (Photinus pyralis). Luc2P is a synthetically derived luciferase sequence with humanized codon optimization that is designed for high expression and reduced anomalous transcription. The luc2P gene contains hPEST, a protein destabilization sequence. The protein encoded by luc2P responds more quickly than the protein encoded by the luc2 gene upon induction. The vector backbone contains an ampicillin resistance gene to allow selection in E. coli and a mammalian selectable marker for hygromycin resistance.

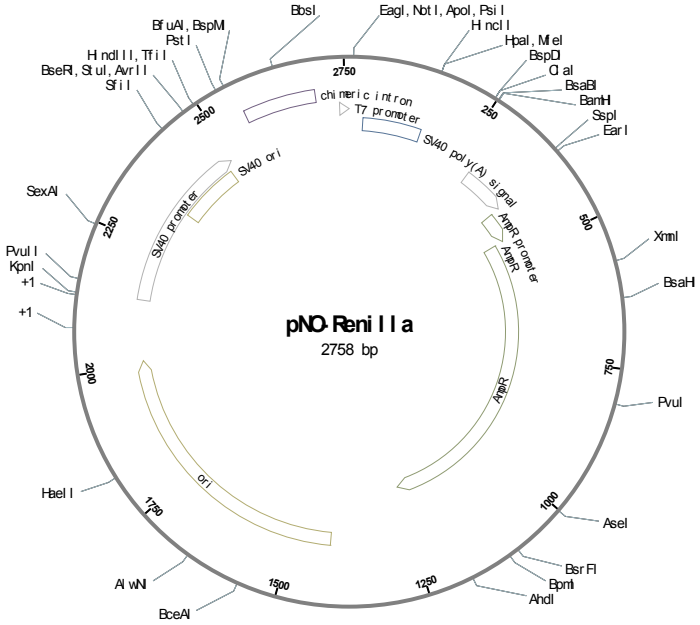

Figure 3A: pNO-Renilla maps. The plasmid has the same structure of the pRL-SV40 except the Renilla Luciferase gene.

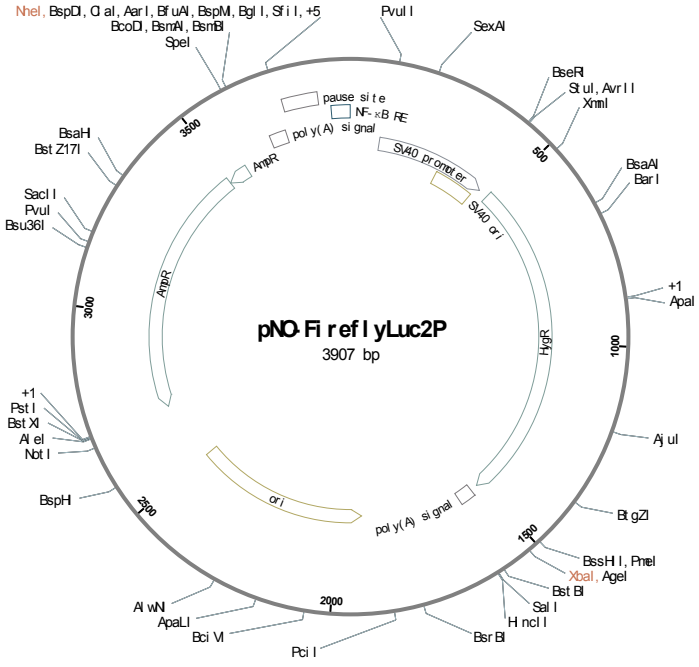

Figure 4A: pNO-FireflyLuc2P. The plasmid contains all the information of the pGL4.32[luc2P/NF-kB-RE/hygro]Vector except for the Firefly Luciferase gene **.**

APPENDIX B

Table 1B: LOPAC Plates Layout. The Table shows the layout of the 4 plate with the related LOPAC ID number of the compounds present in each plate. A: plate P1401; B plate P1402; C plate P1403; D plate P1404.

A

	1	2	3	4	5	6	7	8	9	10	11	12	13	14	15	16	17	18	19	20	21	22	23	24
A	Activity	Activity	120693	A 7250	291552	A7824	A 0500	A 8723	A 1260	A 9501	A 2129	A 9834	A 3539	SML0877	A 4508	A-145	SML1081	A-178	A 5909	SMI0888	A 6671	B 0753	SORBINIL	Blank
B	Activity	Activity	SML0492	SML0551	B 3023	C 3662	B 5399	C 4382	B 7651	C 4895	SMI1250	R 7772	B-102	C 6022	SMI1224	M5793	C 0330	C 7632	C 0862	C 8138	C 1671	C 8773	SORBINIL	Blank
C	Activity	Activity	144509	A 7275	SMI0773	SML0075	SMI1042	SML1249	A 1755	A 9512	A 2169	P 9623	Y4877	SML0894	A 4562	A-155	A 5282	S 3316	T 9034	SMI0908	SML0505	S 5192	SORBINIL	Blank
D	Activity	Activity	B 2134	SML0552	B 3501	C 3909	S 7067	C 4397	B 7777	C 4911	G6548	S 0693	SMI1179	G5794	B-161	C 6895	SMI1165	C 7861	C 0987	C 8145	C 1754	C 8903	SORBINIL	Blank
E	Activity	Activity	SML1041	SML0476	861804	A 8003	A 0760	A 8835	SML0511	A 9561	A 2251	A 9899	SML1506	SMI0882	A 4638	SML1138	A 5330	A-201	A 5922	C 6617	A 6883	SML0113	SORBINIL	Blank
F	Activity	Activity	B 2292	C 3025	B 3650	C 3912	B 5681	C 4418	B 7880	C 4915	S7701	C 5793	B-112	C 6048	B-168	C 7005	C 0400	C 7897	SMI0843	C 8221	B 6311	L5420	SORBINIL	Blank
G	Activity	Activity	194336	A 7410	A 0152	A 8404	A 0779	A 9013	A 1784	I4409	A 2385	A 9950	A 3773	A-129	A 4669	A-162	A 5376	A-202	A 6011	A-254	SML0189	B 1266	SORBINIL	Blank
H	Activity	Activity	B 2377	C 3130	B 4555	C 3930	B 5683	C 4479	B 8262	C 5020	G6423	L4545	B-121	C 6305	B-169	C 7041	C 0424	C 7912	C 1159	I0160	C 2235	C 9510	SORBINIL	Blank
I	Activity	Activity	211672	A 7655	A 0257	A 8423	SMI1166	A 9251	A 1824	A 9657	A 3085	H3288	F3680	A-138	SMI0881	A-164	A8001	O 5889	A 6134	A-255	A 7009	SMI1241		
J	Activity	Activity	B 2390	C 3270	B 4558	G 5918	B 6506	C 4520	B 8279	C 5040	SML0796	C 5923	SML1514	C 6506	B-173	SMI1497	C 0625	C 7971	C 1172	C 8395	P5749	SML0524		
K	Activity	Activity	246379	SMI1403	A 0382	A 8456	A 0937	A 9256	A 1895	SMI1068	A 3134	A-013	A 3940	A-140	S 9318	SML1447	A 5626	A-230	SML1514	A-263	A 7127	T6951		
L	Activity	Activity	B 2417	SML0550	B 5002	C 4024	B 7005	C 4522	B 8385	C 5134	SML0564	D8696	B-135	C 6628	B 5311	C 7255	C 0737	C 8011	C 1251	A9361	C 2505	A0487		
M	Activity	Activity	246557	A 7762	A 0384	A 8598	A 0966	SML0517	A 1910	L 6668	A 3145	A-022	SML1465	A-142	A4910	S 0568	T3955	A-236	SML0860	A-265	A 7148	SMI1084		
N	Activity	Activity	B 2515	C 3412	B 5016	C 4042	B 7148	C 4542	A0232	C 5259	B-016	SMI1498	B138	C 6643	SMI1005	C 7291	C 0750	C 8031	C 1290	C 8645	C 2538	C 9754		
O	Activity	Activity	265128	A 6476	A 0430	A 8676	R 0875	SML1445	SMI0896	A 9809	D-033	SMI0719	A 4393	A-143	A 5006	A8981	A 5879	A-242	SMI1461	B 0385	A 7162	B 2009		
P	Activity	Activity	B 2640	C 3635	B 5275	C 4238	B 7283	C 4662	SML0530	C 5270	SMI0846	C 6019	D 3943	C 6645	S3322	C 7522	C 0768	C 8088	C 1610	D6321	C 2755	C 9758		

B

	1	2	3	4	5	6	7	8	9	10	11	12	13	14	15	16	17	18	19	20	21	22	23	24
A	Activity	Activity	C 9847	P 9248	SMI0937	D 7644	C-141	SMI1560	C-199	D 9035	SML0584	D 9891	D 1306	SMI1066	D 2521	D-104	D 3689	SMI0797	D 4505	A5181	D 5564	E 1279	SORBINIL	Blank
B	Activity	Activity	S 3567	G-002	SML0613	P0099	E 8375	H 1377	E-101	H 2775	U6758	H 5752	F 6020	H 8125	F 6886	H 9002	F 9427	H 9882	SML0666	SMI1545	C 1625	I 1149	SORBINIL	Blank
C	Activity	Activity	C 9901	D 6035	C-106	D 7802	Y 0503	I6659	C-203	D 9128	D 0411	D-002	D 1413	M 7945	SMI1264	D-108	D 3768	A8054	D 4526	D1920-6	D 5689	E 1383	SORBINIL	Blank
D	Activity	Activity	E 3149	G-007	E 3876	G-133	N 3911	H 1384	T5648	H 3132	F 2802	H 6036	F 6145	H 8250	F 6889	H 9003	F 9552	H-108	G 0639	S0323	B7273	SML0130	SORBINIL	Blank
E	Activity	Activity	C 9911	D 6140	C-108	C1493	C-144	SML1085	T0202	D 9175	D 0540	D-003	D 1414	I 9532	C3993	D-122	D 3775	D-134	SMI1519	D-193	D 5766	E 1779	SORBINIL	Blank
F	Activity	Activity	E 5156	SMI1070	E 4375	G-154	E 8875	H 1512	E-114	SML0091	SML1109	Z4902	F 6300	H 8502	SML0639	SML0179	F 9677	SMI1111	G 0668	SMI1087	G 6416	I 1637	SORBINIL	Blank
G	Activity	Activity	SmI1173	D 6518	C-117	D 7909	SMI1474	C0256	C-223	D 9190	D 0670	SML1558	D 1507	D-047	D 2763	D126608	D 3900	D-138	D 5290	S 4443	D 5782	SmI1038	SORBINIL	Blank
H	Activity	Activity	E 3256	SML0660	E 4378	H 0126	E 9750	H 1753	SMI1193	H 4001	F 3764	H 7250	G4796	H 8627	N 2538	M 7445	F-100	SMI1244	SML0282	I 0157	G 6649	I 1656	SORBINIL	Blank
I	Activity	Activity	E9531	D 6899	C3618	D 7910	C-147	SMI1195	C-231	D 9305	D 0676	SML0594	D 1542	D-052	D 2926	N 2288	SMI1473	SMI1245	D 5294	V7264	D 5794	C 8863	SORBINIL	Blank
J	Activity	Activity	E 3263	G-110	E 4642	H 0131	P0111	H 1877	F 0778	L 4408	F 4303	H 7258	F 6513	H 8645	F 8257	H 9523	F-114	H-127	G 2128	I 0375	G 6793	M 1195	SORBINIL	Blank
K	Activity	Activity	SMI0837	SML0601	C-125	D 7938	C-191	D 8555	SMI1040	D 9628	D 1064	SMI1239	SMI1054	D-054	D 3630	D-129	D 4007	D14204	SML1530	E 0137	C0494	E 2375	SORBINIL	Blank
L	Activity	Activity	E 3380	J4829	E 7138	H 0627	E-006	H 2138	F 0881	H 4759	F 4381	J4137	F 6627	H 8653	F 8791	L 2167	F-124	H-128	G 2536	SMI1563	N2540	G0419	SORBINIL	Blank
M	Activity	Activity	C-101	SMI1532	C1335	SML1522	C-192	D9071	C-239	D 9766	D 1260	D-031	D 1916	N1415	D 3634	SMI1592	SML0586	SML0252	D 5385	SMI1528	SML0940	SMI1067	SORBINIL	Blank
N	Activity	Activity	R0158	G-117	SML0610	H 0879	D7443	B5437	F 1016	SML0191	F 4646	H 7779	E7906	SML005	F 8927	H 9772	F-131	H-135	G 3126	SML1594	G 8134	I 2279	SORBINIL	Blank
O	Activity	Activity	C-102	D 7505	C-130	D 8040	C-197	S 5567	C-271	D 9815	D 1262	A9605	S4572	D-103	D 3648	D-131	D 4434	B6813	D 5439	E 0516	D 5891	E 3132	SORBINIL	Blank
P	Activity	Activity	G9797	G-119	E 7881	H 1252	E-100	H 2380	F 1553	H 5257	F 4765	SMI0936	F 6800	H 8876	F 9397	H 9876	F-132	H-140	SML0527	I 0782	SML0634	I 2760	SORBINIL	Blank

C

	1	2	3	4	5	6	7	8	9	10	11	12	13	14	15	16	17	18	19	20	21	22	23	24
A	Activity	Activity	I 2764	T5576	I 5879	SMI1100	I 7627	M 1387	I 9890	SML0667	I-135	M 2901	A1362	M 3668	K 3888	M 4531	SML1102	M 5391	L 5025	SML0886	SMI0912	M 6690	SORBINIL	Blank
B	Activity	Activity	M 8046	N-144	M 9511	SMI0598	M-108	SMI1082	M-149	O 3752	SML0221	O-111	O0766	P 0878	PZ0111	P 1918	E2535	SML0698	N 7510	P 4543	N 8652	P 5514	SORBINIL	Blank
C	Activity	Activity	SML0264	L-109	I 6138	L-134	F8682	M 1404	I-106	M 2398	I-138	SML0223	K 0250	SML1226	U 6881	M 4659	SMI1625	M 5435	SML0653	M 6383	N 0287	M 6760	SORBINIL	Blank
D	Activity	Activity	M 8131	N-149	M 9651	N-170	SML0612	O 1008	N4163	SMI1089	S7198	P 0130	N 2001	P 0884	N 4148	P 2016	N 5501	P 4015	N 7634	P 4651	N 8659	P 5654	SORBINIL	Blank
E	Activity	Activity	I 2892	SMI0040	SML0247	L-135	SMI1073	M 1514	SMI1590	M 2525	M 1818	SMI0741	K 1003	M 3778	L 0258	M 4796	SML1587	M 5441	L 5647	M 6500	R 0529	M 7033	SORBINIL	Blank
F	Activity	Activity	SMI0962	N-151	SML1149	SMI0914	M-110	O 2378	M3071	O 8757	M-226	T2705	N 2034	P 1061	N 4159	P 2116	N 5504	SML0234	N 7758	P 4668	N 8784	SMI1075	SORBINIL	Blank
G	Activity	Activity	I 3639	SmI1626	I 6504	L119	I 8250	M 1559	I-117	SMI1591	I-146	M 3127	K 1136	D9446	L 0664	M 4910	L 2906	SML0233	L 5783	M 6517	L 9664	M 7065	SORBINIL	Blank
H	Activity	Activity	SML0683	N-153	M-001	N-183	M-116	O 2751	SMI1071	O 9126	L8668	P 0453	N 2255	P 1675	N 4382	P 2278	N 5636	P 4394	N 7778	P 4670	N 9007	P 6126	SORBINIL	Blank
I	Activity	Activity	I 3766	B175	I 7016	M 0763	SML1169	SMI0932	I-119	M 2547	A0606	M 3184	K 1751	M 3935	L 1011	M 5154	L 3791	M 5560	A6664	M 6524	L 9756	M 7277	SORBINIL	Blank
J	Activity	Activity	M 9020	SML0630	F 0430	SML0518	D 0943	O 2881	Z 4626	SML0557	N 0630	P 0547	N 3136	L9793	SML1639	P 2607	N 5751	P 4405	M2199	SML1124	T8703	P 6402	SORBINIL	Blank
K	Activity	Activity	I 4883	SMI1152	I 7378	M 0814	I 8898	B 1686	SMI1251	SML0658	I-160	M 3262	SMI1595	M 4008	SML0644	M 5171	L 4376	M 5644	L 8401	M 6545	SMI1624	M 7684	SORBINIL	Blank
L	Activity	Activity	M 9125	SML1198	M-104	O 0250	M-129	O 3011	M-184	S 3442	N 1016	SMI1490	N 3398	P 1784	N 4779	No-id-in-sdf	N 7127	SML0744	SML0711	P6499	N-115	P 6500	SORBINIL	Blank
M	Activity	Activity	SML0195	SML0269	I 7379	M 1022	SML1480	M 1809	I-122	M 2727	I18008	M 3281	K 2628	M 4145	C5493	M 5250	L 4762	M 5685	L 8533	M 6628	L 9908	SMI1606	SORBINIL	Blank
N	Activity	Activity	M 9292	N-158	M-105	O 0383	M-137	O 3125	SML098	SMI1493	N 1392	P 0667	N 3510	P 1793	SML1640	A0233	N 7261	P 4509	SMI1108	P 5295	S 6319	P 6503	SORBINIL	Blank
O	Activity	Activity	I 5627	L-131	I 7388	M 1275	S3572	F7932	S8822	M 2776	SMI0954	SML1610	K 3375	R 8404	L 2037	M 5379	L 4900	M 6191	L 8539	E4660	L-106	D 8941	SORBINIL	Blank
P	Activity	Activity	SML0227	B 2185	M-107	O 0877	ES406	O 3636	S 5321	O-100	N 1530	P 0778	N 3529	P 1801	N 5023	P 3510	N 7505	P 4532	N 8534	P 5396	N-142	P 6628	SORBINIL	Blank

D

	1	2	3	4	5	6	7	8	9	10	11	12	13	14	15	16	17	18	19	20	21	22	23	24
A	Activity	Activity	P 6656	R 0758	P 7412	SMI0995	SMI0994	R 8900	P 8782	R-108	P 9233	R-140	P 9879	A6733	P-118	S 2501	P-162	S7947	SML0704	I 5409	Q 3251	S 8010	SORBINIL	Blank
B	Activity	Activity	S 8567	SMI0938	S-008	T 7947	S-154	T 9262	T 0410	T-122	T 1516	U 4125	T 2528	U-103	SMI1523	U-116	B9311	V 8879	T 5625	W-104	T 6764	Y 3125	SORBINIL	Blank
C	Activity	Activity	P 6777	R 1402	P 7505	R 5648	P 8293	R 9525	P 8813	R-115	P 9297	S 0278	P-101	SML0752	B 4311	S 2812	P-178	SMI1525	SML0678	S 7389	SMI1504	SMI0842	SORBINIL	Blank
D	Activity	Activity	S 8688	T 7508	S-009	SML0216	A2729	T 9652	T 0625	T-123	T 1633	U 5882	T 2879	U-104	T 4264	U-120	SMI1014	A 2731	T 6031	A4233	T 6943	Y-101	SORBINIL	Blank
E	Activity	Activity	P 6902	R 2625	P 7561	R 6152	SMI0957	R 9644	P 8828	R-116	P 9375	S 0441	P-102	SMI1003	P-120	S 2816	SMI0989	S 3378	P63204	S 7395	Q-102	S 8139	SORBINIL	Blank
F	Activity	Activity	SML0275	SMI1112	D9571	SML0255	S-168	T 9778	F4429	T-144	T 1694	C9369	T 2896	U-105	K4144	SML1518	O1141	SML1115	T 6050	W-108	T 7040	Y-102	SORBINIL	Blank
G	Activity	Activity	P 6909	R 2751	P 7780	R 6520	P 8386	R-101	P 8852	H8664	P 9391	D5446	P-103	S 1875	G9048	S 2876	P-203	S 4063	Q 0125	C1494	L3169	S 8251	SORBINIL	Blank
H	Activity	Activity	Z1252	T 7665	S-106	T 8516	S-174	T-101	T 0891	A8852	T 1698	SML0134	T 3146	SML1529	T 4376	V 4629	SML0841	M0253	T 6154	SMI1539	T 7165	Z 0878	SORBINIL	Blank
I	Activity	Activity	218359	R 3255	P 7791	R 7150	SML1026	R-103	P 8887	R-121	P 9547	S 0752	SMI1119	T2952	P-126	SML1011	SMI0997	S 4250	Q 0875	S 7771	Q-109	I7160	SORBINIL	Blank
J	Activity	Activity	S 9186	SMI1547	S-143	T 8543	S-180	T-103	T 1132	H9415	SMI1527	SMI1550	SML0777	SML1237	T 4425	SML0776	SML0226	W 1628	B9685	X 1251	P0122	Z 2001	SORBINIL	Blank
K	Activity	Activity	P 7136	R 3277	P 7912	R 7385	P 8511	SMI1121	P 8891	SML0597	T6580	S 0758	B5063	S 2201	SML1448	S 3065	B 5556	S 5013	S8197	SML1495	Q-110	SML0209	SORBINIL	Blank
L	Activity	Activity	S 9311	SML0218	B6436	T 9025	G3796	T-104	T 1443	SML0229	T 2067	U 7500	T 3757	C0993	C0996	V 6383	SMI1000	SML0864	T 6376	S4568	T 7254	C1119	SORBINIL	Blank
M	Activity	Activity	P 7295	R2530	P 8013	B 5435	P 8688	I5784	K 1015	R-134	Z2777	SML0720	B9061	S 2250	SMI1110	SML0246	SML1446	S 5890	Q 1250	S 7882	SML0245	S 8442	SORBINIL	Blank
N	Activity	Activity	SML0679	B7688	S 2671	SML1559	T 0254	X4753	T 1505	T-200	T 2265	U-100	SML0824	U-111	T 4500	V 8138	SML1103	A7111	T 6394	X 6000	SML1543	O 7389	SORBINIL	Blank
O	Activity	Activity	P 7340	R 5010	P 8139	R 8875	P 8765	SML0993	P 9178	T6950	P 9797	SML1517	E9658	A9861	P-154	A8231	A1237	T7080	Q 2128	S 7936	R 0500	S 8502	SORBINIL	Blank
P	Activity	Activity	S-006	T 7883	S-153	I2285	T 0318	SMI1025	T 1512	SMI1552	T 2408	U-101	T 4143	U-115	T 4512	V 8261	SML0817	SMI0977	SMI1027	SML0892	T 7313	Z-101	SORBINIL	Blank

Table 2B: Percentage of inhibition of the 89 compounds identified through HTS. The Table shows the percent inhibition of the 89 compounds identified with the HTS with the L-Idose, their validation and the % of inhibition with HNE. For each compound the delta of inhibition between L-Idose (considering the mean of the first value and the one obtained from the validation) and HNE was calculated. The compounds in red are the hits that were selected for the best differential inhibition. The compounds in green are known AKR1B1 inhibitors.

Plate position	CAS NUMBER	% Inhibition L-Idose	% Inhibition L-Idose Validation	% Inhibition Screening HNE	Delta %L-Idose - %HNE
P1401C21	40180-04-9	61.77	70.34	70.95	-4.89
P1401D07	152121-30-7	29.29	12.24	9.52	11.25
P1401I13	403811-55-2	34.44	35.21	23.05	11.77
P1401K09	4431-00-9	88.08	75.44	75.00	6.76
P1401K12	136765-27-0	59.73	53.49	61.76	-5.15
P1401L11	183322-45-4	50.61	40.01	55.25	-9.95
P1401M10	132866-11-6	30.58	24.69	27.11	0.53
P1401M11	520-36-5	79.10	74.99	74.18	2.87
P1401M12	89073-57-4	42.04	47.53	51.16	-6.38
P1401M22	182135-66-6	28.45	48.70	34.69	3.88
P1401N22	64-86-8	29.10	34.14	38.67	-7.05
P1401N05	186185-03-5	69.93	51.03	53.99	6.49
P1402A21	486-35-1	42.46	66.86	87.79	-33.13
P1402B19	1300031-49-5	39.35	49.44	45.77	-1.38
P1402C06	486-66-8	27.76	34.89	41.91	-10.58
P1402C15	147098-20-2	25.99	28.54	26.03	1.24
P1402D12	263717-53-9	81.42	94.83	86.08	2.04

P1402E10	14663-23-1	31.09	28.82	20.30	9.65
P1402E11	2379-57-9	32.08	41.27	54.59	-17.91
P1402F16	136381-85-6 (anhydrous)	90.29	91.94	92.88	-1.77
P1402F21	220904-83-6	47.79	64.78	67.82	-11.54
P1402G03	136790-76-6	24.74	29.23	10.45	16.53
P1402G18	190908-40-8	86.95	93.76	96.19	-5.84
P1402H21	446-72-0	35.86	45.26	45.88	-5.32
P1402J22	17560-51-9	47.66	63.87	65.78	-10.01
P1402K03	4506-66-5	34.93	28.02	36.37	-4.89
P1402K21	14513-15-6	45.53	61.60	39.12	14.45
P1402L11	54-31-9	44.71	51.01	39.15	8.70
P1402L16	79558-09-1	66.27	70.60	76.08	-7.64
P1402L21	426834-69-7	31.47	40.83	25.32	10.83
P1402M09	115066-14-3 (free base)	50.12	52.19	51.46	-0.31
P1402N08	MFCD16879055 (MDL number)	51.18	50.62	44.51	6.39
P1402N12	65646-68-6	45.53	54.68	75.26	-25.16
P1402O16	7659-29-2	25.02	35.39	32.42	-2.22
P1402P05	518-82-1	25.58	32.10	28.30	0.54
P1402P10	555-55-5	49.67	51.41	57.34	-6.80
P1402P12	163451-81-8	62.53	72.18	58.23	9.13
P1402P19	82159-09-9	84.83	99.50	108.87	-16.70
P1403A06	172732-68-2	55.11	60.56	57.19	0.65
P1403B13	99754-06-0	49.03	53.21	45.96	5.16
P1403B21	104869-31-0 (anhydrous)	43.76	52.45	41.91	6.20
P1403C03	63735-71-7	26.78	33.24	23.35	6.66
P1403C17	210353-53-0	28.58	43.94	56.63	-20.37
P1403C20	362-07-2	30.27	46.61	23.13	15.31
P1403C22	529-44-2	40.25	59.01	63.55	-13.92
P1403D16	567-02-2 2016	26.23	40.85	18.26	15.28
P1403E07	101714-41-4	57.92	67.00	62.54	-0.08
P1403E21	293762-45-5	45.38	54.24	37.30	12.51
P1403G09	54197-31-8	71.57	66.34	52.69	16.27
P1403G13	74103-07-4	65.52	57.01	61.95	-0.68
P1403G18	199666-03-0	48.32	47.87	3.79	44.30
P1403H07	17560-51-9	69.72	65.56	55.22	12.42
P1403I08	18642-23-4	27.66	27.54	23.84	3.76
P1403K05	53-86-1	54.02	50.06	35.88	16.16
P1403K14	654055-01-3	53.93	50.68	51.95	0.36

P1403L04	165538-40-9	78.72	76.36	64.25	13.29
P1403L15	107254-86-4	67.99	64.76	54.70	11.68
P1403M21	934389-88-5	32.62	42.15	40.49	-3.11
P1403N16	648450-29-7	27.11	32.54	24.10	5.73
P1403O13	492-27-3	39.49	59.30	57.89	-8.50
P1403P03	863405-60-1	29.42	52.17	31.01	9.78
P1404A10	125628-97-9	90.88	92.64	103.07	-11.31
P1404A17	1852-38-6	28.74	30.85	8.70	21.09
P1404B20	138091-43-7	31.43	25.55	3.20	25.29
P1404C06	82-08-6	45.98	37.64	28.37	13.44
P1404C10	12236-82-7	85.81	83.99	79.16	5.74
P1404D16	MFCD25977152 (MDL number)	45.57	23.67	6.77	27.85
P1404E17	139262-76-3	43.04	45.61	39.01	5.32
P1404E22	38194-50-2	89.23	87.20	94.82	-6.60
P1404F21	2826-26-8	26.70	27.76	47.74	-20.51
P1404G19	6151-25-3	35.41	39.12	34.62	2.65
P1404H04	126433-07-6	92.94	93.82	103.59	-10.21
P1404H15	T 402-71-1	46.95	39.02	18.93	24.06
P1404H17	69049-73-6	62.12	62.71	56.74	5.67
P1404H22	37762-06-4	32.95	43.74	30.38	7.96
P1404I15	50-58-8	25.64	29.33	44.69	-17.21
P1404I17	88095709 (SID)	44.01	41.85	28.97	13.97
P1404J06	83373-60-8	28.62	36.07	16.51	15.84
P1404J10	105624-86-0	29.14	22.12	13.72	11.91
P1404K05	60-82-2	31.77	22.62	24.43	2.76
P1404K22	219766-25-3	31.29	31.69	17.25	14.24
P1404L11	148741-30-4	29.17	19.85	22.12	2.38
P1404M13	90357-06-5	40.21	34.91	14.80	22.76
P1404M21	145040-37-5	26.36	31.45	12.57	16.34
P1404N05	129-46-4	94.28	90.53	94.33	-1.93
P1404N06	186497-07-4	50.46	44.60	74.55	-27.02
P1404P07	53902-12-8	64.88	64.88	86.04	-21.16
P1404P15	24198-97-8 (anhydrous)	38.17	47.69	49.08	-6.15
P1404P18	149904-87-0	26.79	43.24	40.79	-5.78

7. REFERENCES

- Abu-Reidah I.M., Arráez-Román D., Lozano-Sánchez J., Segura-Carretero A. and Fernández-Gutiérrez A. (2013). Phytochemical characterization of green beans (Phaseolus vulgaris L.) by using high-permormance liquid chromatography coupled with time-of-flight mass spectrometry. Phytochem Anal 24(2): 105-116.
- American Diabetes Association (2014). Diagnosis and Classification of Diabetes Mellitus. *Diabetes Care 37, 1: S81-S90*.
- Asano T., Saito Y., Kawakami M., Yamada N., Fiderestat Clinicla Pharmacology Study Group. (2002). Fidarestat (SNK-860), a potent aldose reductase inhibitor, normalizes the elevated sorbitol accumulation in erythrocytes of diabetic patients. *Journal of Diabetes and its Complications Volume 16 Issue 2: 133-138*.
- Ba M.Y., Xia L.W., Li H.L., Wang Y.G., Chu Y.N., Zhao Q., Hu C.P., He X.T., Li T.X., Liang K.Y., Zhang Y.H., Yang L., Xie W.H., Yang H. and Sun M.R. (2019) Concise synthesis of 2-methoxyestradiol from 17β-estradiol through the C(sp 2)-H hydroxylation. *Steroids 146:99-103*.
- Baeuerle P.A. and Baltimore D. (1996). NF-kB: Ten years after. *Cell, 87: 13-20*.
- Balestri F., Barracco V., Renzone G., Tuccinardi T., Pomelli C.S., Cappiello M., Lessi M., Rotondo R., Bellina F., Scaloni A., Mura U., Del Corso A., and Moschini R. (2019). Stereoselectivity of Aldose Reductase in the Reduction of Glutathionyl-Hydroxynonanal Adduct. *Antioxydants, 8: 502*.
- Balestri F., De-Leo M., Sorce C., Cappiello M., Quattrini L., Moschini R., Pineschi C., Braca A., La-Motta C., Da-Settimo F., Del-Corso A., and Mura U. (2019). Soyasaponins from Zolfino bean as aldose reductase differential inhibitors. *J. Enz. Inhib. Med. Chem. 34: 350-360*.
- Balestri F., Poli G., Pineschi C., Moschini R., Cappiello M., Mura U., Tuccinardi T. and Del Corso A. (2020). Aldose Reductase Differentil Inhibitors in Green Tea. *Biomolecules 10(7): 1003*.

- Balestri F., Quattrini L., Coviello V., Sartini S., Da Settimo F., Cappiello M., Moschini R., Del-Corso A., Mura U., and La-Motta C. (2018). Acid derivatives of Pyrazolo[1,5-*a*]pyramidine as Aldose reductase differential inhibitors. *Cell Chemical biology 24:1414-1418*.
- Balestri F., Rotondo R., Moschini R., Pellegrino M., Cappiello M., Barracco V., Misuri L., Sorce C., Andreucci A., Del-Corso A. and Mura U. (2016). Zolfino Iandrace (*Phaseouls vulgaris* L.) from Pratomagno: general and specific features of a functional food. *Food Nutr Res. 60*.
- Balestri F., Sorce C., Moschini R., Cappiello M., Misuri L., Del-Corso A., and Mura U. (2017). Edible vegetables as a source of aldose reductase differential inhibitors. *Chem, Biol Interact 276: 155-159*.
- Balestri F., Cappiello M.; Moschini R.; Rotondo R.; Buggiani I.; Pelosi P., Mura U. and Del Corso, A. (2015a). L-Idose: an attractive substrate alternative to D-glucose for measuring aldose reductase activity. *Biochem Biophys Res Commun, 456*, *891-895.*
- Balestri F., Cappiello M., Moschini R., Rotondo R., Abate M., Del Corso A. and Mura U. (2015b). Modulation of aldose reductase by aldose hemiacetals. *Biochim Biophys Acta, 1850: 2329-2339.*
- Bergmann M., Hart L., Lindsay M., Barnes P.J., and Newton R. (1998). IkappaBalpha degradation and Nuclear factor-kappaB DNA binding are insufficient for interleukin-1beta and tumor Necrosis factor-alpha induced kappaB-indipendent transcription. Requirement for an addition activation pathway. *J Biol Chem 273(12):6607-10*.
- Biadene M., Hazemann I., Cousido A., Ginell S., Joachimiak A., Sheldrick G.M., Podjarny A. and Scheneider T.R. (2007) The atomic resolution structure of human aldose reductase reveals that rearrangement of a bound ligand allows the opening of the safety-belt loop. *Acta Crystal Section D 63: 665-672*.
- Bohren K.M., Grimshaw C.E., Lai C. J., Harrison D.H., Ringe D., Petsko A.A., and Ganny K.H. (1994). Tyrosine-48 is the proton donor and histidine-110 directs substrate stereochemical selectivity in the reduction reaction of Human Aldose Reductase: enzyme kinetics and crystal structure of the Y48H mutant enzyme. *Biochemistry* 33(8):2021-2032.
- Bradford, M.M. (1976). A rapid and sensitive method for the quantitation of microgram quantities of protein utilizing the principle of protein-dye binding. *Anal. Biochem*. *72, 248–254*.

- Brownlee M. (2001). Biochemistry and molecular cell biology of diabetic complications. *Nature 414: 813-820*.
- Brownlee M. (2004). The pathobiology of diabetic complications. A unifying mechanism. *Diabetes, 54: 1615-1625*.
- Burg M.B. (1995). Molecular basis of osmotic regulation. *Am J Physiol 268 (6 Pt 2): F983-96*.
- Cappiello M., Balestri F., Moschini R., Mura U., and Del-Corso A. (2020). Intra-site differential inhibition of multi-specific enzymes. Journal of Enzyme Inhibition and Medicinal *Chemistry: 840-846*.
- Chang K.C., Li L., Sanborn T.M., Shieh B., Lenhart P., Ammar D., LaBarbera D. V. and Petrash J.M. (2016). Characterization of Emodin as a Therapeutic Agent for Diabetic Cataract. *J Nat Prod. 79(5): 1439-1444.*
- Chaudhry P.S., Cabrera J., Juliani H.R. and Varma S.D. (1983). Inhibition of human lens aldose reductase by flavonoids, sulindac and indomethacin. *Biochem Pharmacol 32(13): 1995-1998.*
- Chiefari E., Arcidiacono B., Foti D. and Brunetti A. (2017). Gestational diabetes mellitus: an updated overview. *J Endocrinol Invest 40: 899-909*.
- Choi J. S., Islam M. N., Ali M. Y., Kim E. J., Kim Y. M. and Jung H. A. (2014). Effects of C-glycosylation on anti-diabetic, anti-Alzheimer's disease and anti-inflammatory potential of apigenin. *Food Chem Toxicol. 64: 27-33.*
- Clements R.S. Jr. (1986). The polyol pathway. *A historical review. Drugs 32 Suppl 2: 3-5*.
- Comahli V., Adem S., Oztekin A. and Demirdag R. (2020). Screening inhibitory effects of selected flavonoids on human recombinant aldose reductase enzyme: *in vitro* and *in silico* study. *Arch Physiol Biochem 28: 1-7.*
- Csala M., Kardon T., Legeza B., Lizak B., Mandl J., Margittai E., Puzkas F., Szaraz P., Szelenyi P. and Banhegyi G. (2015). On the Role of 4-hydroxynonenal in Health and Disease. *Biochim Biophys Acta 1852(5): 826-838*.
- De la Fuente J.A. and Manzanaro S. (2003). Aldose reductase inhibitors form natural sources. *Nat Prod Rep. 20(2): 243-51*.
- DeFronzo R.A. (2004). Pathogenesis of type 2 diabetes mellitus. *The medical clinics of North America 88: 787-835*.

- Del Corso A., Cappiello M. and Mura U. (2008). From a dull enzyme to something else: facts and perspectives regarding aldose reductase. *Current Medicinal Chemistry 15: 1452-1461*.
- Del Corso A., Dal Monte M., Vilardo P.G., Cecconi I., Moschini R., Banditelli S., Cappiello M., Tsai L. and Mura U. (1998). Site-specific inactivation of aldose reductase by 4-hydroxynonenal. *Arch Biochem Biophys* 350(2): 245-8.
- Del-Corso A., Balestri F., Di Bugno E., Moschini R., Cappiello M., Sartini S., La-Motta C., Da-Settimo F., and Mura U. (2013). A new approach to control the enigmatic activity of Aldose reductase. *PLOS ONE, 8, 9: e74076*.
- Deshpande A.D., Hayes M.H. and Schootman M. (2008) Epidemiology of Diabetes and Diabetes-Related Complications. *Physical Therapy 88, 11: 1254-1264*.
- Diaz-Meco M.T., Dominiguez I., Sanz L., Dent P., Lozano J., Municio M.M., Berra E., Hay R.T., Sturgill T.W. and Moscat J. (1994). ζPKC induces phosphorylation and inactivation of IxB-ao in vitro. *The EMBO Journal vol.13 no.12: 2842-2848*.
- Dinelli, G., Bonetti, A., Minelli, M., Marottia, I., Catizone, P., & Mazzanti, A. (2006). Content of flavonols in Italian bean (Phaseolus vulgaris L.) ecotypes. *Food Chemistry, 99, 105- 114*.
- Dworkin J.P. and Miller S.L. (2000). A kinetic estimate of the free aldehyde content of aldoses. *Carbohydr Res 329(2): 359-365*.
- Endo S., Matsunaga T., Mamiya H., Ohta C., Soda M., Kitade Y., Tajima K., Zhao HT., El-Kabbani O. and Hara A. (2009). Kinetic studies of AKR1B10, human aldose reductase-like protein: Endogenous substrates and inhibition by steroids. *Archives of Biochemistry and Biophysics Volume 487, Issue 1: 1-9.*
- Federation, International Diabetes (2017). *IDF Diabetes Atlas. Eighth Edition*
- Ferraris, J.D., Williams, C.K., Jung, K.Y., Bedford, J.J., Burg, M.B. and Garcia- Perez, A.J. (1996). ORE, a Eukaryotic Minimal Essential Osmotic Response Element. The Aldose Reductase Gene in Hyperosomitc Stress. *Biol. Chem 271(31*): 18318-18321.
- Forbes J.M and Cooper M. E. (2013). Mechanisms of diabetic complications. *Physiol Rev Volume 93: 137-188.*
- Fotsis T., Zhang Y., Pepper M.S., Adlercreutz H., Montesano R., Nawroth P.P. and Schwigerer L. (1994) The endogenous oestrogen metabolite 2-methoxyestradol inhibits angiogenesis and suppresses tumor growth. *Nature 368 (6468): 237-9.*

- Gabbay K.H. and Tze W. J. (1972). Inhibition of glucose-induced release of insulin by aldose reductase inhibitors. *Proc Natl Acad Sci U S A. 69(6): 1435-1439.*
- Gao J., Yao L., Xia T., Liao X., Zhu D. and Xiang Y. (2018). Biochemistry and structura studies of kynurenine 3-monooxygenase reveal allosteric inhibition by Ro 61-8048. *The FASEB Journal 2036:2045.*
- Grewal A.S., Bhardwaj S., Pandita D., Lather V., and Sekhon B. S. (2016). Updates on aldose reductase inhibitors for management of Diabetic complications and Non-diabetic diseases. *Mini-Reviews in Medicinal Chemistry, 16: 120-162*.
- Gucalp A., Tolaney S., Isakoff S.J., Ingle J.N., Liu M.C., Carey L.A., Blackwell K., Rugo H., Nabell L., Forero A., Stearns V., Doane A.S., Danso M., Moynahan M.E., Momen L.F., Gonzalez J.M., Akhtar A., Giri D.D., Patil S., Feigin K.N., Hudis C.A., Traina T.A. and Translational Breast Cancer Research Consortium (TBCRC 011). (2013) Phase II trial of bicatulamide in patients with androgen receptor-positive estrogen receptor-negative metastatic Breast Cancer. *Clin Cancer Res. 19(19): 5505-12.*
- Harteneck C. (2013). Pregnenolone Sulfate: From Steroid Metabolite to TRP Channel Ligand. *Molecules 18: 12012-12028.*
- Hashimoto Y., Yamagishi S.I., Mizukami H., Yebe-Nishimura C., Lim S.W., Kwon H.M., Soroku Y. (2011). Polyol pathway and diabetic nephropathy revisited: Early tubular cell changes and glomerulopathy in diabetic mice overexpressing human aldose reductase. *J Diabetes Investig. 2(2): 111-122.*
- Hirakawa H., Sawada H., Yamahama Y., Takikawa S.I., Shintaku H., Hara A., Mase K., Kondo T. and Iino T. (2009). Expression analysis of the aldo-keto reductases involved in the novel biosynthetic pathway of tetrahydrobiopterin in human and mouse tissues. *J Biochem 146(1):51-60.*
- Hotta N., Akanuma Y., Kawamori R., Matsuoka K., Oka Y., Shichiri M., Toyota T., Nakashimi M., Yoshimura I., Sakamoto N. and Shigeta Y. (2006). Long-term clinical effects of Epalrestat, an aldose reductase inhibitor, on diabetic peripheral neuropathy: the 3-year, multicenter, comparative Aldose reductase inhibitor-Diabetes complications trial. *Diabetes Care 29, 7: 1538-1544.*

- Hwang S. H., Kim H. Y., Quispe Y. N. G., Wang Z., Zuo G. and Lim S. S. (2019). Aldose Reductase, Protein Glycation Inhibitory and Antioxidant of Peruvian Medicinal Plants: The Case of *Tanacetum parthenium* L. and Its Costituents. *Molecules 24(10): 2010.*
- Iannuzzi A.M., Moschini R., De Leo M., Pineschi C., Balestri F., Cappiello M., Braca A., and Del-Corso A. (2020). Chemical profile and nutraceutical features of *Salsola soda* (Agretti): anti-inflammatory and antidiabetic potential of its flavonoids. *Food Bioscience 37.*
- Inagaki K., Miwa I. and Okuda J. (1982). Affinity Purificatio and Glucose Specificity of Aldose Reductase From Bovine Lens*. Arch Biochem Biophys 216(1): 337-344*.
- International Diabetes Federation (2017). IDF DIABETES ATLAS. Eighth edition.
- Iwata T., Sato S., Jimenez J., McGowan M., Moroni M., Dey A., Ibaraki N., Reddy V.N. and Carper D. (1999). Osmotic response element is required for the induction of aldose reductase by tumor necrosis factor-alpha. *J Biol Chem 274(12): 7993-8001.*
- Jang D.S., Lee G. Y., Kim Y. S., Lee Y. M., Kim C. S., Yoo J. L. and Kim J.S. (2007). Anthraquinones from the seeds of Cassia tora with inhibitory activity on protein glycation and aldose reductase. *Biol Pharm Bull 30(11): 2207-2210.*
- Jez J.M., Flynn G. and Penning T.M. (1997) A new nomenclature for the Ald-Keto Reductase Superfamily. *Biochemical Pharmacology Volume 54: 639-647*.
- Kasajima H., Yamagishi S., Sugai S., Yagihashi N., and Yagihashi S. (2001). Enhanced in situ expression of aldose reductase in peripheral nerve and renal glomeruli in diabetic patients. *Virchows Archiv Int J Pathol 439,1: 46-54*.
- Kato A., Higuchi Y., Goto H., Kizu H., Okamoto T., Asano N., Hollinshead J., Nash R. J., and Adachi I. (2006). Inhibitory effects of Zingiber officinale Roscoe derived components on Aldose reductase activity in vitro and in vivo. *J. Agric. Food Chem. 54: 6640-6644*.
- Kim S. B., Hwang S. H., Wang Z., Yu J. M. and Lim S.S. (2017). Rapid Identification and Isolation of Inhibitors of Rat Lens Aldose Reductase and Antioxidant in *Maackia amurensis. Biomed Research International: 4941825.*
- Kim T.H., Kim J.K., Kang Y.H., Lee J.Y., Kang I.J., and Lim S.S. (2013). Aldose reductase inhibitory activity of compounds from *Zea mays* L. *BioMed Research International*.
- Kim Y.S., Kim N. H., Jung D. H., Jang D. S., Lee Y. M., Kim J. M. and Kim J. S. (2008). Genistein inhibits aldose reductase activity and high glucose-induced TGF-beta2 expression in human lens epithelial cells. *Eur J Pharmacol 594(1-2): 18-25.*

- Kinoshita J.H., Merola L.O. and Dikmak E. (1962). Osmotic changes in experimental galactose cataracts. *Exp Eye Res. 1: 405-10*.
- Ko, B.C.B., Ruepp, B., Boheren, K.M., Gabbay, K.H. and Chung, S.S.M. (1997). Identification and Characterization of multiple osmotic response sequences in the Human Aldose reductase gene. *J. Biol. Chem. 272 (26): 16431-16*437.
- Kovacic J.C., Castellano J.M., Farkouh M. E. and Fuster V. (2014). The relationships between cardiovascular disease and diabetes: focus on pathogenesis. *Endrocrinol Metab Clin North Am. 43(1): 41-57.*
- Koya D., Haneda M., Najagawa H., Isshiki K., Sato H., Sugimoto T., Yasuda H., Kashiwagi A., Wayas D. K., King G., L., and Kikkawa R. (2000). Amelioration og Accelerated Diabetic Mesangial Expansion by Treatment with a PKC Beta Inhibitor in Diabetic db/db Mice, a Rodent Model for Type 2 Diabetes. *FASEB J. 14(3): 439-47.*
- Krans H.M. (1992). Recent clinical experience with aldose reductase inhibitors. *J Diabetes Complications 6(1): 39-44.*
- Laemmli U.K. (1970). Cleavage of structural proteins during the assembly of the head of bacteriophage T4. *Nature 227(5259):680-685.*
- Lee A. Y. W., and Chung S. S. M. (1999). Contributions of polyol pathway to oxidative stress in diabetic cataract. *FASEB J13: 23-30.*
- Lee K.H., Cho J. H., Choi I. S., Park H. M., Lee M. G., Choi B. J. and Jang I. S. (2010). Pregnenolone sulfate enhances spontaneous glutamate release by inducing presynaptic Ca2+ induced Ca2+ release. *Neuroscince 171(1): 106-116.*
- Lee Y.S., Kang Y.H., Jung J.Y., Kang I. J., Han S. N., Chung J. S., Shin H.K. and Lim S.S. (2008). Inhibitory Costituents of Aldose Reductase in the Fruiting Body of *Phellinus linteus*. *Biol Phamr Bull 31(4): 765-768.*
- Lin L.Z., Harnly J.M., Pastor-Corrales M.S. and Luthria D.L. (2008). The polyphenolic profiles of common bean (*Phaseolus vulgaris* L.). *Food Chem 107(1): 399-410.*
- Milackova I., Kapustova K., Mucaki P. and Hosek J. (2017). Artichoke Leaf Extract Inhibits AKR1B1 and reduces NF-kB activity in Humna Leukemic Cells. *Phytother Res 31(3): 488-496.*
- Nelson D. L., and Cox M. M. (2018). Lehninger's Principles Of Biochemistry. (E. Melloni, Trad. Bologna: *Zanichell*i.

- Paek J.H., Shin K.H., Kang Y-H., Lee J-Y., and Lim S.S. (2013). Rapid identification of Aldose reductase inhibitory compounds from *Perilla frutescens. BioMed research International 2013.*
- Petak S. and Sardhu A. (2018). The Intersection of Diabetes and Cardiovascular Disease. *Methodist Debakey Cardiovasc J. 14(4): 249-250.*
- Poli G. and Schaur R.J. (2000). 4-hydroxynonenal in the Pathomechanisms of Oxidative Stress. *IUBMB Life, 50: 315-321*.
- Pribluda V.S., Gubish Jr E.R., Lavalle T.M:, Treston A., Swart G.M. and Green S.J. (2000) 2-Methoxyestradiol: an endogenous antiangiogenic and antiproliferative drug candidate. *Cancer Metastasis Rev 19(1-2):173-179.*
- Ramana K.V. (2011) Aldose reductase: New insights for an old enzyme. *Biomol Concepts. April 1: 2(1-2):103-114.*
- Ramana K.V., Friedrich B., Bhatnagar A. and Srivastava S.K. (2003). Aldose Reductase mediates cytotoxic signals of hyperglycemia and TNF-alpha in Human Lens Epithelial Cells. *FASEB J 17(2): 315-317*.
- Ramana, K.V., Friedrich, B., Tammali, R., West, M.B., Bhatnagar, A. and Srivastava, S.K. (2005) Requirement of aldose reductase for the hyperglycemic activation of protein kinase C and formation of diacylglycerol in vascular smooth muscle cells. *Diabetes 54: 818–829*.
- Ramirez M.A. and Borja N.L. (2008). Epalrestat: an aldose reductase inhibitor for the treatment of diabetic nerupathy. *Pharmacotherapy 28(5): 646-655.*
- Sampath C., Sang S and Ahmedna M. (2016). In vitro and in vivo inhibition of aldose reductase and advanced glycation end products by phloretin, epigallocatechin 3-gallate and [6]-gigerol. *Biomed Pharmacother 84: 502-513.*
- Schaur R.J., Siems W., Bresgen N. and Eckl P.M. (2015). 4-hydroxy-nonenal- A Bioactive Lipid Peroxudation Product. Biomolecules, 5: 2247-2337.
- Schellhammer P. F. and Davis J. W. (2004). An evaluation of bicatulamide in the treatment of prostate cancer. *Clin Prostate Cancer 2(4): 213-219.*
- Smith J.R., Jamie J.F. and Guillemin G.J. (2016). Kynurenine-3-monooxygenase: a review of structure, mechanism and inhibitors. *Drug Discov Today. 21(2): 315-324.*

- Snow A., Shieh B., Chang K.C., Pal A., Lenhart P., Ammar D., Ruzycki P., Palla S., Reddy G. B., and Petrash J. M. (2015). Aldose reductase expression as a risk factor for cataract. *Chem Biol Interact 5, 234: 247-253.*
- Sotriffer C.A., Kramer O. and Klebe G. (2004) Probing flexibility and 'indiced-fit' phenomena in aldose reductase by comparative crystal structure analysis and molecular dynamics simulations*. PROTEINS: Structure, Function and Bioinformatics Volume 56: 52-66.*
- Srivastava S., Chandra A., Bhatnagar A., Srivastava S.K. and Ansari N.H. (1995). Lipid Peroxidation Product, 4-Hydroxynonenal and Its Conjugate with GSH Are Excellent Substrates of Bovine Lens Aldose Reductase. *Biochemical and Biophysical Research Communications, 217: 741-746.*
- Srivastava S., Watowich A.J., Petrash J.M., Srivastaca S.K., and Bhatnagar A. (1999). Structural and kinetic determinants of aldehyde reduction by Aldose Reductase. *Biochemistry 38(1): 42-54*.
- Srivastava S.K., Ramana K.V. and Bhatnagar A. (2005). Role of aldose reductase and oxidative damage in diabetes and the consequent potential for therapeutic options. *Endocr. Rev. 26: 380–392.*
- Stitt A.W., Lois N., Medina R.J., Adamson P., and Curtis T.M. (2013). Advances in our understanding of diabetic retinopathy. *Clin Sci (Lond) 125(1):1-17*.
- Tao H., Mei J. and Tang X. (2019). The anticancer effects of 2-Methoxyestradiol on human huh7 cells in vitro and in vivo. *Biochem Biophys Res Commun. 512(3): 635-640.*
- Tarr J. M., Kaul K., Chopra M., Kohner E.M., and Chibber R. (2013). Pathophysiology of Diabetic Retinopathy. *ISRN Ophthalmology 2013: 343560*.
- Tošović, J., & Marković, S. (2015). Simulation of the UV/Vis spectra of flavonoids. *Conference Paper - 15th international Conference on Bioinformatics and Bioengineering (BIBE)*, (p. 1-6).
- Urzhumtsev A., Tete-Favier F., Mitschler A., Barbanton J., Barth P., Urzhumtseva L., Biellmann J.F., Podjarny A., and Moras D. (1997). A "specificity" pocket inferred from the crystal structures of the complexes of aldose reductase with the pharmaceutically important inhibitors tolrestat and Sorbinil. *Structure 5(5): 601-12.*
- Vijan S. (2015). In the clinic. Type 2 diabetes. *Annals of internal Medicine 162(5): ITC1-16.*

- Wellington K. and Keam S. J. (2006). Bicatuamide 150mg: a review of its use in the treatment of locally advanced prostate cancer. *Drugs 66(6): 837-850.*
- Wilson D.K., Bohren K.M., Gabbay K.H., and Quiocho F.A. (1992). An unlikely sugar substrate site in the 1.65 A structure of the human aldose reductase holoenzyme implicated in diabetic complications. *Science 257(5066): 81-4.*
- World Health Organization (2016). Global Report On Diabetes. *World Healt Organization*.
- Wu S.L. (2015). Staging of type 2 diabetes mellitus. *Genetics and Molecular Research Volume 4: 2118-2121.*
- Zhang H. and Forman H. J. (2017). Signaling by 4-hydroxy-2-nonenal: Exposure protocols, target selectivity and degradation. *Arch Biochem Biophys. Mar 1; 617: 145-15*4.
- Zhang, J.H., Chung, T.D., Oldenburg, K.R. (1999). A simple statistical parameter for use in evaluation and validation of high throughput screening assay. *J. Biomol. Screen, 4: 67-73*.
- Zheng X., Zhang L., Zhai J., Chen Y., Luo H. and Hu X. (2012). The molecular basis for inhibition of sulindac and its metabolites towards human aldose reductase. *FEBS Lett 586(1): 55-9.*